Numerical studies of thermal-mechanical responses of embankments under a changing climate in two first nation communities, Saskatchewan, Canada

Zubair Akhter

A Thesis

In

The Department

Of

Building, Civil, and Environmental Engineering

Presented in Partial Fulfillment of the Requirements

For the Degree of

Master of Applied Science (Geotechnical Engineering) at

Concordia University

Montréal, Québec, Canada

July 2023

CONCORDIA UNIVERSITY

School of graduate studies

This is to certify that the thesis is prepared

By: Zubair Akhter

Entitled: Numerical studies of thermal-mechanical responses of embankments under a changing climate in two first nation communities, Saskatchewan, Canada.

and submitted in partial fulfillment of the requirements for the degree of

Master of Applied Science (Geotechnical Engineering)

complies with the regulations of the University and meets the accepted standards with respect to originality and quality.

Signed by the final Examining Committee:

_____ Chair

Dr. A. M. Hanna

_____ Examiner

Dr. G. Hafeez

_____ Examiner

Dr. A. M. Hanna

_____ Supervisor

Dr. A. Nazemi

_____ Supervisor

Dr. B. Li

Approved by: Dr. C. An

Graduate Program Director

22nd August 2023 Mourad Debbabi

Dean of faculty

ABSTRACT

Numerical studies of thermal-mechanical responses of embankments under a changing climate in two first nation communities, Saskatchewan, Canada.

Zubair Akhter

Records show that ongoing global warming has changed the thermal condition of the ground in seasonally frozen areas of Canada, causing widespread ground surface settlement and harm to infrastructure, particularly embankments. In the current study, finite element numerical analysis is conducted to evaluate how climate change may influence the thermal-mechanical (TM) regimes in road embankments that are under climate conditions in two Indigenous communities in Saskatchewan, Canada, namely Yellow Quill and James Smith. This evaluation includes the analysis of embankment on the climate data from 1975 till 2100, where the data is divided into different time periods of Historical (1975-2000), Future-1 (2023-2048), Future-2 (2049-2074) and Future-3 (2075-2100. From each period, 5 representing years including extreme cold, extreme hot, expected hot, expected cold, expected mean years are considered to simulate the TM regimes with and without traffic loads. The relation for temperature-dependent thermal expansion coefficients of soils is derived and included in the modeling based on the ice content and a mixture theory. Temperature dependent mechanical properties are also involved to account for freeze-thaw induced stress redistribution and the related potential plastic deformation. According to the coupled thermal-mechanical study, which takes into account the Linear Drucker-Prager

yield criterion for the stress analysis at critical location of embankments, cases with an extreme cold climate indicates the worst effect on the embankment foundation. It is reflected by the more significant temperature variations causing larger plastic zones in the toe of the embankment when compared with other climate scenarios. The extreme hot cases tend to generate more displacement on the road surface as the climate is getting warmer. The present study only sheds light on the thermal-mechanical aspect, and it does not include pore water flow behavior due to frost actions. Therefore, the result on the heave or settlement of embankment surface is not significant. Nevertheless, the inclusion of temperature-dependent thermal expansion coefficients considering the ice contents provides a better estimation of thermal-mechanical responses.

Key words: Finite element analysis, climate change, embankment, thermal-mechanical response, nonlinear thermal expansion coefficient

ACKNOWLEDGEMENTS

Accomplishing this thesis was not an individual achievement. I'd like to thank the followings for their assistance in getting me to the finish line:

My supervisor, Dr. Biao Li, for taking me under his supervision and for all his advice, support, and suggestions regarding problem-solving. He also worked incredibly hard to teach me the necessary software skills and techniques during my master's program, which undoubtedly helped me remain determined despite the ups and downs of my research work.

Dr. Ali Nazemi, my co-supervisor, for introducing me to this project, guidance for in understanding environmental details and helping me to achieve my research objectives.

Sohail Akhtar, my elder brother, played an important role in making complex programming easy for me and supported my thesis completion.

Finally, I would like to express my gratitude for the financial assistance provided by Faculty Research Support (FRS) program from University of Concordia and Bursary from New Frontiers in Research Fund to carry out this research.

TABLE OF CONTENTS

LIST OF FIGURES

LIST OF TABLES

LIST OF SYMBOLS, ABBREVATIONS, AND NOMENCLATURE

b_i	Body force
C	Mohr-Coulomb model cohesion
C_{ijkl}	Elastic stiffness tensor
D	Drucker-Prager model cohesion
$\bar{\varepsilon}^{pl}\|_0$	Initial plastic strain
$\dot{\varepsilon}^{pl}$	Equivalent plastic strain rate
F	Yield function
G	Flow potential
I_1	First stress tensor invariant
J_2, J_3	Second and Third stress deviator invariants
k	Thermal conductivity of soil
L	latent heat of fusion for freezing and thawing water
L_s	Latent heat of fusion for soil
n	Porosity
P	Equivalent pressure stress
P_1	Uniform characteristic load
P_2	concentrated characteristic load

P	equivalent load
ρ	Deviatoric length
ρ_b	Bulk density
ρ_d	The dry density of soil
ρ_s	The density of solid minerals
ρ_w	Density of water
q	Mises equivalent stress
r	Third deviatoric stress invariant
S	Stress deviator
T	Temperature
T	Time
$\vec{u}$	Displacement vector
V_s	Volume of solid minerals
V_w	Volume of water
W_{ice}	Volume fraction of ice over total solid
W_s	Volume fraction of solid minerals over total solid
w	Water content
w_u	Unfrozen water content

Ω	Gravimetric water content of soil or pavement material
β	Mohr-Coulomb model friction angle
β_e	Equivalence thermal expansion coefficient of soil
β_{ice}	Equivalent thermal expansion of ice
β_s	Equivalent thermal expansion of solids
Σ	Stefan-Boltzmann constant
σ_{ij}	Stress tensor
ε_{kl}	Strain tensor
θ	Angle of similarity
ξ	Hydraulic length
Ψ	Dilation angle in the p–t plane
Φ	Drucker-Prager model friction angle

1 Introduction

1.1 Background

The road network is an essential infrastructure that connects the communities for the essentials of life. However, in cold regions, the habitants are facing issues to maintain the lifespan of these infrastructures due to global warming. The energy balance at the ground surface is basically altered by meteorological factors such as rain, radiation from the sun, wind, and construction, which leads to temperature swings below the ground. The access road to the Umiujaq airport, Nunavik, Quebec has experienced subsidence of 0.85 m within period of 18 years (1991 to 2009) as is indicated in Fortier et al. (2011). The warming of frozen ground was observed close to the study site, which causes the underlying permafrost thawing and thaw consolidation, as shown in Figure 1.1. Similarly, the complicated freeze-thaw processes disrupt the embankments in cold region (Luo et al., 2019) and cause irregular settlements (Figure 1.2), and longitudinal cracks (Figure 1.3) along Shiwei-Labudalin Highway of S201 Line in Inner Mongolia Autonomous Region, China (Zhang et al., 2020). Alaska has been declared one of the Earth's fastest-warming regions (Reidmiller et al. 2018) and is warming more quickly than any other state. Lepage et al. (2016) presented the permafrost thawing induced road damages along the Alaska highway. Instead of draining to the side of the road, water from the thawing ground tends to pool in settlement regions and increases the risk of aquaplaning (Figure 1.4).

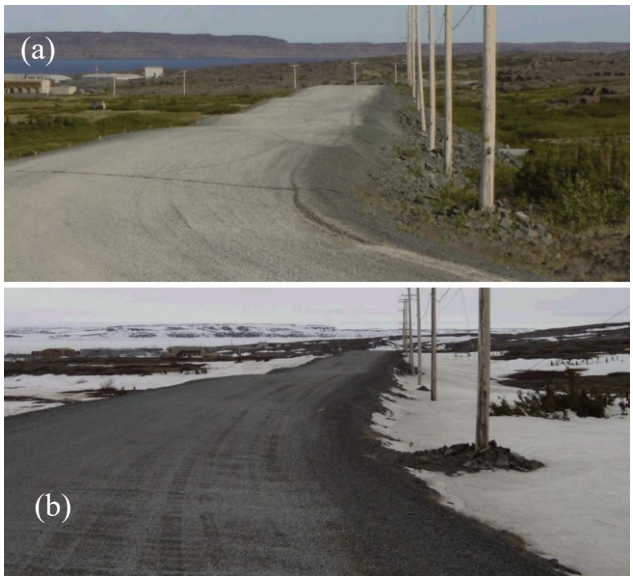

Figure 1.1 Images of the localized zones of thaw subsidence along the Umiujaq Airport access road in (a) summer and (b) winter (Fortier et al., 2011)

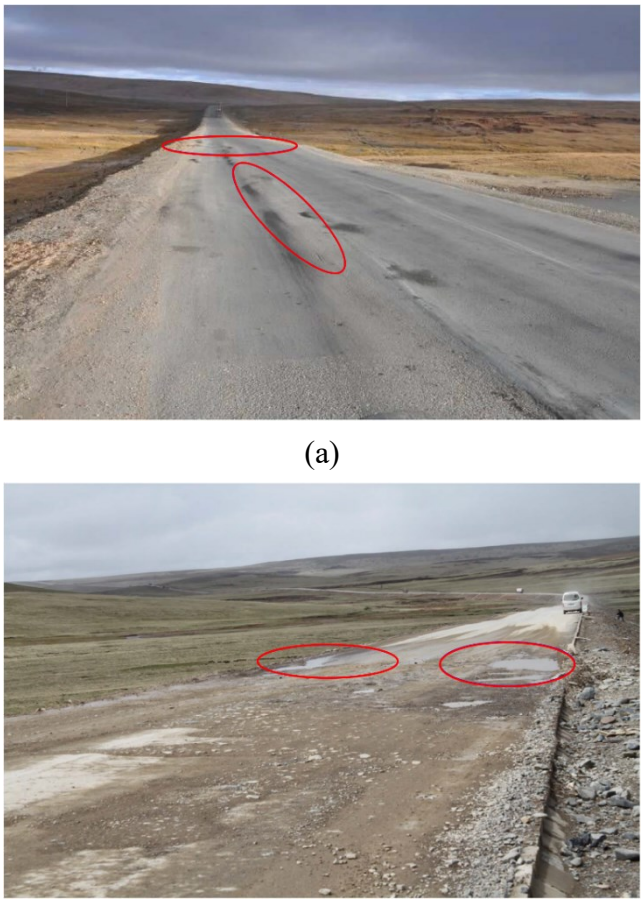

(a)

(b)

Figure 1.2 Frost heave (a) and thaw (b) settlement of embankment in cold regions (Luo et al., 2019).

Figure 1.3 Shi-La Highway longitudinal cracks induced by the freeze-thaw cycle (Zhang et al., 2020)

(a) (b)

Figure 1.4 (a) Differential settlement with water ponding and (b) Potholes (Lepage et al., 2016)

NASA's Global Climate Change Assessment has reported that in 2022, the Annual Average Anomaly was 0.89 °C (1.6 °F) (Global surface temperature, 2023). The graph (Figure 1.5) shows "the change in global surface temperature compared to the long-term average from 1951 to 1980. The year 2020 statistically tied with 2016 for the hottest year on record since recordkeeping began in 1880 (NASA/GISS)"(Global surface temperature, 2023).

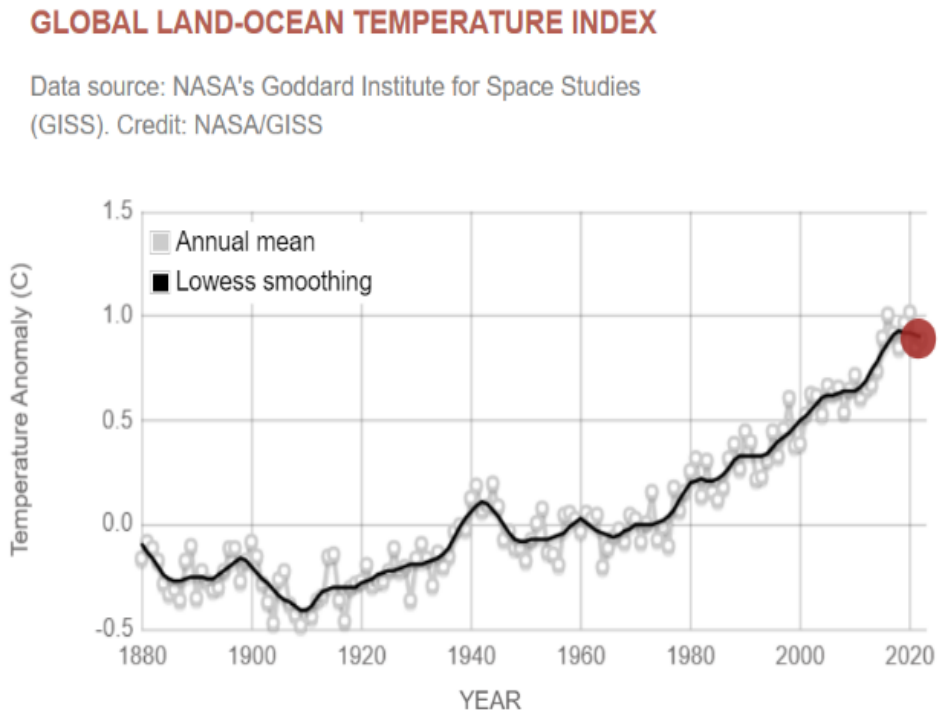

Figure 1.5 Global land-ocean temperature index (Global surface temperature, 2023).

According to the IPCC sixth assessment report by Forster et al. (2021), the global surface temperature increased by 0.99 °C between 1850-1900 and the initial two decades of the twenty-first century (2001-2020), and by 1.09 °C between 1850-1900 and 2011-2020. The most current climate change report released by the Canadian government notes that the country's temperature is rising at a rate twice as fast as the

world average, with winter seeing the highest levels of warming (Canada, 2018; Bush and Lemmen, 2019).

Cold regions are sensitive to temperature variations that could cause local infrastructure to perform poorly. In terms of social and economic advantages and retaining their integrity, development in these regions is essential. Many First Nations settlements can be found in Canada, which are also particularly wealthy in mineral, petroleum, and hydroelectric energy resources. To preserve connections with these populations and to extract natural resources, road, rail, and air communications are crucial for the development of these areas. Climate change and the deterioration of the soil's engineering properties over the course of these projects' anticipated lifespans must be considered in the design and upkeep of new infrastructure.

The study of how temperature affects infrastructure has gained more attention in the domains of science and engineering with the emergence of projects involving northern infrastructure and climate change. As ground temperatures rise, some frozen soil is thawing as a result of climatic and human-caused changes. This may cause non-recoverable shear deformations and differential settlements (Brown 1967). Researchers are looking into mitigation strategies, some of which entail permafrost preservation, to lessen the potential impact on infrastructures. As these issues are handled from various angles, this heightened interest could, in turn, aid in enhancing communication between geoscientists and geotechnical engineers. Even in non-permafrost regions, climate change may also have a negative impact on the embankments. Previous studies mainly

focus on the ground temperature variation or pore pressure changes at different depths due to climate change, as mentioned in Burgess et al. (2001) and Smith et al. (2005). However, there is very limited research focusing on the thermal-mechanical responses of embankments under freeze-thaw cycles. The nonlinear thermal-elastic deformation behavior of soils was not considered in previous studies because of not having enough data related to temperature dependent mechanical properties. Frozen soil is a mixture of solid minerals, ice, water, and air. At different frozen temperatures, the soil will display different thermal expansion potentials since the thermal expansion coefficient of ice is highly dependent on temperatures. A reliable characterization of the stress re-distributions in soil formations due to temperature disturbance relies on the accuracy of the applied thermal expansion coefficients. It is necessary to develop temperature-dependent thermal expansion coefficients for soils and apply them to the thermal mechanical responses of embankments. In addition, there is a lack of database showing the vulnerability of embankments in first nation communities under a changing climate.

1.2 Objectives of the Current Study

In consideration of the research significance of thermal-mechanical responses of embankments and limitation of previous studies, the following three major objectives will be achieved through this study:

1) To derive a relationship between temperature and equivalent thermal expansion coefficients of soils under freeze-thaw cycles.

2) To carry out the thermal-mechanical modeling of road embankments in two first nation communities of Saskatchewan, Canada under various future climate scenarios. Cases with and without traffic loads will be addressed.
3) To analyze the results and identify the potential risks in road embankments due to climate change.

1.3 Structure of thesis

This thesis is comprised of 6 chapters. The purpose of this work is to perform numerical modeling of embankments which are subjected to various climate conditions to analyze the thermal-mechanical responses of embankments. Chapter 1 introduces the background and brief content about thesis. Chapter 2 summarizes previous research on geotechnical analysis, including numerical modeling approach for settlements, ground temperature regime and stress analysis in embankments. Chapter 3 includes the constitutive model, governing equations and introduces the development of the temperature dependent equivalent thermal expansion coefficients of soils. Chapter 4 includes the methodology of carrying out finite element modeling of thermal-mechanical responses of embankments. Chapter 5 presents the responses of soil on the application of different climate data sets on the embankments in first nation communities. Chapter 6 concludes the summary, conclusions, and recommendations for further work on the embankments facing global warming.

1.4 Original Contributions

Previous researchers' work on embankments focuses only on analysis based on recorded or historical climate data and on continuous predicted future climate data, and the mechanical analysis includes only settlements and stress strategies. In this study, we work on thermal-mechanical analysis of road embankments in two first nation communities of Saskatchewan, Canada. This work considers the non-linear thermal expansion of soils to analyze the stress-strain conditions of ground. Four different sets of predicted climate data are applied to observe the reaction of embankments under a changing climate. This research includes the yielding analysis and plastic strain monitoring of key sections of the embankment based on finite element modeling.

2 Literature Review

2.1 Introduction

The analysis and seeking solutions for the infrastructure failures in cold regions due to various meteorological conditions are creating a great interest for researchers and engineers. The cause of stress and strain creation in seasonally frozen soil is basically from the temperature variation with time.

This chapter provides the geography of Canadian ground classification based on permafrost or frozen situations, location of interested sites of Saskatchewan, Global warming scenarios on cold region embankments, and also previous researchers work on the climatic impact on embankments by mentioning their theoretical and numerical analysis.

2.2 Frozen ground distributions in Canada

By geography, Canada is distributed in various types of permafrost. Permafrost is defined as ground (soil or rock) that has been continuously at 0°C or below for at least two years (Heginbottom et al., 1995). Figure 2.1 is showing the Canadian territory division in permafrost types (Heginbottom et al., 1995). Arctic and Polar regions are associated with continuous permafrost. With the exception of deep lakes and major rivers, continuous permafrost covers the entire surface area in this region. The Subarctic zone is connected to discontinuous permafrost. Most of the discontinuous permafrost

is substantially more recent, having formed only a few thousand years ago. There are no widely accepted thermal specifications for sporadic permafrost's southern limit. The existence of sporadic permafrost is frequently dependent on the availability of organic soils, which aids in the preservation of permafrost in milder climates. The distribution of isolated patchy permafrost, and no-permafrost terrain is common. This study locations, James Smith and Yellow Quill are in Saskatchewan province, as shown in Figure 2.1, which is in the central part of Canada. The studying sites are in non-permafrost zones, where the ground is subjected to seasonally freeze-thaw actions.

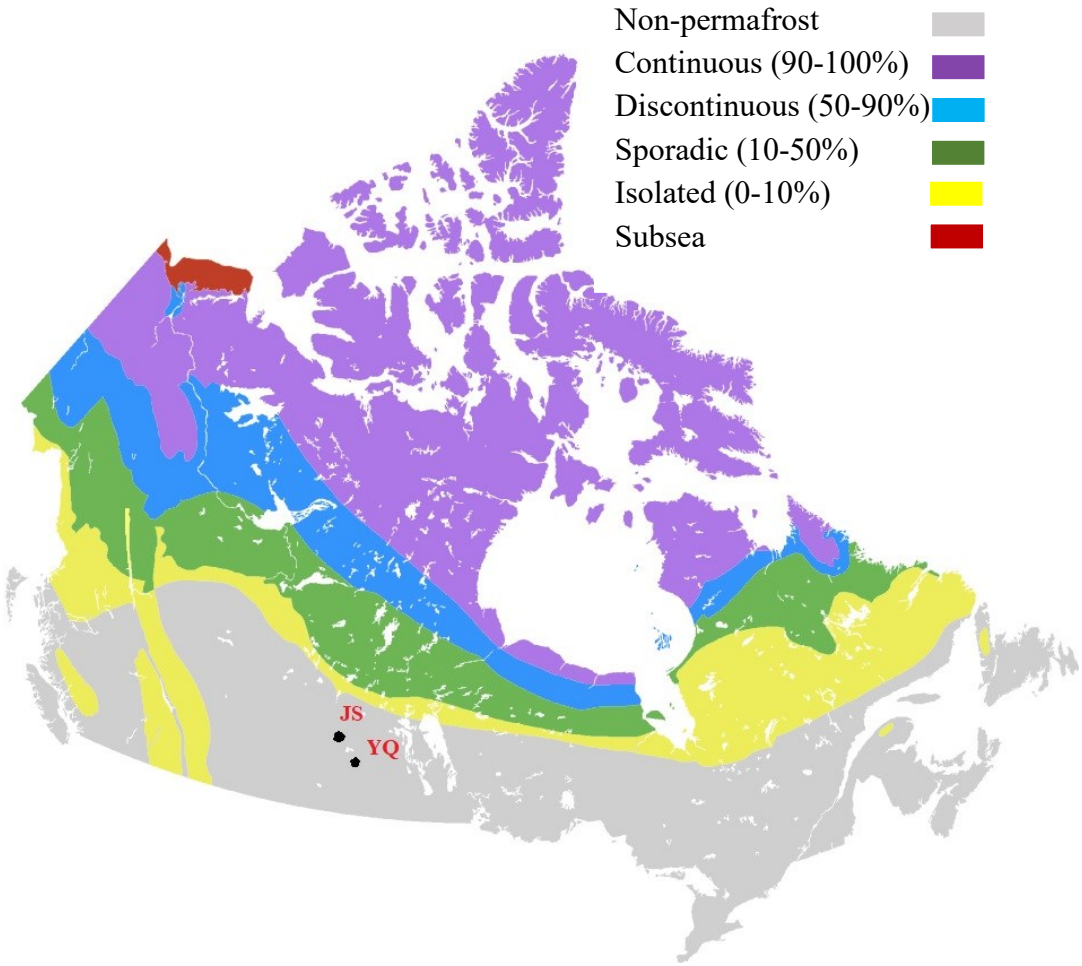

Figure 2.1 Locations of first nations of, James Smith and Yellow Quill, in Saskatchewan, Canada, modified after Heginbottom et al. (1995).

2.1 Numerical Modeling

Finite element method (FEM), boundary element method (BEM), finite difference method (FDM), and discrete element method (DEM), are some of the numerical techniques used for modelling the responses of infrastructures in cold regions. Most numerical modeling focuses on the thermal modeling part, and some thermal-mechanical coupled modeling work is significant in recent years.

2.1.1 Thermal Modeling

The locations of this study are in the non-permafrost (seasonally frozen) territory of Canada. Most previous studies are conducted in discontinuous permafrost regions or isolated patches ground locations. Very limited work has been done on non-permafrost or seasonally frozen soils, where the top layer of the ground freezes seasonally throughout the winter. The term “frost penetration depth” refers to the depth at which the ground freezes. According to Armstrong and Csathy (1963), frost penetration depth is influenced by several parameters, including as the soil’s thermal characteristics, the severity of the winter, the amount of vegetation, the state of the groundwater, and the relief of the surface (elevations/depressions). Frost actions develop due to the formation of ice in the soil pores during the freezing period followed by thaw weakening in the thawing season (Andersland and Ladanyi, 2004).

Alfaro et al. (2009b) conducted a study on Provincial Road (PR) 290 near Gillam in Northern Manitoba to examine the vulnerability of road infrastructure to further permafrost deterioration because of embankment construction and climate

change. To accurately simulate the conditions and trends in the subsurface thermal regime beneath the embankment, a geothermal model was created using field observations of ground temperatures over a three-year monitoring period. In the numerical modelling, TEMP/W, a commercially available software, was employed to investigate the future ground thermal regime. TEMP/W is a finite element software product for simulating heat transmission and phase change processes in porous media (*Geostudio*, *2010*). The results of the numerical modeling indicated that the permafrost can deteriorate due to the installation of road embankments, especially close to the toe. The permafrost beneath road embankments is degrading more quickly because of expected global warming.

The vulnerability of sub ground thermal condition can cause huge settlements by a change in climate. Similarly, a subsidence of 0.85 m was observed on the access road to the Umiujaq airport, Nunavik, Quebec within a period of 18 years (1991 to 2009) (Figure 2.2), which was in a discontinuous permafrost region (Fortier et al., 2011). After the air temperature reported along the east coast of Hudson Bay since 1992, the permafrost warming was noticed close to the study site. To predict the effects of the recent rise in air temperature in Nunavik, numerical modelling of the thermal regime of the road embankment and subgrade was carried out. Electronic and optical levels were used to assess the elevation of the road surface on July 12, 2008, July 24, 2008, and June 7, 2009. The as-built plans for the Umiujaq Airport's airfield and access road can be compared to these elevation data (MTQ 1991), as shown in Figure 2.2. To simulate

the effects of the recent rise in air temperature observed in Nunavik and the thermal insulation of the heavy snow cover collecting on the road shoulders and toes, numerical modelling of the thermal regime of road embankment and subgrade was carried out. The results show that the underlying permafrost thawing and thaw consolidation at the origin of the observed thaw subsidence are explained by the concurrent impacts of climatic warming and snow's thermal insulation on the road embankment and subgrade. The anticipated thaw subsidence rises linearly with time, and it is suggested that the road is still useful for traffic even after the thaw subsidence. A constructed structure can be vulnerable to permafrost degradation without a thorough evaluation of the permafrost conditions in advance of any project, especially if its design ignores the simultaneous effects of global warming and snow's thermal insulation on the thermal regime of an embankment and subgrade (Fortier et al., 2011).

Kurz (2014) performed thermal modelling at two locations: Provincial Road PR391, which is located roughly 18 km northwest of Thompson, and the 138 kV Radisson-Churchill transmission line built by Manitoba Hydro. For the simulation of 10 years, TEMP/W was used for the thermal modelling of PR391, which is in the region of discontinuous permafrost, under three different sets of surface boundary conditions: 'Kurz', 'Sine', and 'CCCma'. These boundary conditions stand in for the measured climatic data (Kurz), the simplification of those data using a sine function (Sine), and the forecast temperature data using the same sine function simplification (CCCma). The findings revealed an increase in temperature of about 0.4°C over a period of ten years

at 1.0 m below the embankment's toe and 0.3°C at 2.0 m below the embankment's mid-slope. The 138 kV Radisson-Churchill transmission line traverses' areas of both discontinuous and continuous permafrost. Kurz (2014) did the thermal modeling of this transmission tower foundations by TEMP/W for two different scenarios of foundation; shallow foundation (depth 0.0 m) and deep foundation (depth 3.7 m) by considering the climate data of 21 years (01 April 1987 and 31 March 2008) and also the insulating sheet, as shown in Figure 2.3, was modelled in two sizes: 2.5 m by 2.5 m and 4.0 m by 4.0 m. This led to insulation lengths in the axisymmetric models for both deep and shallow foundations of 1.25 m and 2.0 m. Results indicate that because of global warming and also several freeze thaw cycle within year, may influence the current water (influx or drainage), frost heave, and subsequent settlement, which may impact the superstructure's performance in shallow foundations. The model for deep foundations suggests that annual frost thawing may not necessarily have a negative impact on the performance of the superstructure because deep foundations are anchored on non-active layers. Longer insulation may aid in reducing rising ground temperatures at deep, according to results and trends in a warming climate (Kurz, 2014).

Gholamzadehabolfazl (2015) analyzed the thermal regime of the low road embankment PR391, about 18 km north-west of Thompson, and which is in the region of discontinuous permafrost (Figure 2.4), instead of using TEMP/W in Kurz (2014), Gholamzadehabolfazl (2015) used the finite element package ABAQUS/CAE due to its capability of considering thermal-mechanical behavior in a subsequent analysis.

Thermal modeling was performed for 12 years from 1 January 2002 until 31 October 2014 as there are some available data for validation for the studying period. The results revealed that the model accurately represented the temperature regime of the ground beneath the embankment. The predicted depth of zero annual temperature (0 °C) amplitude beneath the embankment is around 8 meters, which is consistent with the temperatures observed. Under the embankment, there is a frost bulb or zone of frozen earth. It varies periodically, but it continuously deteriorates over time and is most likely the primary cause of the embankment's continuous shifts. The frost bulb will fully vanish within 20 years, and possibly much sooner, based on anticipated future air temperatures or global warming.

For the simulation of thermal regime comparisons between natural ground and newly build structures on frozen grounds, Zheng et al. (2018) used a modified Finite Element Method which is called as Mixed Hybrid FEM (MHF) with the consideration of phase change of water and the latent heat influence. The research was on an embankment at the Harbin-Dalian railway, which is the first high-speed railway ever built in a region that experiences seasonal freezing temperatures. The numerical simulation demonstrates that the thermal regime of the natural ground experienced some turbulence as a result of the foundation work for the high-speed railway. The frozen depth in the first year following foundation construction is greater than that in the second year. The heat energy contained in the foundation is to be thoroughly assessed. Furthermore, the unequal frozen depth in the foundation and its shoulder may

result in uneven frost heave of the foundation. The high-speed railway's safety will be compromised as a result. Zheng et al. (2018) also observed that the foundation part had a greater frozen depth. This is due to the thermal qualities of the foundation fill materials, which is from the natural soil.

To predict the potential implications of climate change, Pk et al. (2018) did the numerical analysis on a typical highway embankment with two different construction fill materials (sand and silt) in southern Ontario, Canada. For this study, predicted future climatic data for 90 years was obtained from the Laboratory of Mathematical Parallel Systems (LAMPS) at York University in Toronto, Canada. Three general circulation models (GCMs), CCSM4, GFDL-ESM2M, and NorESM1-M, were chosen from a total of 33 GCMs for this study. The 90-year (2011-2100) time span and all four Representative Concentration Pathways (RCPs) were included in the future climate dataset. It was divided into three segments with each lasting 30 years. Pore water pressures (PWPs) were calculated using a commercial 2D finite element (FE) hydrological modelling program called HYDRUS-2D. The PWPs were then employed in the slope stability model SLOPE/W to calculate the stability of embankments under climate change. The findings show that both sand and silt embankments have been less stable as a result of climate change. For both embankments, an estimated 10% drop in FOS was seen, which may result in failure. The results for different temporal periods of precipitation show that the hydraulic qualities of fill materials influence the response to climate change. The high permeable sand embankment drains water fast without

affecting stability, making it less vulnerable to heavy precipitation events. Repeated precipitation events with lower resolutions, in contrast, produce stronger positive PWPs and lower FOS for the silt embankment. In its conclusion, the study highlights the significance of taking into account realistic resolution of precipitation data and precise assessment of hydraulic parameters in embankment design.

For the analysis of change in thermal regime (temporal and spatial distribution of ground temperature) of the ground due to global warming, Marrah (2021) basically used the field and thermal modeled data from Crawford and Legget (2002) work, which was on the Ottawa clay soil between May 1954 and April 1955 for the validation of his model. He analyzed the thermal regime of ground at three regions; Ottawa, Toronto, Sudbury, for the four time periods; 2020-2040, 2041-2060, 2061-2080 and 2081-2100, and the data for each city is considered under three predicted climate change scenarios with representative concentration pathways (RCP) values of RCP 2.5, RCP 4.5, and RCP 8.5 (Government of Canada, 2019). RCP8.5 is a high global emission scenario that predicts a 3.2 to 5.4°C global warming range by 2090 and a 4.9°C mean temperature increase by 2100. RCP4.5 is a medium global emission scenario that includes climate change mitigation strategies. This scenario predicts global average warming of 1.7 to 3.2°C by 2090, with a 1.9 °C increase in mean temperature by 2100. RCP2.6 is a low-emission global scenario that necessitates significant mitigation measures. This scenario predicts global average warming of 0.9 to 2.3°C by 2090, with a 4°C mean temperature increase by 2100. A model for the ground thermal regime was

created using Geo-Slope International Ltd TEMP/W software suite. The analysis shows that in the three chosen cities, the mean average ground temperature, and the depth of the frost both somewhat decline over the first 40 years, then significantly decline over the next 40 years. This non-linear impact suggests that some considerable changes could occur quickly, and that climate change will continuously alter the temperature profile of the ground for a long period. In the three typical sites, the results indicated a steady decrease in frost penetration depth because of climate change and by 2100, the normally frozen ground in Ottawa and Toronto will be completely gone.

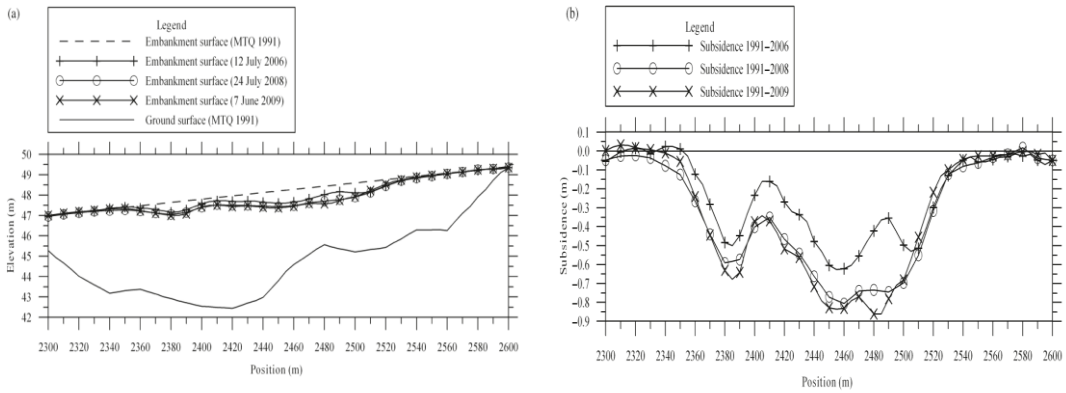

Figure 2.2 (a) Elevation (relative to the mean sea level) of the ground surface before the road completion and road surface in 1991, 12 July 2006, 24 July 2008, and 7 June 2009. (b) Thaw subsidence of the road surface from 1991 to 2006, 2008, and 2009 (Fortier et al., 2011).

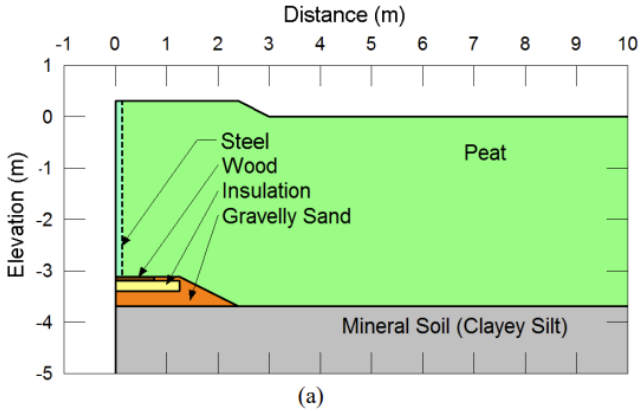

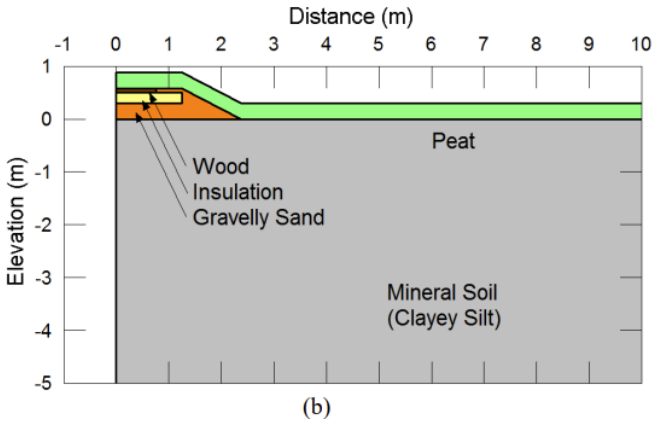

Figure 2.3 Model Cross Sections for transmission tower (a) deep foundation (showing steel) and (b) shallow foundation (no steel) (Kurz, 2014).

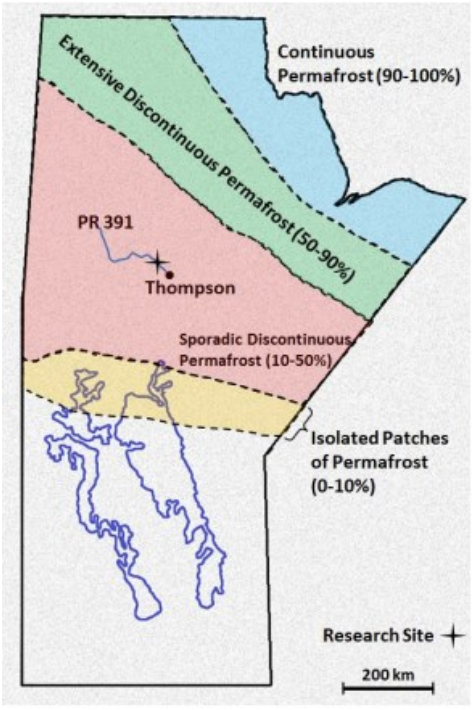

Figure 2.4 Permafrost types and location of the research site (Gholamzadehabolfazl, 2015).

2.1.2 Coupled Modeling

In earlier investigations, a relatively small work on coupled thermo-hydro-mechanical modelling of frozen soils utilizing the finite element approach was established. In coupled modeling, thermal and stress-deformation studies are resolved

in a coupled way in a single analysis. As a result, the model received simultaneous assignments of its thermal, mechanical, and hydraulic material properties.

To simulate the thaw consolidation of the permafrost beneath the embankment section in the Kaixinling hilly area on the Qinghai-Tibet plateau, Qi et al. (2012) created a sequentially coupled stress-deformation numerical model. Two steps made up their model: a thermal analysis and a consolidation analysis. Qi et al. (2012) employed Fast Lagrangian Analysis of Continua in 3 Dimensions (FLAC3D) as their numerical modelling framework. The findings of their study demonstrate that certain factors, such as effective consolidation time and characteristic drainage length, regulate how the thawed permafrost layer behaves. The degree of consolidation tends to grow throughout the initial operation years of the investigated highway embankment segment. Because the underlying permafrost continues to thaw, the characteristic drainage length grows and the effective consolidation time reduces, the freshly thawed layer cannot complete consolidation in the same year. Consolidation requires some residual consolidation time to complete. Even after the permafrost layer entirely thaws, the residual consolidation time may accrue to a high degree due to the accumulation of pore water pressure. As a result, consolidation will take a long time to complete, and hence settlement of the embankment will continue for a long period.

Gholamzadehabolfazl (2015) presents the effects of the thawing of frost bulb, shown in Figure 2.5, on the deformations of the road embankment using numerical modeling for climate data of 2012 to 2014. The functioning mechanisms of

deformations caused by the melting frost bulb beneath the road embankment were examined using a fully coupled (in which selected methods are called simultaneously) and a sequentially coupled (a type of coupling in which a class requires its methods to be called in a specific order) thermo-hydro-mechanical analysis. The road embankment's vertical as well as lateral displacements were accurately modelled by the model. Modified Drucker-Prager Cap (MDPC) was used as the constitutive model to reflect the elasto-plastic behavior of soils at the location. MDPC is designed to model cohesive geological materials with pressure-dependent yield, such as soils and rocks, and is based on the addition of a cap yield surface to the Drucker-Prager plasticity model (Extended Drucker-Prager models), which provides an inelastic hardening mechanism to account for plastic compaction and aids in the control of volume dilatancy when the material yields in shear. The findings show that the mechanical performance of the soil beneath the embankment and the resulting deformations of the embankment are both influenced by the slow degradation of the frost bulb beneath the embankment.

Rasmussen et al. (2018) established a Coup-Model, which is a process-based numerical package for modelling heat and mass movement in the soil-plant-atmosphere continuum (Jansson, 2012). Rasmussen et al. (2018) simulates the heat and mass transfer in soil, to understand the present and future thermal regimes of permafrost in Zackenberg Valley of Northeast Greenland. For modelling, the study uses on-site data and samples in frozen and thawed permafrost of an emerged delta and an alluvial fan

in the Zackenberg Valley to evaluate the sensitivity of active layer thermal properties in relation to sediment types and soil water contents. The results show that, at a site with a snow patch, the yearly mean ground temperatures were 1 °C higher than at a nearby site with a comparable sediment type but usual landscape scale snow depth. This is primarily due to snow insulation in the winter. Permafrost temperatures down to 18 m were found to be sensitive to surface temperature increases of +3° and +6 °C respectively, and after 19 years of increased surface temperature, roughly half of the additional forcing (1.5 °C and 3.5 °C, respectively) had reached a depth of 18 m. Due to the additional force, the active layer rose from 0.83 m to 1.5 m and 2 m, respectively. To continue with the thermo-hydro-mechanical simulations, Marrah (2021) used the GeoStudio software, a finite element package that includes several modelling programs of GeoStudio, including SEEP/W to model groundwater flow in saturated and unsaturated conditions in porous materials (*GEO-SLOPE International Ltd, 2012*), SIGMA/W for stress and deformation analysis of soil and structural materials (*GEO-SLOPE International Ltd, 2013*), and TEMP/W for modelling heat transfer and phase changes through fully or partially saturated and fully or partially thawed material (Veinović et al., 2020). These three programs were coupled to perform thermal-hydro-mechanical coupled analysis of three sites; Ottawa, Toronto, Sudbury, for the four time periods; 2020-2040, 2041-2060, 2061-2080 and 2081-2100. Government of Canada (2018) presents projection maps with a spatial resolution of around 10 km and temporal resolution accessible at seasonal and yearly scales to show climate change predictions.

For four-time frames, these interactive maps model climate change under the following three emission scenarios: RCP2.6 (low global emission scenario), RCP4.5 (medium global emission scenario), and RCP8.5 (high global emission scenario). Two climate change scenarios, RCP4.5 and RCP8.55 were taken into consideration for sensitivity analysis in the current work (*Government of Canada*, 2018). The results were showing that as the ground temperature will continuously increase in this non-permafrost regions from 2020 up to 2100, the rise will range between 1°C to 4°C. According to the coupled hydro-mechanical research, the soil settling in Canada's non-permafrost regions won't be considerably impacted by upcoming climatic changes.

To simulate coupled thermo-hydrologic (TH) processes in frozen soils of the upper reaches of Heihe River Basin (HRB) on the northeastern Qinghai-Tibet Plateau (QTP), Hu et al. (2022) created and used a computational fluid dynamic (CFD) based cryo-hydrogeological model (darcyTHFOAM). Thermo-hydrologic processes happening on the north- and south-facing slopes of a valley in the upper reaches of the Qinghai-Tibet Plateau (HRB) were then better understood using numerical models, as shown in Figure 2.6. The numerical simulations of two transects, one with a slope facing south and the other with a slope facing north, showed that the aspect of a slope significantly affects the soil temperature and moisture distribution in frozen soils. In comparison to a south-facing slope, a slope facing north is colder, wetter (liquid, ice, and total water storage), and thaws later. In contrast to the south-facing slope, the north-facing slope can stay frozen for longer and can hold more water, as shown in Figure

2.7. To advance a mechanistic and predictive understanding of the thermo-hydrologic processes under freeze thaw cycles in the Heihe River Basin, the influence of local topographic factors (slope aspect) on soil temperature, moisture, and total water storage was investigated at the hillslope scale with high spatio-temporal resolutions (1 mm, half-hour) (Hu et al., 2022).

Chen et al. (2023) investigated the influence of climate change on the Qinghai-Tibet Railway in the Beiluhe Basin, which is endangered by ground subsidence from excess ice melt. It is a typical continuous permafrost area in the central Tibetan Plateau. In their analysis, a Climate model (GFDL-ESM2G) was considered under Representative Concentration Pathway RCP 2.6 and RCP 8.5 emission scenarios. The simulations, which covered the period from 2020 to 2100, demonstrate that future ground warming will eventually cause infrastructure failure due to ground subsidence when the thaw depth hits the ice-rich ground, as shown in the Figure 2.8 (a-f). According to simulations using the RCP8.5 scenario, there is a possibility of serious destabilization commencing in the 2030s and complete failure because of the settlement of the embankment structure around the middle of the century if global warming continues unabated.

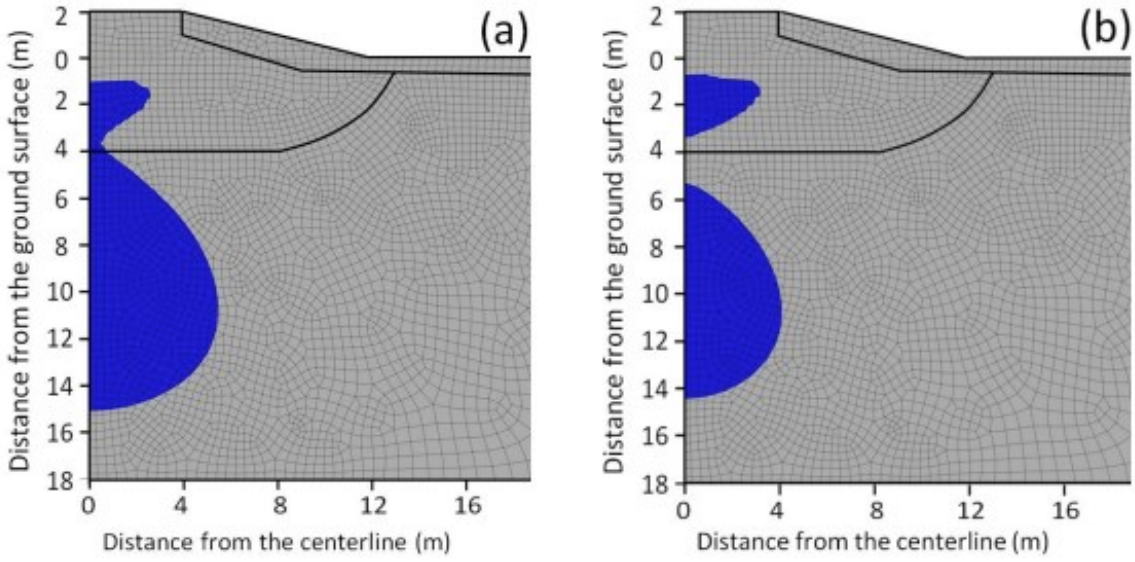

Figure 2.5 The location and size of the frost bulb under PR 391 road embankment from thermal modeling: (a) August 2013 and (b) August 2014 (Gholamzadehabolfazl, 2015).

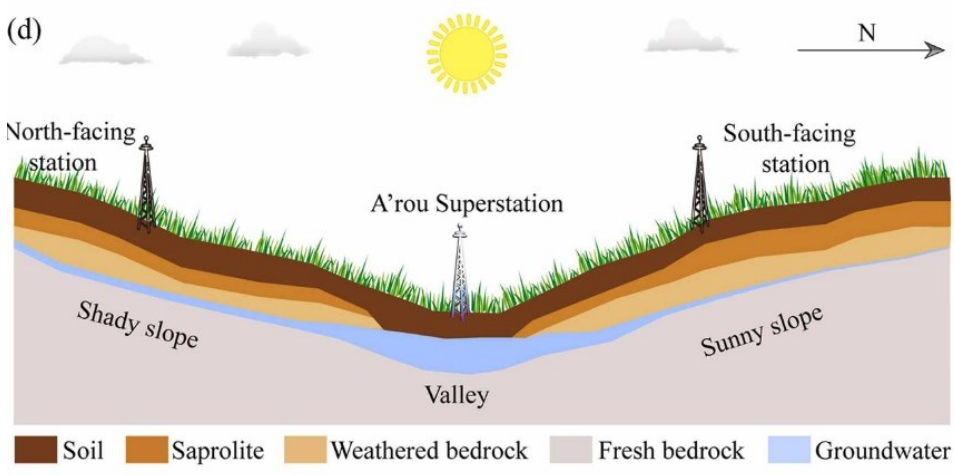

Figure 2.6 Stations for hydrometeorology along the 2D transect (Hu et al., 2022).

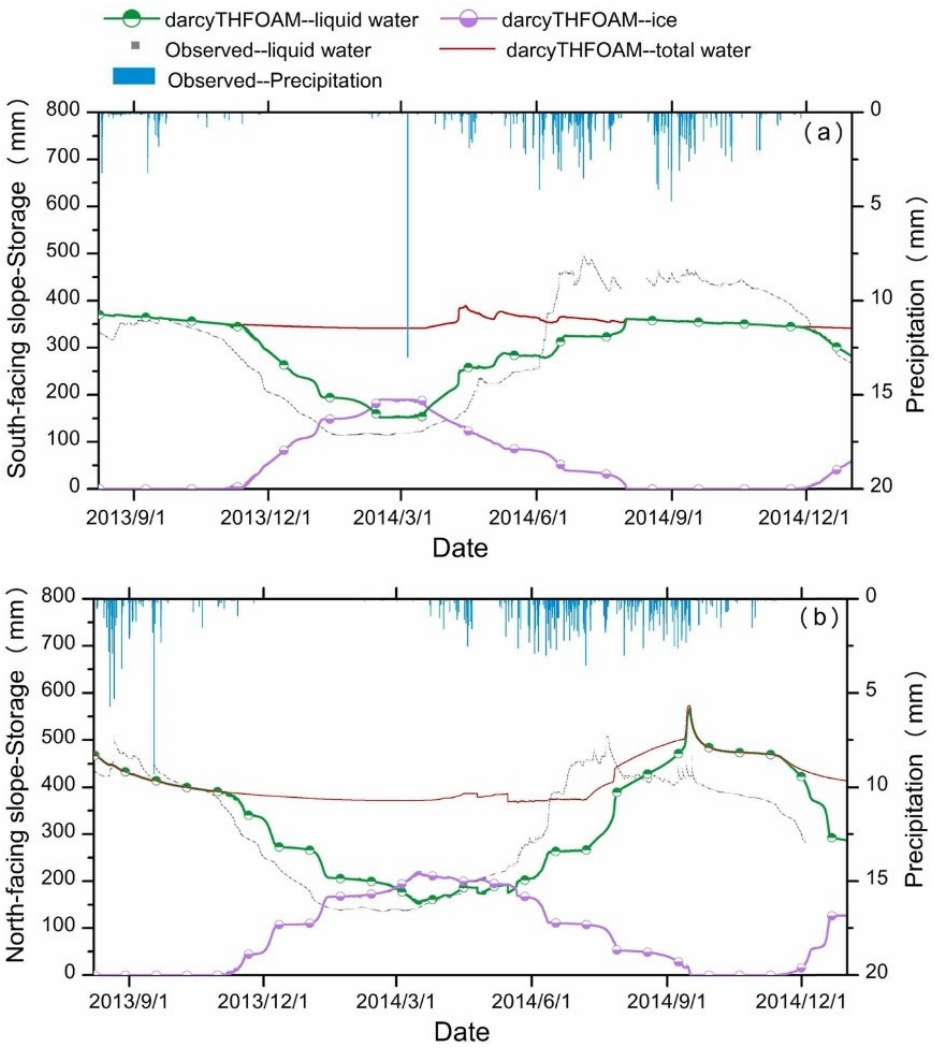

Figure 2.7 Storage of liquid water and precipitation (simulated and observed), ice (simulated), and total water (simulated) at 10-120 cm for (a) south-facing slope and (b) north-facing slope (Hu et al., 2022).

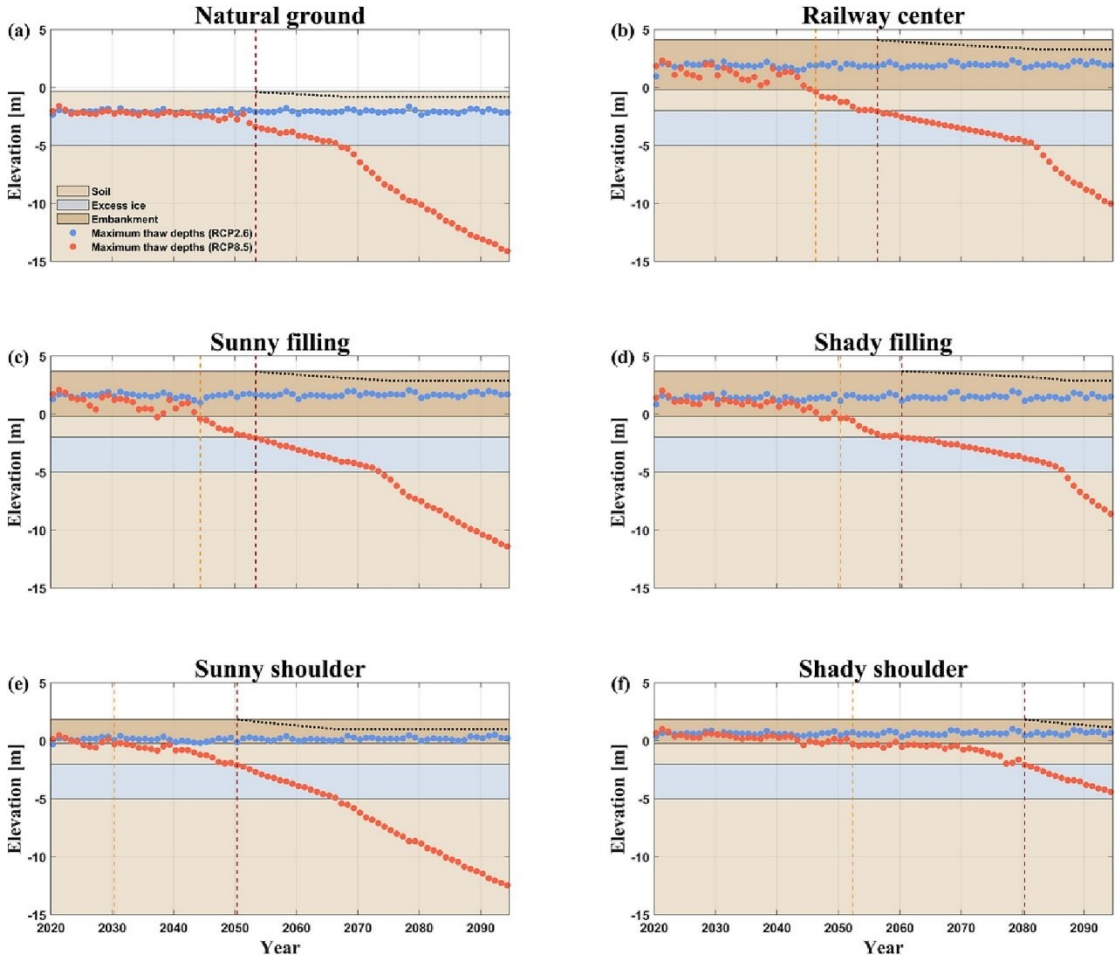

Figure 2.8 The status of a railway embankment through time as a result of climate change. The dashed vertical lines depict the embankment's stability loss under the RCP8.5 warming scenario (orange: the start of sub-grade persistent destabilization, dark red: the start of subsidence) (Chen et al., 2023).

2.2 Justification of the research

The vastness of Western Canada's non-permafrost (seasonally frozen) areas, as well as their importance as foundation soils for these regions' infrastructure, highlight the importance of carrying out research on thermal-mechanical responses of ground under a changing climate. This huge region of mostly non-permafrost country, including Manitoba, Saskatchewan, etc., which is home territory for first nation communities, have a dense network of highways. The economic development of these

areas depends heavily on the functionality of the transportation infrastructure. These non-permafrost locations are typically isolated areas and facing the climate warming, which has effects on ground thermal condition. In addition, it is very necessary to estimate the ground responses under a changing climate.

In this research, the embankment Geometry is obtained in relevance to the PR391 highway, about 18 km north-west of Thompson, Manitoba, which has a typical highway embankment geometry in Canada. In-depth field and laboratory investigations have been conducted by Batenipour et al. (2014a), who began the research in 2008, Kurz (2014), and Flynn et al. (2016a), to comprehend the behaviour of the road embankment and to determine the thermal and mechanical parameters of the soil at the PR 391 location. These researchers' field studies and laboratory experiments have produced data that have made it possible to conduct an extensive numerical modelling. Since soils from the Manitoba site studied by Batenipour et al. (2014a) are typical clay silt and silty clay soils, which are widespread across the princes of Saskatchewan and Manitoba. The physical properties are also used for the thermal- mechanical analysis of the embankment on the projected temperature of two first nation communities in Saskatchewan under climate change conditions.

The author's research aims to create a thorough pair thermal-mechanical model to examine the mechanical behaviour of the ground because of a shift in thermal regime brought on by climate change. For ground thermal regime and mechanical behaviours, a lot of researchers work on GeoStudio software, but because of the strong capabilities

in dealing with frost-heave ground problems, ABAQUS/CAE, a finite element method (FEM) software was chosen as the modelling platform. A Complete ABAQUS Environment, ABAQUS/CAE offers a straightforward, standardized interface for developing, publishing, tracking, and analyzing simulation results. Each module in ABAQUS/CAE defines a logical step in the modelling process, such as defining the geometry, specifying material characteristics, creating a mesh, and sending analysis jobs (Abaqus, 2014).

3 Governing equations and constitutive laws

3.1 Governing equations

A coupled thermal-mechanical (TM) finite element formulation is used in this study. The simulation of seasonally frozen soil considers the interactions between heat transfer and mechanical deformation. The mechanical governing equations can be written as:

$$\sigma_{ij,j} + b_i = 0 \tag{3.1}$$

$$\sigma_{ij} = C_{ijkl}\varepsilon_{kl} \tag{3.2}$$

$$\varepsilon_{kl} = \frac{1}{2}\left(\frac{\partial u_k}{\partial x_l} + \frac{\partial u_l}{\partial x_k}\right) \tag{3.3}$$

where $\boldsymbol{b_i}$ is the body force, σ_{ij} is the stress tensor, ε_{kl} is the strain tensor, C_{ijkl} is the fourth order elastic stiffness tensor, {ijkl} are tensor indices and $\vec{\boldsymbol{u}}$ is the displacement vector.

The plastic deformation behavior should also be considered in the present analysis. The Linear Drucker-Prager plasticity model is adopted here and will be illustrated in the subsequent section. The related equivalent plastic strain (PEEQ) is defined as:

$$\bar{\varepsilon}^{pl}|_0 + \int_0^t \dot{\varepsilon}^{pl}\, dt \tag{3.4}$$

where $\bar{\varepsilon}^{pl}|_0$ is the initial plastic strain at time zero and $\dot{\varepsilon}^{pl}$ is the equivalent plastic strain rate.

In addition, an energy balance equation should be applied to govern the heat transfer process considering the water-ice phase transfer.

3.2 Constitutive model

The constitutive model of seasonally frozen soils should be carefully chosen as a major input for the numerical analysis. In this work, we examine how climatic fluctuations and traffic loads affect the embankment of seasonally frozen soils. This embankment body's failure behavior should be able to be described by the applied failure criterion. It is also important to consider the soil's temperature-dependent mechanical parameters.

The elastic limit and the point at which a material begins to deform plastically in response to potential combined states of stresses are defined by the yield criteria. In the current research we used Linear Drucker-Prager model for the numerical modeling of embankment. This is an expanded version of the Drucker-Prager model, which is used to simulate frictional materials, such as soils and rocks.

Both ABAQUS/Standard and ABAQUS/Explicit support the linear Drucker-Prager Model, where a linear shear failure line is adopted as the failure criterion (Abaqus 2014). The two invariants for yield stress surface are the mean equivalent stress (P) and Mises equivalent stress (q):

$$P = -\frac{1}{3}trace(\sigma) \tag{3.5}$$

$$q = \sqrt{\frac{3}{2}(S:S)} \tag{3.6}$$

where, $trace$ is the summation of matrix diagonal entities, (:) is double dot product and the stress deviator S is defined with the usage of unit tensor I as:

$$S = \sigma + PI \tag{3.7}$$

The third deviatoric stress invariant is also included in the Drucker-Prager model:

$$r = (\frac{9}{2}S.S:S)^{\frac{1}{3}} \tag{3.8}$$

where (.) and (:) are tensor notations (dot and double dot operators). The yield criterion for the Linear Drager-Prager model is given as:

$$F = t - ptan\beta - d = 0 \tag{3.9}$$

where β and d are the friction angle and cohesion of material, respectively. t for our case can be explain as

$$t = \frac{1}{2}\, q[1 + \frac{1}{K} - (1 - \frac{1}{K})(\frac{r}{q})^{3}] \tag{3.10}$$

K is the ratio of the yield stress in triaxial tension to the yield stress in triaxial compression (Abaqus, 2014). As is displayed in Figure 3.1, the condition of K = 1, t =

q, indicating that the von Mises circle in the deviatoric primary stress plane is the yield surface (Abaqus, 2014).

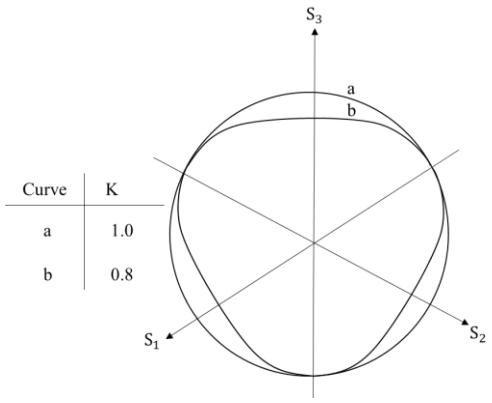

Figure 3.1 Yield/flow surfaces in the deviatoric plane

For the plastic flow in this model, the flow potential G can be written as:

$$G = t - ptan\psi \tag{3.11}$$

where ψ is the dilation angle in the p–t plane.

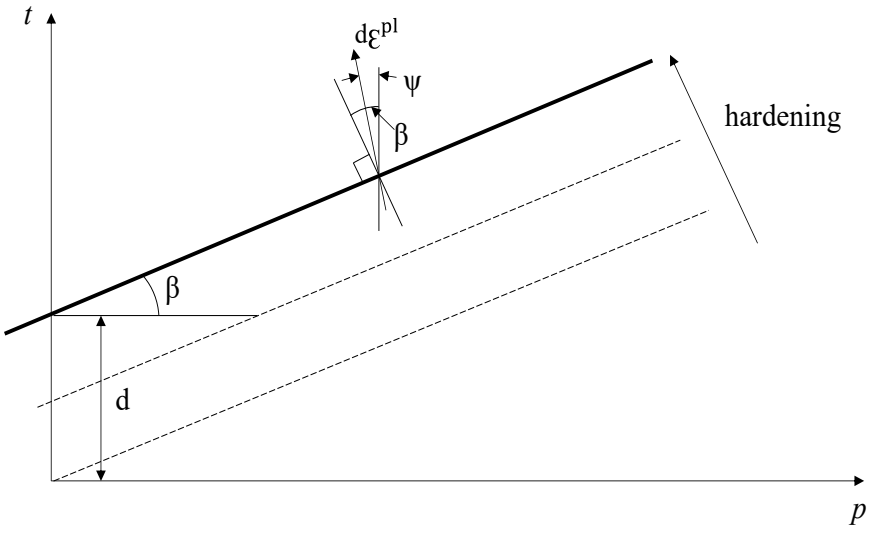

Figure 3.2 Linear Drucker-Prager model: yield surface and flow direction in the p–t plane.

3.3 Derivation of equivalent thermal expansion coefficients for soils

3.3.1 Theoretical development

Although thermal expansion is more noticeable in gases and liquids, it can significantly affect solids (Barron et al., 1980). Frozen soil is a mixture of solid minerals, ice, water, and air. In this study, we focus on the water-saturated soils as a preliminary investigation. Since the thermal expansion coefficient of ice is highly dependent on temperatures, the soil will display different thermal expansion potentials at varying temperatures. The derivation of the equivalent thermal expansion coefficients for soils will be based on the mixture theory by treated the bulk soil as a homogenized porous media (Li and Wong, 2017). The total solid is composed of ice and solid soil minerals. The derivation of equivalence thermal expansion coefficient of soil (β_e) primarily dependent on volume fraction of ice over total solid (W_{ice}), volume fraction of solid soil minerals over total solid (W_s), equivalent thermal expansion of ice (β_{ice}) and equivalent thermal expansion of solids (β_s). Mathematically the equivalent thermal expansion coefficient for a soil can be written as:

$$\beta_e = W_{ice}\,\beta_{ice} + W_s\,\beta_s \tag{3.12}$$

where,

$$W_{ice} = \frac{V_{ice}}{V_{solid}} \tag{3.13a}$$

$$W_s = \frac{V_s}{V_{solid}} \tag{3.13b}$$

The derivation of equations for (W_{ice}) and (W_s) depends on unfrozen water content (w_u) in soil. Unfrozen water content can be expressed as:

$$w_u = \frac{\rho_w V_w}{\rho_s V_s} \tag{3.14}$$

where (ρ_s) and (ρ_w) are the densities of solid minerals and water respectively, and V_s and V_w are the volumes of solid minerals and water, respectively. Accordingly, V_s can be expressed as:

$$V_s = \frac{\rho_w V_w}{\rho_s w_u} \tag{3.15}$$

The bulk volume of soil, V is given by summing up the volumes of each component:

$$V = V_{ice} + V_w + V_s \tag{3.16}$$

The porosity, n can be calculated by:

$$n = \frac{V_{ice} + V_w}{V} \tag{3.17}$$

Thus, the volume of ice, V_{ice} can be given as:

$$V_{ice} = n \cdot V - V_w \tag{3.18}$$

After some rearrangement, we can get:

$$\frac{V_w}{V} = \frac{(1-n)\rho_s w_u}{\rho_w} \tag{3.19}$$

By putting equation (3.19) in porosity (3.17) we get:

$$\frac{V_{ice}}{V} = n - \frac{(1-n)\rho_s w_u}{\rho_w} \tag{3.20}$$

$$\frac{V_s}{V} = 1 - n \tag{3.21}$$

Rearranging equation (3.20) and (3.21), and the ratio of $\frac{V_{ice}}{V_s}$ is given as:

$$\frac{V_{ice}}{V_s} = \frac{n - \frac{(1-n)\rho_s w_u}{\rho_w}}{1-n} \tag{3.22}$$

$$V_{solid} = V_{ice} + V_s \tag{3.23}$$

After substituting (3.22) and (3.23) in (3.13b), we can get (W_s) and (W_{ice}),

$$W_s = \frac{V_s}{V_{ice} + V_s} = \frac{1}{\frac{V_{ice}}{V_s} + 1} = \frac{1-n}{1 - \frac{(1-n)\rho_s w_u}{\rho_w}} \tag{3.24}$$

$$W_{ice} = 1 - W_s \tag{3.25}$$

The given derived formula for volume fraction (W_s) of soil minerals over total solid, contains the overall density of solid minerals (ρ_s). The density of solid minerals (ρ_s) can be calculated based on data of soil dry density and porosity using:

$$\rho_s = \frac{\rho_d}{1-n} \tag{3.26}$$

3.3.2 Application to the studying sites

In the above-mentioned method of calculating the equivalent thermal expansion coefficient of frozen soils, the unfrozen water content (w_u) is an essential input. The unfrozen water content is defined as weight of water divided by weight of dry soil (Anderson et al., 1973). The liquid water (unfrozen water content) in soils decreases as a result of the liquid water's phase change into ice during the freezing process. According to Williams (1964), unfrozen water is still present in soils at temperatures below the soil freezing point, even as low as -70 °C. Unfrozen water content greatly affects the thermal-mechanical characteristics of soil and, as a result, leads to a variety of engineering issues, such as pavement cracking and damage to structures and substructure. During the freezing and thawing process, the amount of unfrozen water has an influence on the thermal (Zhang et al., 2018; Shen et al., 2018) and mechanical (Li et al., 2018; Xu et al; 2019) properties of soils. Also, according to Li et al., (2015), an essential indicator of the stability of engineering in cold climates is the amount of unfrozen water present, which has a significant impact on active layer heat and mass transfer processes.

The Anderson et al. (1973) equation can be used to express the unfrozen water content as a function of frozen temperature:

$$w_u = A(-T)^B \tag{3.27}$$

where A and B are constants, and which are related to the specific surface values of soils.

The adoption of constants, A and B, depends on the type of soil in Nixon (1991). For the studying silty clay and clayey silt in the present study sites, the unfrozen water contents are presented in Figure 3.3. The selecting of parameters A and B are based on values of liquid limit and specific surface area with relevant to some published data from the literature (Dasog et al., 1987; Nixon, 1991; Yukselen-Aksoy and Kaya, 2010).

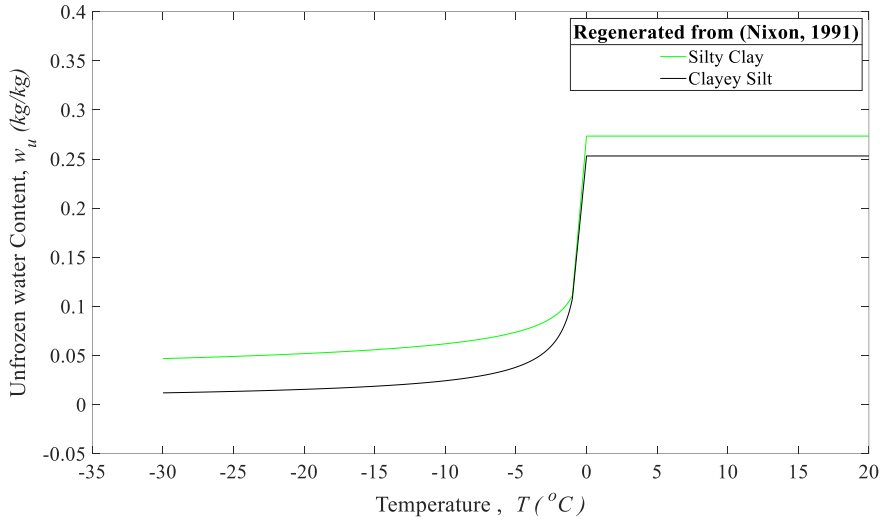

Figure 3.3 Unfrozen water content of silty clay and clayey soil.

In the case of warm conditions, when all water content is unfrozen in soils, then the water content is calculated by using Eq 3.28, as shown in Table 3.1.

$$w_u = \frac{n\rho_w}{\rho_d} \tag{3.28}$$

Table 3.1 Unfrozen water content in warm condition (Positive temperature).

Soil type	$\boldsymbol{\rho_d}(^{\boldsymbol{kg}}/_{\boldsymbol{m^3}})$	$\boldsymbol{w}$	$\boldsymbol{n}$
Silty clay	1500	0.273333	0.41
Clayey silt	1620	0.253086	0.41

As the derived equation (3.12) presents that the equivalence thermal expansion depends on the volume fraction of ice over total solid (W_{ice}), volume fraction of solid minerals over total solid (W_s), equivalent thermal expansion of ice (β_{ice}) and equivalent thermal expansion of solids (β_s).

According to Li and Wong (2017), the thermal expansion coefficient (β_s) of solid mineral in soils can be given as $11.3 * 10^{-6}$. Based on the empirical equation by Butkovich (1959), the thermal expansion coefficient of ice is nonlinearly related to temperature by:

$$\beta_{ice}.10^6 = 52.5186 - 0.18525T + 0.008854T^2 - 0.00023712T^3 \qquad (3.29)$$

where the temperature T is given in °C.

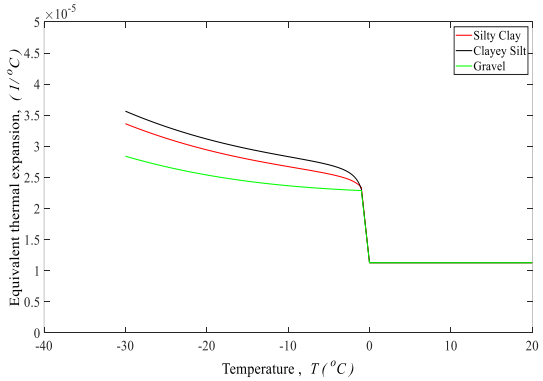

Figure 3.4 Estimated temperature dependent equivalence thermal expansion of soils in the studying sites.

Using Equation 3.12, the equivalence thermal expansion coefficients of soils are derived plotted against temperature, as shown in Figure 3.4. Related values of gravel are also given as they are needed for the thermal-mechanical modeling of embankments. The results will be included in the subsequent numerical modeling tasks. Previously the

thermal expansion coefficient of frozen soil was usually treated to be equal to ice or solid soil minerals. By using the proposed new model, the equivalent thermal expansion coefficient will be provided with more reliability since the weight of different components have been well considered.

4 Finite element modeling of thermal-mechanical responses of embankments

4.1 Introduction

This study is generally analyzing the effect of global warming on the ground of two First Nation communities, Yellow Quill and James Smith, Saskatchewan, which are in the non-permafrost region. Finite element numerical analysis will be conducted to evaluate how temperature variations may influence the thermal-mechanical (TM) responses in road embankments. The derived temperature-dependent thermal expansion coefficients presented in Chapter 3 will be used in the modeling with an aim to improve the accuracy of characterizing thermal-mechanical behaviors. Other thermal-mechanical properties along with boundary conditions for the numerical modeling tasks will be reported in this chapter.

4.2 Climate data consideration for numerical modeling

The interactions between soil and climate have a significant impact on the geotechnical characteristics of the ground, such as its strength, texture, and compressibility. Climate is one of the primary regulating variables of ground behavior.

The projected climate data used in this study is from National Aeronautics and Space Administration (NASA) (Yip, 2021). So, according to Thrasher et al. (2022), to simulate the historical and future climate data (1975-2100), the most recent version of

the NASA Earth Exchange Global Daily Downscaled Projections (NEX-GDDP-CMIP6), which is Phase 6 of the Climate Model Intercomparison Project (CMIP6), is utilized. This recent version of the NEX-GDDP archive (NEX-GDDP-CMIP6) is not only modified prediction based on the newer CMIP6 output, but this also include a broader range of variables, e.g., Surface downwelling longwave radiation ($^{W}/_{m^2}$), Surface downwelling shortwave radiation ($^{W}/_{m^2}$), near-surface air temperature, etc. The monthly bias correction/spatial disaggregation (BCSD) methodology described in Wood et al. (2004), is a daily variant of the statistical downscaling algorithm used to generate the NEX-GDDP datasets. This variant method uses information derived from a comparison of the original GCM (Global climate model) output with corresponding climate observations over a common reference duration to modify future climate projections, to make them more in line with historical climate records and, presumably, more realistic for the spatial domain of interest. The daily BCSD technique is predicated on the assumption that the relative spatial patterns identified during the reference period will stay consistent under future climatic change. Climate Model Intercomparison Project Phase 6 (CMIP6) simulations are employed under Shared Socioeconomic Pathways (SSPs) of 1-1.9, 1-2.6, 2-4.5, 3-7.0, and 5-8.5. SSP1-1.9 (Very ambitious scenario to meet the 1.5°C goal of the Paris Agreement) is the most optimistic scenario, in which global CO_2 emissions are nil by 2050. In SSP1-2.6 (Sustainable development scenario), global CO_2 emissions are significantly reduced but slowly with the objective of zero emissions reached after 2050. In SSP2-4.5 (Middle of the road scenario), CO_2

emissions stay around current levels before beginning to decline by mid-century and temperatures rise by 2.7°C by the end of the century. In SSP3-7.0 (Regional rivalry scenario), greenhouse gas emissions and temperatures continue to climb, with CO_2 emissions nearly doubling from current levels and average temperatures rising by 3.6°C by the end of the century. The SSP5-8.5 (Fossil fuel-driven development scenario) is the worst-case scenario, in which current CO_2 emissions nearly double by 2050 and the average global temperature rises by 4.4°C by 2100 (Pörtner et al., 2022)

In this study, both Yellow Quill and James Smith sites have different projected climate data but have the same number of time episodes. Projected Climate data contains the near surface mean daily temperature (at 2 meters) for these two communities. For each community, one Historical (1975-2000) and three Future time episodes (Future 1: 2023-2048; Future 2: 2049-2074; Future 3: 2075-2100) were used. Each future episode under two potential radiative forcing, i.e., Low Radiative Forcing (LRF), which correspond to SSP 2–4.5, in which global warming of 4.5 W/m2 forces will occur at end of century and High Radiative Forcing (HRF), which correspond to SSP 5–8.5 follows 8.5 W/m2 forcing. This makes 7 episodes for each community. For each episode, 5 representative years are provided, which makes 35 years for each community and when we take both communities into account then we have 70-year worth of daily simulation, as shown in a general outline for each community in Figure 4.1.

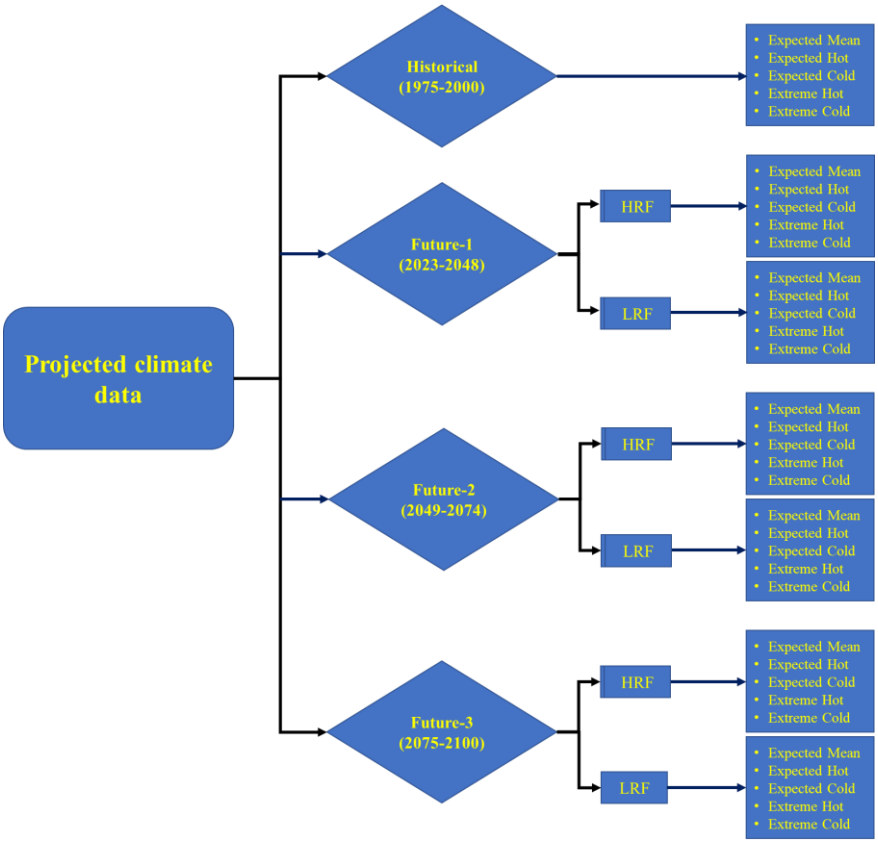

Figure 4.1 Simplification of projected climate data.

For each of these four-time episodes e.g., Historical (1975-2000), NEX-GDDP-CMIP6 had 35 climate models, out of which 14 have been used in this study. The details of these 14 models, from Lim Kam Sian et al. (2021), are shown in Table 4.1. Each model will yield simulated data covering 25 years. Each model's hot and cold years are easily distinguished by comparing the annual average temperature. For a specific model, the year with the greatest annual average temperature is considered the hot year and the year with the lowest annual average temperature is considered the cold year. The expected year is simply calculated by averaging the daily temperature simulation over the span of 25 years. After calculating the cold, hot, and expected years for each model, the extreme cold year, expected cold year, expected mean year, expected hot year, and

extreme hot year are possible to calculate for each period/time episode. Among all 14 models, the coolest year is designated as an extreme cold year, the average of cold years is taken as an expected cold year, the average of all expected years is taken as an expected mean, the average of hot years is taken as an expected hot year, and the hottest year is taken as an extreme hot year. This projected climate data is used in our study for numerical modelling of the embankments. The five representative years of climate data for James Smith and Yellow Quill location are shown in Figure 4.2 and 4.3.

Table 4.1 List of 14 CMIP6 GCMs, as well as their reporting agencies, countries, and grid increment horizontal resolutions (Lim Kam Sian et al., 2021).

Model Number	Model Name	Modeling Center/Nation	Horizontal Resolutions (Lat. × Lon.)
1	BCC-CSM2-MR	Beijing Climate Center China / Meteorological Administration China	1.125°×1.125°
2	CanESM5	Canadian Centre for Climate Modelling and Analysis/Canada	2.8°×2.8°
3	CNRM–CM6–1	Centre National de Recherches Météorologiques–Centre Européen de Recherche et de Formation Avancée en Calcul Scientifique/France	1.4° × 1.4°
4	GFDL–CM4-gr1	NOAA Geophysical Fluid Dynamics Laboratory/USA	1°× 1.25°
5	GFDL–CM4-gr2	NOAA Geophysical Fluid Dynamics Laboratory/USA	1°× 1.25°
6	GFDL–ESM4-gr1	NOAA Geophysical Fluid Dynamics Laboratory/USA	1°× 1.25°
7	INM–CM4–8	Institute for Numerical Mathematics, Russian Academy of Science/Russia	1.5°× 2°
8	IPSL–CM6A–LR	L'Institut Pierre–Simon Laplace/France	1.26° × 2.5°
9	MIROC6	Japan Agency for Marine–Earth Science and Technology, Atmosphere and Ocean Research Institute, The University of Tokyo	1.4° × 1.4°
10	MIROC–ES2L	National Institute for Environmental Studies, and RIKEN Center for Computational Science/Japan	2.8° × 2.8°
11	MPI–ESM–1–2–HR	Max Planck Institute for Meteorology/Germany	0.9375° × 0.9375°

`12	MPI–ESM–1–2–LR	Max Planck Institute for Meteorology/Germany	1.875° × 1.875°
13	MRI–ESM2–0	Meteorological Research Institute /Japan	1.125° × 1.125°
14	NorESM2–MM	Norwegian Climate Centre/Norway	0.9375° × 1.25°

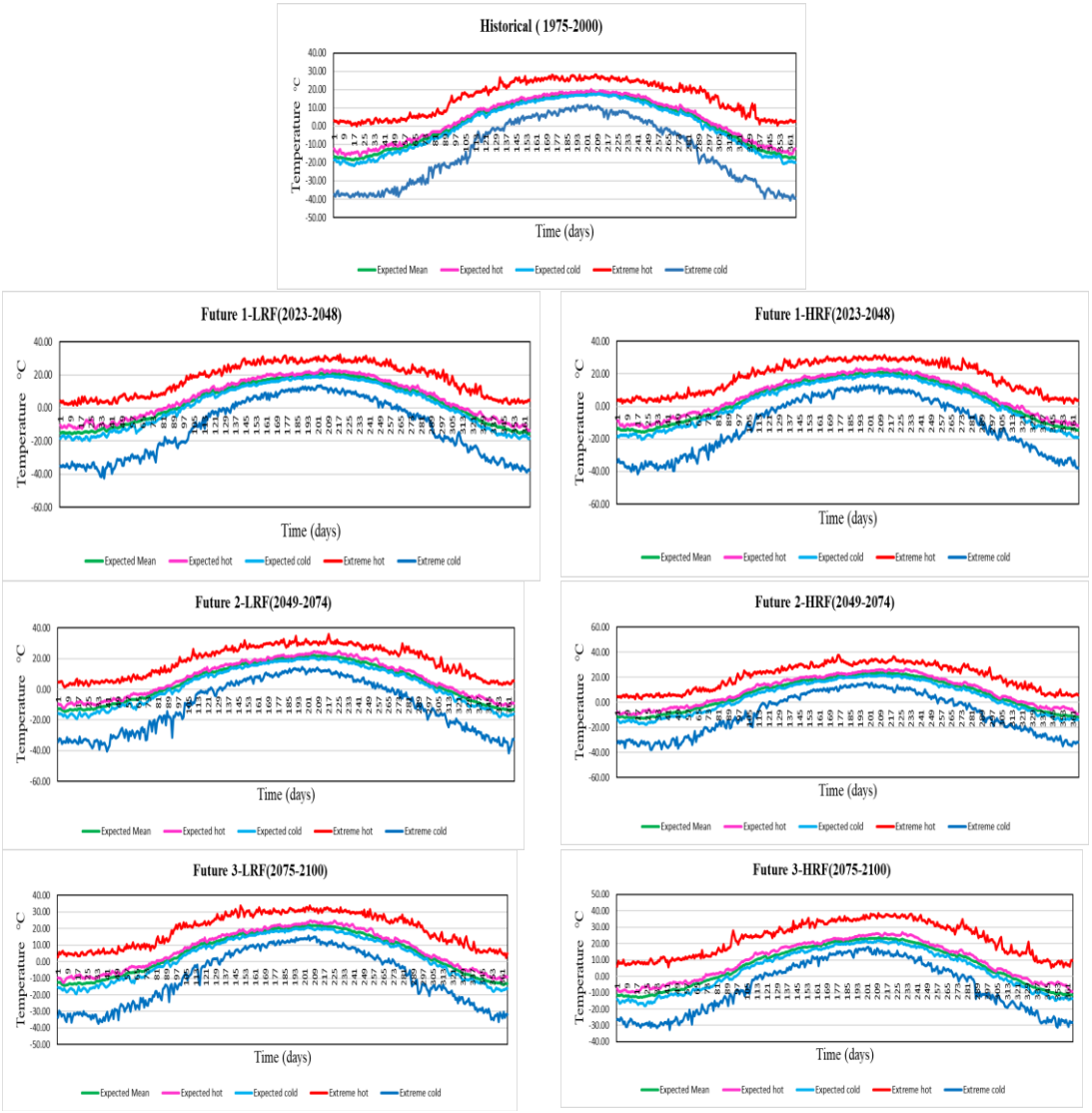

Figure 4.2 Climate scenarios for James Smith location.

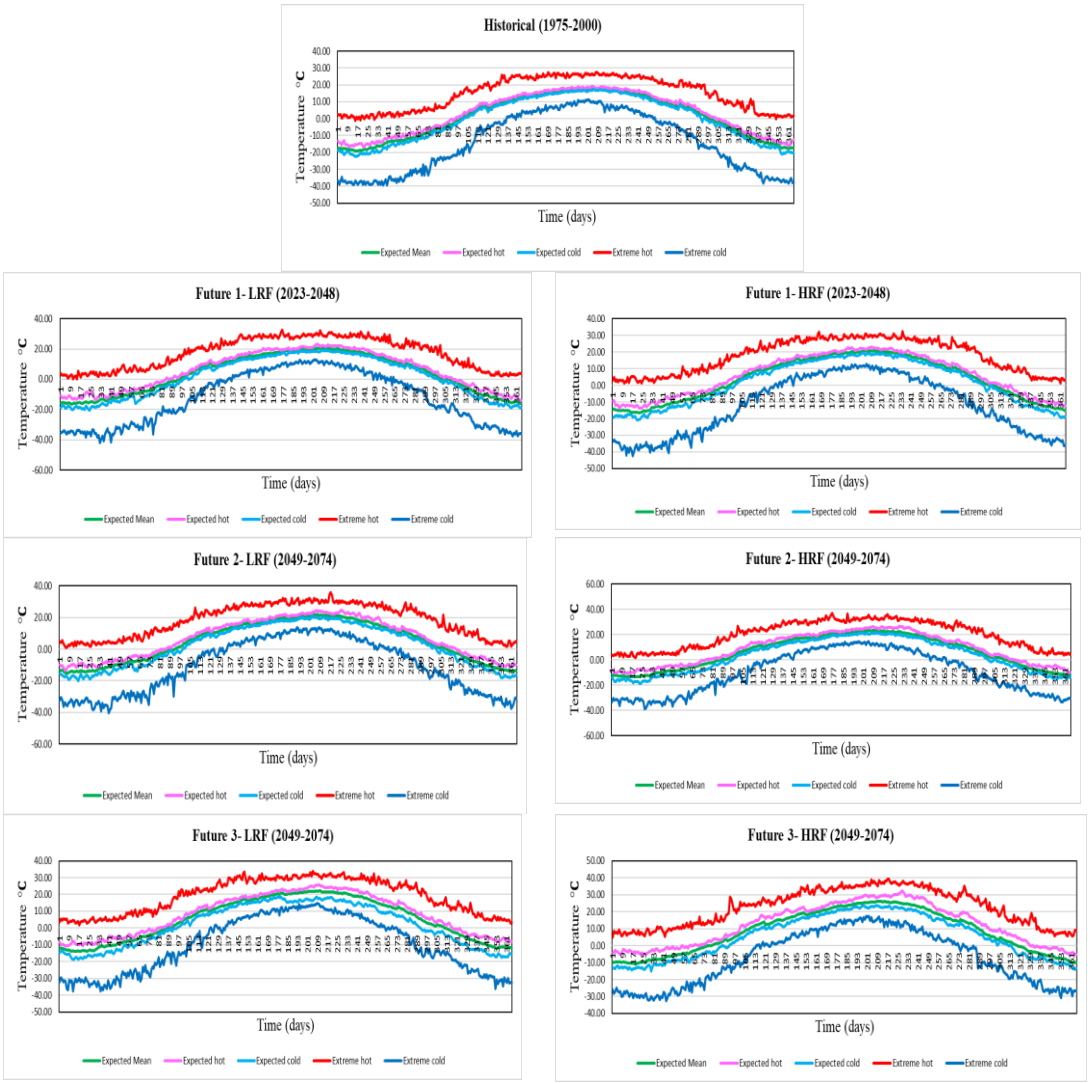

Figure 4.3 Climate scenarios for Yellow Quill location.

4.3 Soil profile

In this study, the profile of embankment is according to a project in Thompson, Manitoba. Half cross section of embankment is taken because of symmetry, which starts from center of pavement and end after 40 meters on right side (Batenipour et al., 2014b; Kurz et al., 2015; Flynn et al., 2016a). Three separate soil layers make up the embankment. Most of the soil used for embankment filling is gravel, with a thin layer of clayey silt on the slope that extends to the ground's surface. Underneath these two

soil layers is silty clay soil, as shown Figure 4.4. The depth of embankment is 18 meters below the ground level.

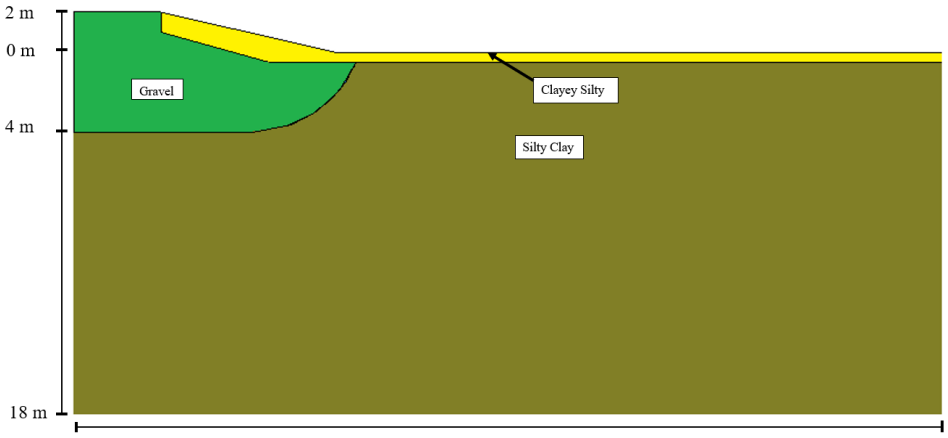

Figure 4.4 Embankment profile.

4.4 Geotechnical properties

Numerical modeling requires the inputs of many soil parameters under frozen and unfrozen conditions. In this study we consider the soil to be water saturated and adapt effective stress principle to describe its behavior for saving computational time. The parameters needed for simulations include equivalent thermal expansion coefficient of soils, thermal conductivity, heat capacity, latent heat, cohesion strength, friction angle, and elastic deformation properties. Data of equivalent thermal expansion coefficient of soils were obtained using the approach presented in Chapter 3. Some temperature dependent thermal and mechanical properties are from the literature. Major data source is from Alfaro et al. (2009a), Batenipour et al. (2009b, 2009a, 2010), Batenipour (2012), and Gholamzadehabolfazl (2015) .

The 'solidus' and 'liquidus' temperatures in ABAQUS/CAE serve as the corresponding descriptors for the ice and water phases. The temperature below which soil freezes with the least amount of unfrozen water is known as the solidus temperature. Similar to the freezing point, the liquidus temperature is the temperature at which a soil is unfrozen, with a volumetric water content equal to the soil's porosity at full saturation. According to Flynn et al. (2016a), the solidus and liquidus temperatures of the clay materials were assumed to be, respectively, -4°C and 0°C for the silty clay, -3°C and 0°C for the clayey silt, -0.75°C and 0°C for gravel, respectively in this study. These temperatures were chosen based on observations in the field and values reported in the literature (Batenipour, 2012; Gholamzadehabolfazl, 2015; Kurz et al., 2015; Flynn et al., 2016a).

4.4.1 Thermal conductivity

In Kurz et al. (2015), thermal conductivities of clayey silt, gravel and silty clay materials were measured for frozen and unfrozen conditions. The frozen and unfrozen values for thermal conductivity of silty clay are 173000 ($^{J}/_{day.\,m.\,°C}$) and 117000 ($^{J}/_{day.\,m.\,°C}$), for clayey silt are 207000 ($^{J}/_{day.\,m.\,°C}$) and 123000 ($^{J}/_{day.\,m.\,°C}$), and for gravel are 355000 ($^{J}/_{day.\,m.\,°C}$) and 230000 ($^{J}/_{day.\,m.\,°C}$), respectively.

4.4.2 Heat Capacity

Gholamzadehabolfazl (2015) calculated the heat capacity of soils in frozen and unfrozen states. The frozen and unfrozen heat capacity of silty clay are 1020 ($^{J}/_{kg.\,°C}$)

and 1450 ($^{J}/_{kg.\,°C}$), for clayey silt are 1000 ($^{J}/_{kg.\,°C}$) and 1380 ($^{J}/_{kg.\,°C}$), and for gravel are 890 ($^{J}/_{kg.\,°C}$) and 800 ($^{J}/_{kg.\,°C}$), respectively.

4.4.3 Latent heat

Latent heat is a representation of the energy gained or lost when the pore fluid water in soil transitions from ice to liquid water. Gholamzadehabolfazl (2015) calculated the latent heat values for silty clay, clayey silt, and gravel, which are 57850 ($^{J}/_{kg}$), 51180 ($^{J}/_{kg}$), and 40660 ($^{J}/_{kg}$), respectively, as shown in Table 4.1.

Table 4.2 Thermal properties of soils.

Soil type	**Thermal conductivity** ($^{J}/_{day.\,m.\,°C}$)		**Specific Heat Capacity** ($^{J}/_{kg.\,°C}$)		**Latent Heat** ($^{J}/_{kg}$)	**Liquidus Temperature (°C)**	**Solidus Temperature (°C)**	**ρ** ($^{kg}/_{m^3}$)
	Unfrozen	**Frozen**	**Unfrozen**	**Frozen**				
Gravel	230000	355000	800	890	40660	0	-0.75	1900
Silty Clay	117000	173000	1450	1020	57850	0	-4	1500
Clayey silt	123000	207000	1380	1000	51180	0	-3	1620

4.5 Mechanical parameters

The mechanical characteristics of soil are surprisingly complex. While designing structures, soil engineers may now take a wide range of mechanical qualities into account because of advancements in both theoretical and empirical soil mechanic's research. For all the materials, the Poisson's ratio and modulus of elasticity are used in the model to describe the elastic deformations. For this study, the modulus of elasticity (E) and Poisson's ratio (v) for gravel and silty clay are obtained from the work of Ming

et al. (2018), which is basically dependent on temperature, as shown in Figure 4.5. The reason of applying mechanical properties from Ming et al. (2018) is due to the similarity in soil basic physical characteristics (e.g., soil type, bulk density)

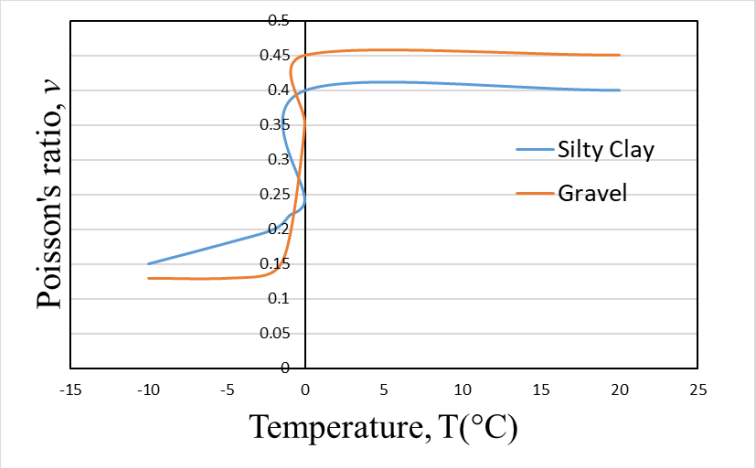

(a)

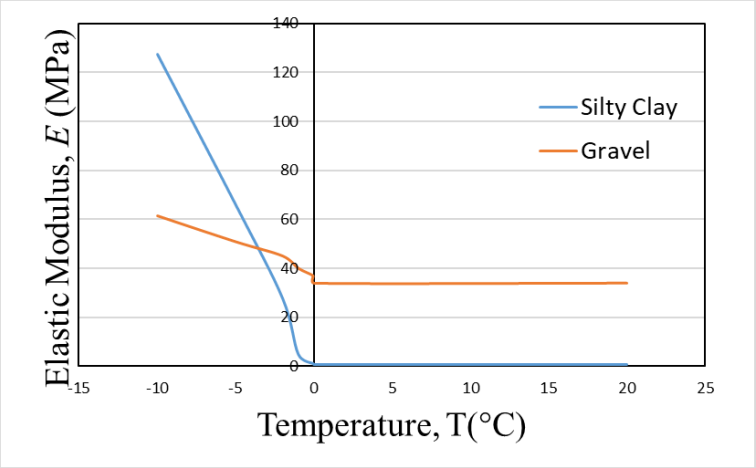

(b)

Figure 4.5 Temperature-dependent (a) Poisson's ratio and (b) modulus of elasticity of soils, data is from Ming et al. (2018).

As we are considering the associative flow rule for yielding scenarios of our numerical modeling, values of dilation angle and friction angle are the same. The friction angle (φ) and cohesion (c) for the gravel and silty clay were given in Ming et al. (2018). Since we are using the Linear Drucker-Prager yield criterion, the Drucker-

Prager version of angle of friction (β) and cohesion strength (d) should be obtained based on Equation 4.1 and 4.2 (Puzrin 2012). The temperature dependent friction angle (β) and cohesion are shown in Figure 4.6.

$$tan\beta = \frac{6Sin\varphi}{3 - sin\varphi} \tag{4.1}$$

$$d = \frac{6cCos\varphi}{3 - Sin\varphi} \tag{4.2}$$

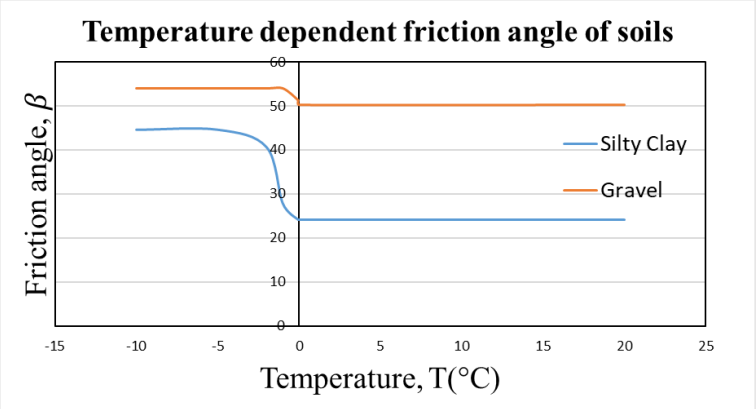

(a)

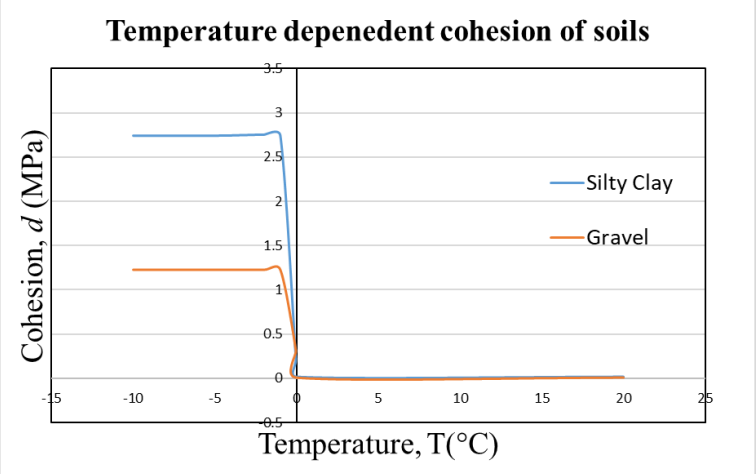

(b)

Figure 4.6 (a) Friction angle and (b) Cohesion of soils.

4.6 Thermal-mechanical modeling of embankments

4.6.1 Configuration and FEM mesh

The embankment model geometrical details are basically taken from Gholamzadehabolfazl (2015) and is treated as a 2D plane strain problem. A road embankment is typically a long structure that is situated on several subsoils which are not homogenous. For a section of this embankment, plane strain (2D) conditions can be taken into consideration, where the longitudinal strain can be assumed to be zero between the segment's two ends. The dimensions and soil's locations are shown in Figure 4.7. The embankment has three types of soil, and filling mainly contains gravel, and clayey silt covers from the slope to the end of ground. Finally, the bottom up to the depth of 18 meters contains silty clay. For the purpose to make the simulation less expansive, the embankment is meshed in two types. The embankment is meshed by elements of size 0.2 m^2 up to the depth of 8.25 meters from the ground surface and the rest of the bottom is meshed by 0.3 m^2 elements. The linear quadratic dominated element type is used for this modeling as shown in Figure 4.7. The quadratic element is a 2D double order element used for the 2D FEM analysis.

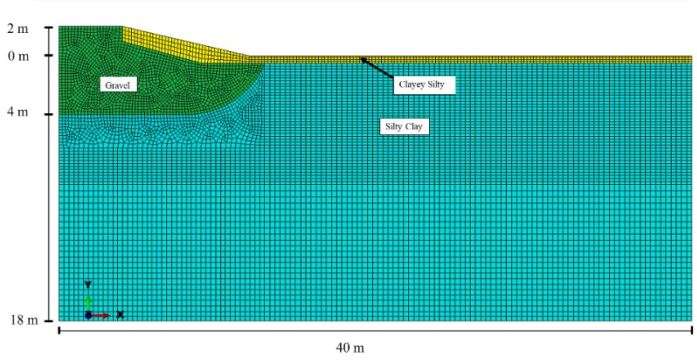

Figure 4.7 The applied mesh of embankment for FEM modeling.

4.6.2 Boundary conditions

There are three boundary conditions needed for the modelling: (1) the foundation boundary condition at the bottom of the cross-section, represented by a constant temperature; (2) the boundary conditions at the left and right vertical boundaries; and (3) the ground surface boundary condition on top of the meshed field, which is primarily controlled by daily air temperatures that vary seasonally with time.

For the bottom boundary condition, average recorded temperatures at a depth of 18 m below the surface of the ground were used. Below the entire embankment model, a constant temperature of 1°C was applied. In case of vertical boundary conditions, "No-heat-flow" boundaries were established for both the left and right borders based on symmetry.

The link between climate and the thermal regime of the active layer is dependent on ground surface temperature (Lachenbruch et al., 1988). Unfortunately, because of the radiative and convective energy flows at the surface and the challenge of keeping a sensor in place, it is challenging to monitor ground surface temperature. Nominal surface temperature readings are frequently taken a few centimeters below the surface due to these challenges (Riseborough, 2003). Efforts to measure such near-surface ground temperatures are growing as autonomous data-collecting systems become more accessible and compact (Taylor 1995; Smith et al., 2001). The year is divided between freezing and thawing seasons in many straightforward models of the relationship between climate and permafrost, which use the freezing index (I_F) and

thawing index (I_T) to describe the annual regime. The definition of a seasonal index is the seasonally integrated temperature, which is roughly equivalent to the total of daily mean temperatures over the period of a season. such as the surface thawing index (Klene et al. 2001) is:

$$I_{TS} = \int_0^{\theta_s} T_S - T_F dt \approx \sum_0^{\theta_s} \bar{T}_S \tag{4.3}$$

where, θ_s is the duration of the thawing season, days, T_F is the temperature of the freezing point (0°C), T_S is the surface temperature °C and $\bar{T}_S$ daily mean surface temperature. Using temperature index data on near-surface temperatures to compile values for n factors and analyze the results to discover how various land covers behave in a particular way is a crucial application. The n-factors were employed to convert air temperatures to temperatures near the ground's surface (Lunardini 1978). Site-specific variables, like surface type and snow cover (Fortier et al. 2011)), can affect the surface n-factors. So according to Gholamzadehabolfazl (2015) the current model also has three surfaces, as shown in Figure 4.6. The gravel surface, which is the pavement's top layer, is always clear of snow and vegetation. The area between the shoulder and the toe of the embankment is known as the slope surface. In the winter, this surface is covered in snow; in the summer, it is hidden by bushes and short vegetation. The surrounding natural land is covered in a clay covering. In the winter, this surface is likewise covered in snow, and in the summer, it is hidden by bushes and short vegetation. So seasonal

air temperature and ground surface temperature are related by n-factors (Lunardini, 1978). For instance, the surface thawing n factor is defined:

$$n_T = \frac{I_{TS}}{I_{TA}} \tag{4.4}$$

$$n_F = \frac{I_{FS}}{I_{FA}} \tag{4.5}$$

where, n_T and n_F are surface thawing n-factor and surface freezing n-factor. I_{TA} and I_{FA} are air thawing and air freezing index. I_{TS} and I_{FS} are Surface thawing and surface freezing index respectively.

As we are using the similar geometrical model of Gholamzadehabolfazl (2015) and, soils layers and thermal properties are also same. Upon comparison of surface air temperature also, the same n-factors were used here. n_T and n_F for clay (surrounding natural land) are 1 and 0.8, for slope are 1.1 and 0.1, and for gravel surface are 1.2 and 1 respectively.

4.6.3 Establishing the initial thermal regime for simulations

Here the work is done on thermal regime of embankment to find out predefined temperature conditions of ground concerning different surface air temperature for various simulation cases. For numerical analysis, to get the initial thermal regime of ground for each climate scenario, we use Historical climate data for trial. From the output results of which we got the temperature of ground at different depth concerning the day of year and surface temperature and then used as a data base for natural ground temperature of various simulation cases respectively. For the initial historical

simulation, the ground thermal regime was taken of January 2010 from Gholamzadehabolfazl (2015). The flow chart in Figure 4.8 is showing the steps to establish the initial ground thermal regime and for that a numerical simulation is conducted to figure out the relation between surface temperature and ground temperature profile to create a database.

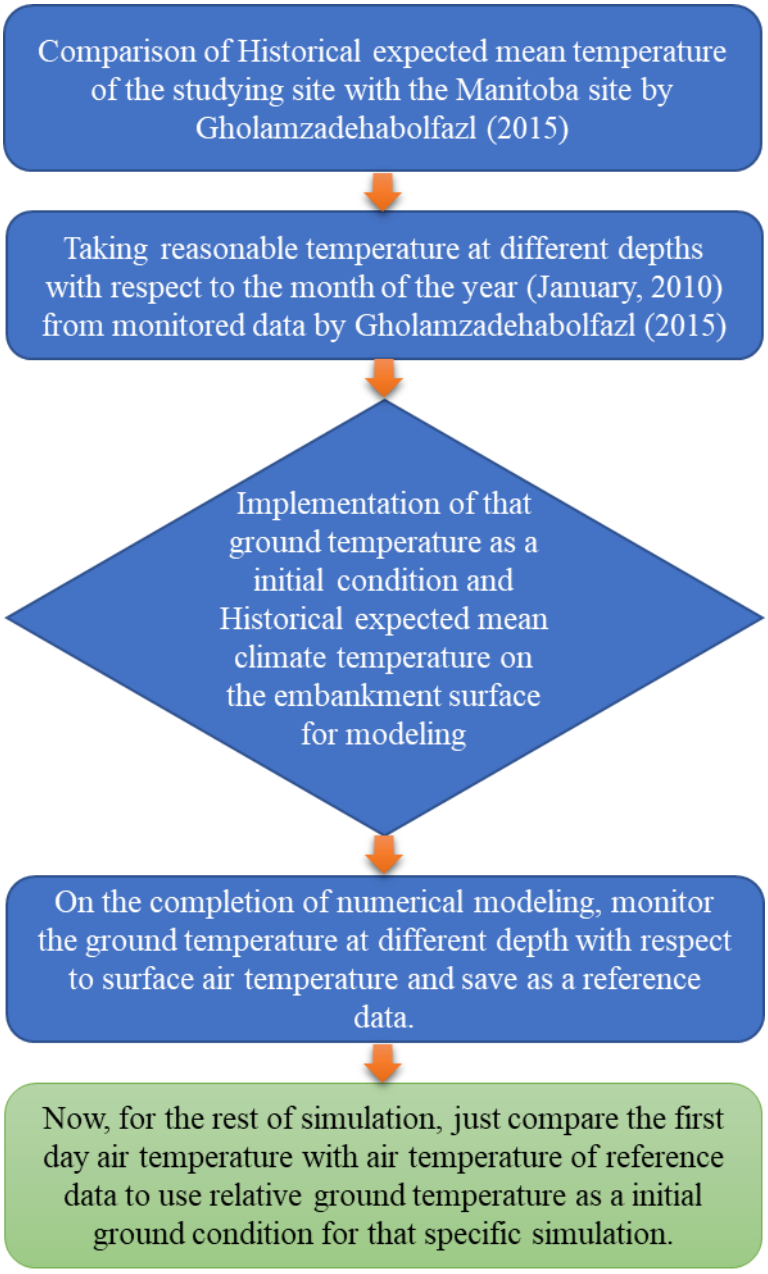

Figure 4.8 Establishment of the initial thermal regime for simulations.

4.6.4 Traffic load consideration

Our study is based on the analysis of embankment stresses and strains under different climate conditions, but at the same time traffic load is also much more important to consider because of its complex effects in the embankment. In addition to being crucial for the security of construction projects, rational estimates of road traffic load for geotechnical and structural evaluations also affect investment costs.

So, for the involvement of traffic load in the analysis of embankment under the changing climate scenarios, this study considered the primary load model from Topolnicki (2020). In the primary model, which applies to geotechnical investigations, the combined action of both traffic load elements, (p1) and (p2), can be replaced by a single uniform load (p), distributed across the entire roadway width (B), and is shown in Figure 4.9 (Topolnicki, 2020) .

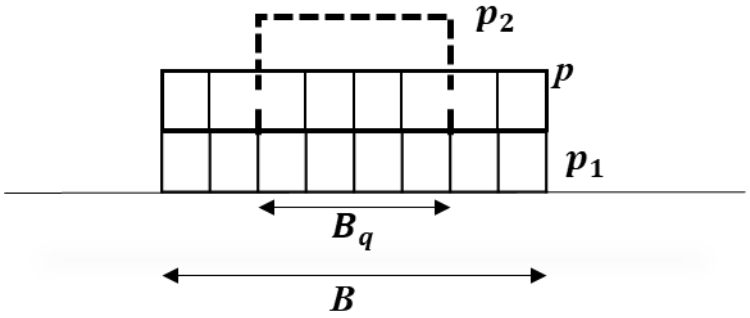

Figure 4.9 Equivalent characteristic traffic load p for the primary load model (Topolnicki, 2020).

$$P = P_1 + P_2 \frac{B_q}{B} \tag{4.6}$$

where, P_1, P_2 and P are uniform characteristic load, concentrated characteristic load and equivalent Load respectively. The calculation of equivalent traffic load for the embankment of this study is done by using the Equation 4.6 and the embankment is shown in Figure 4.10.

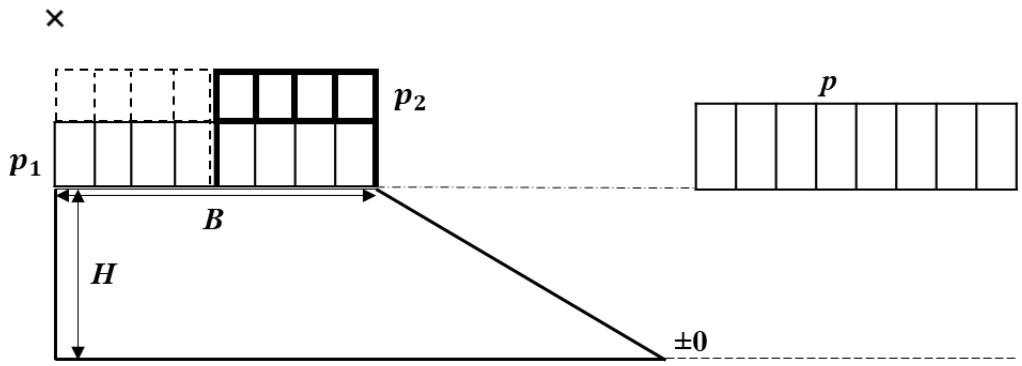

Figure 4.10 A sketch showing the 4 m wide roadway of embankment with the equivalent traffic load.

where H is the effective height of the embankment. The equation proposed by Topolnicki (2020) is applicable to a general group of embankments. Dependent on effective height of the embankment, as H = 2 m < 4m, the referred values taken for P_1 and P_2 calculated by Topolnicki (2020) were 9 kPa and 28.5 kPa respectively. As we considered the whole width (B) as carriage way width (B_q), and the calculated P by using Equation 4.6 is 37500 (Pa), which was then applied on the top (gravel surface) of embankment for numerical analysis.

5 Results

The general clarification of each site climate projected data has been explained in Figure 4.1. The numerical simulation results include monitored temperature, monitored displacements at key monitoring points, stresses, and Equivalent Plastic strain profile (*PEEQ*). As shown in Fig. 5.1, the point A is on the road surface and it is expected to have the maximum displacements when the road is under thermal disturbance. Another chosen point is below the toe of the embankment at the depth of 1.42 meter (point B). The reason of choosing the point B is because the part is critical for an embankment as rain infiltration can pose severe threat to the infrastructure if there is any damage.

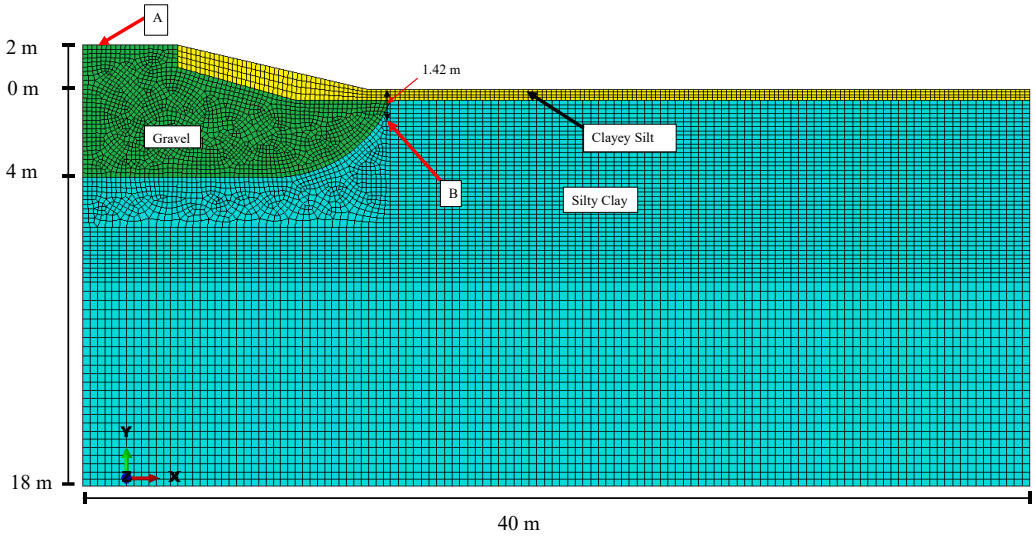

Figure 5.1 Monitored locations on the embankment.

5.1 Monitored temperature

5.1.1 At point A

After the numerical analysis was done, the temperatures at point A of the embankments have been monitored for both locations, James Smith, and Yellow Quill, as shown in Figures 5.2 and 5.3. As is shown in Fig. 5.2a and Fig. 5.3a, very slight temperature increase can be noticed for the future ones when compared with the historical data. However, the differences are better reflected in the plots with cumulative temperatures (Fig. 5.2b and Fig. 5.3b), which are based on an accumulative interval of one day.

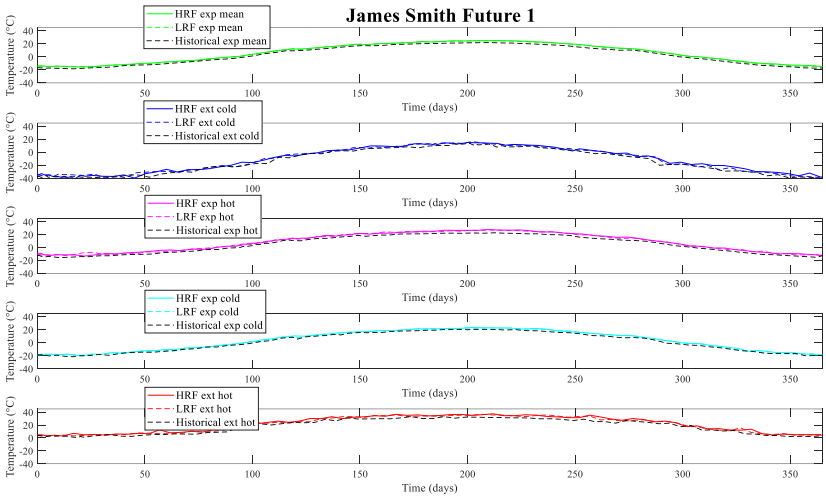

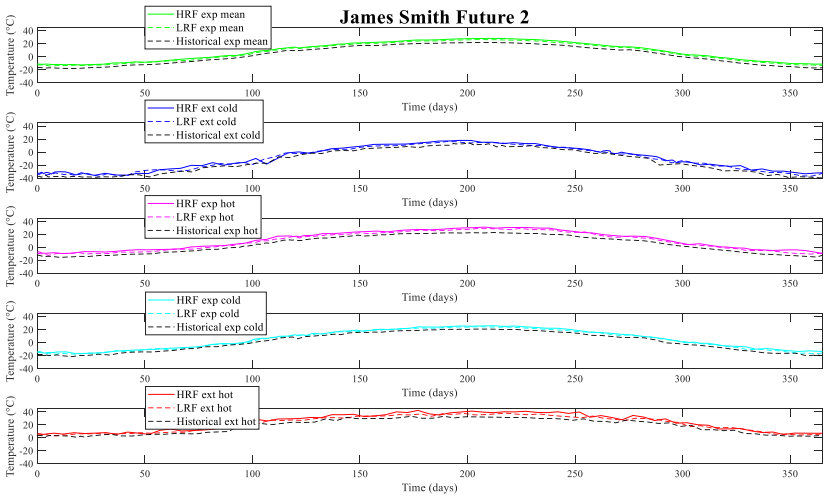

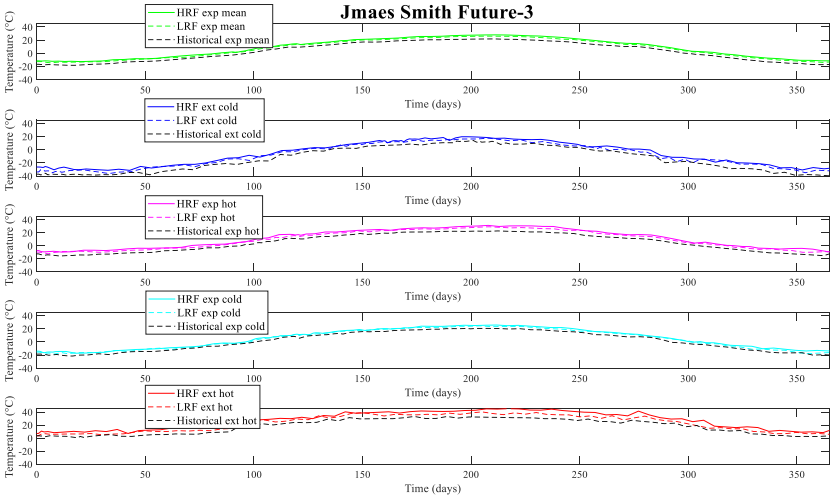
Jmaes Smith Future-3
HRF exp mean
LRF exp mean
Historical exp mean
HRF ext cold
LRF ext cold
Historical ext cold
HRF exp hot
LRF exp hot
Historical exp hot
HRF exp cold
LRF exp cold
Historical exp cold
HRF ext hot
LRF ext hot
Historical ext hot
Temperature (°C)
Time (days)

(a)

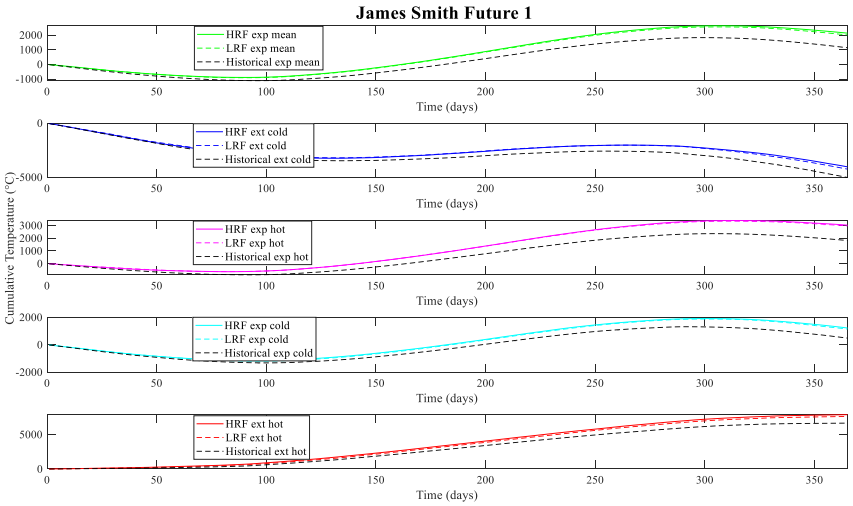
James Smith Future 1
HRF exp mean
LRF exp mean
Historical exp mean
HRF ext cold
LRF ext cold
Historical ext cold
HRF exp hot
LRF exp hot
Historical exp hot
HRF exp cold
LRF exp cold
Historical exp cold
HRF ext hot
LRF ext hot
Historical ext hot
Cumulative Temperature (°C)
Time (days)

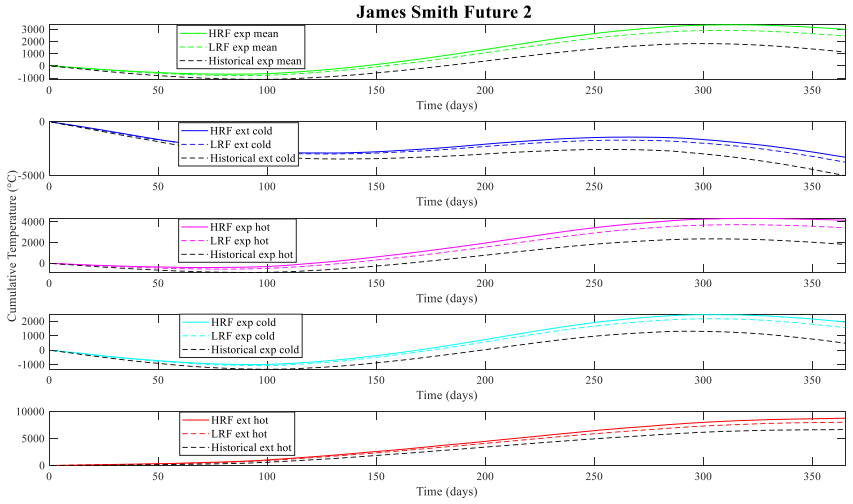
James Smith Future 2
HRF exp mean
LRF exp mean
Historical exp mean
HRF ext cold
LRF ext cold
Historical ext cold
HRF exp hot
LRF exp hot
Historical exp hot
HRF exp cold
LRF exp cold
Historical exp cold
HRF ext hot
LRF ext hot
Historical ext hot
Cumulative Temperature (°C)
Time (days)

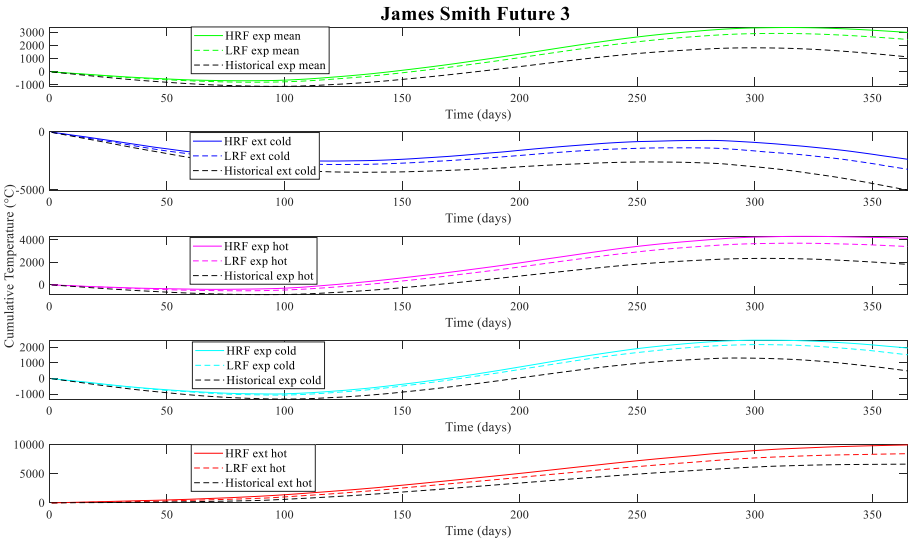

(b)

Figure 5.2 Monitored temperature at point A of James Smith embankment.

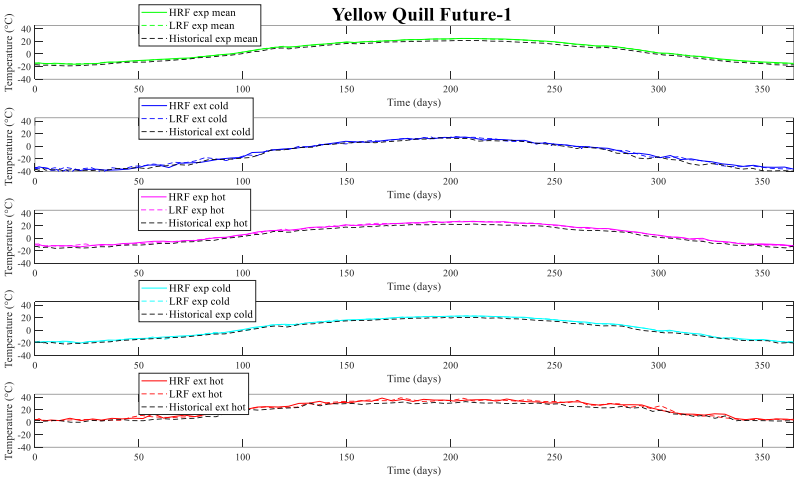

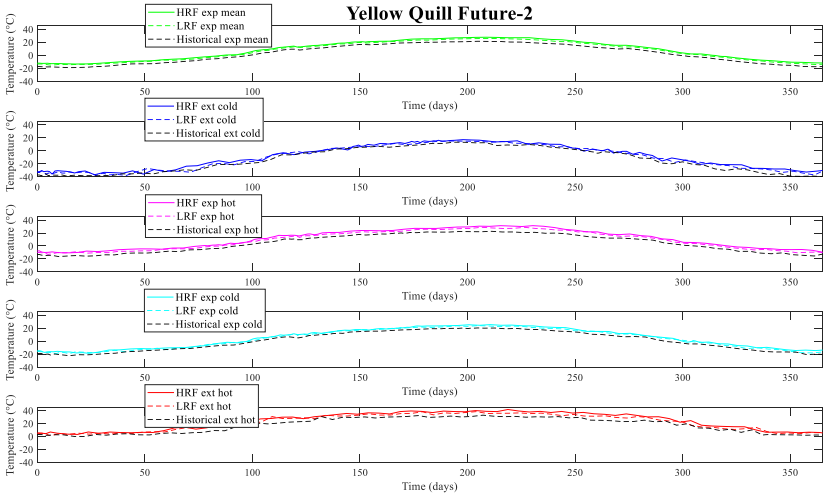

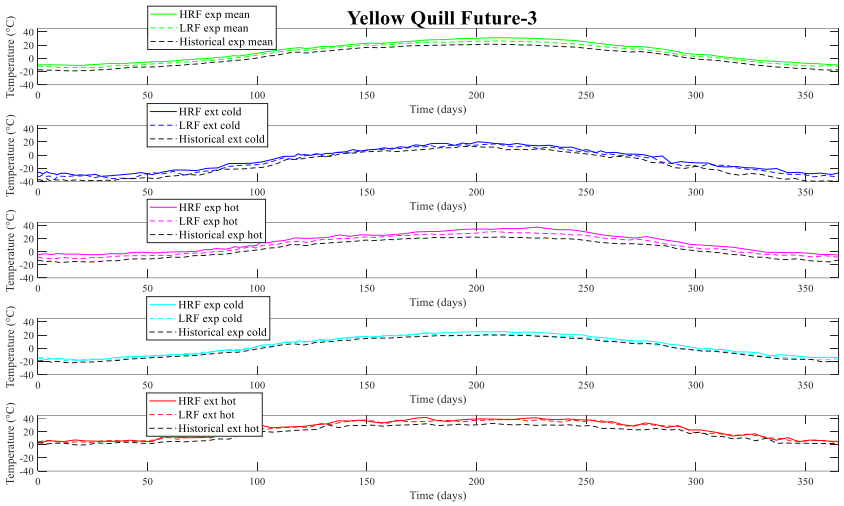
Yellow Quill Future-3
HRF exp mean
LRF exp mean
Historical exp mean
HRF ext cold
LRF ext cold
Historical ext cold
HRF exp hot
LRF exp hot
Historical exp hot
HRF exp cold
LRF exp cold
Historical exp cold
HRF ext hot
LRF ext hot
Historical ext hot
Temperature (°C)
Time (days)

(a)

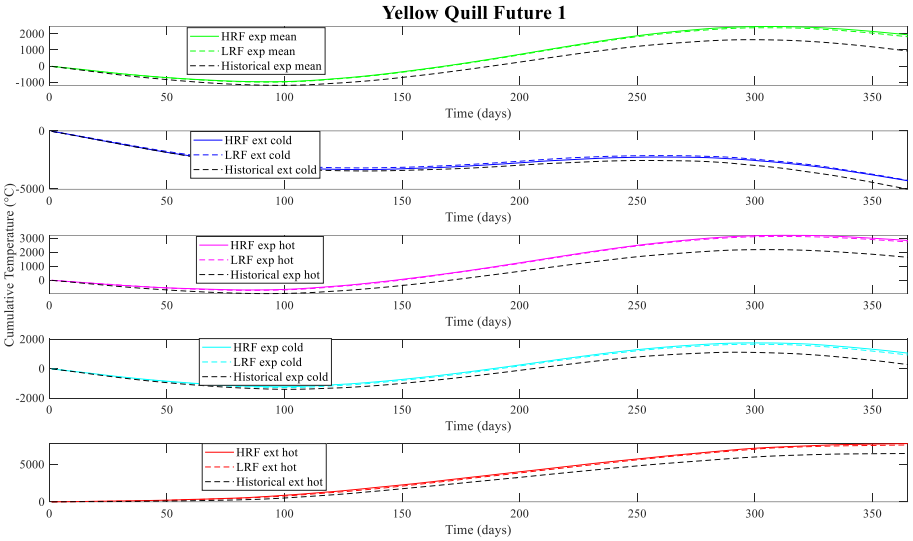
Yellow Quill Future 1
HRF exp mean
LRF exp mean
Historical exp mean
HRF ext cold
LRF ext cold
Historical ext cold
HRF exp hot
LRF exp hot
Historical exp hot
HRF exp cold
LRF exp cold
Historical exp cold
HRF ext hot
LRF ext hot
Historical ext hot
Cumulative Temperature (°C)
Time (days)

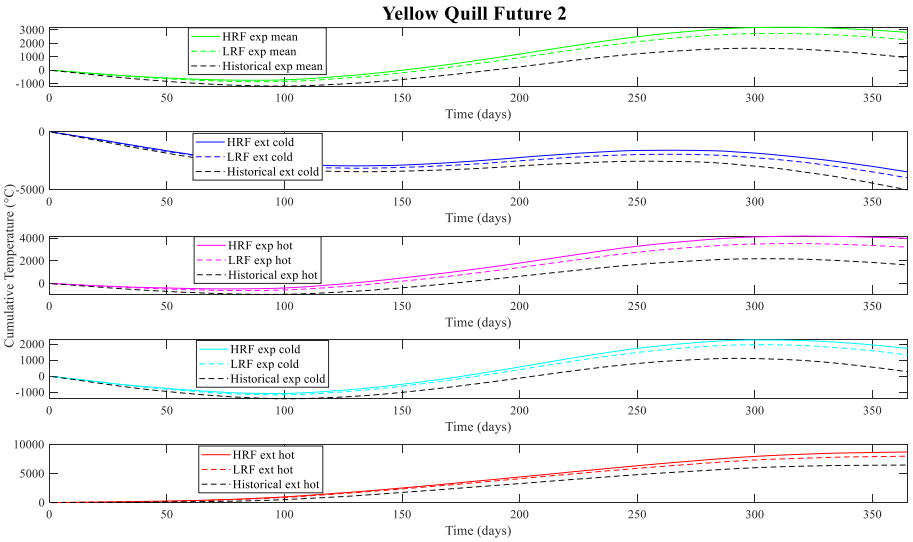
Yellow Quill Future 2
HRF exp mean
LRF exp mean
Historical exp mean
HRF ext cold
LRF ext cold
Historical ext cold
HRF exp hot
LRF exp hot
Historical exp hot
HRF exp cold
LRF exp cold
Historical exp cold
HRF ext hot
LRF ext hot
Historical ext hot
Cumulative Temperature (°C)
Time (days)

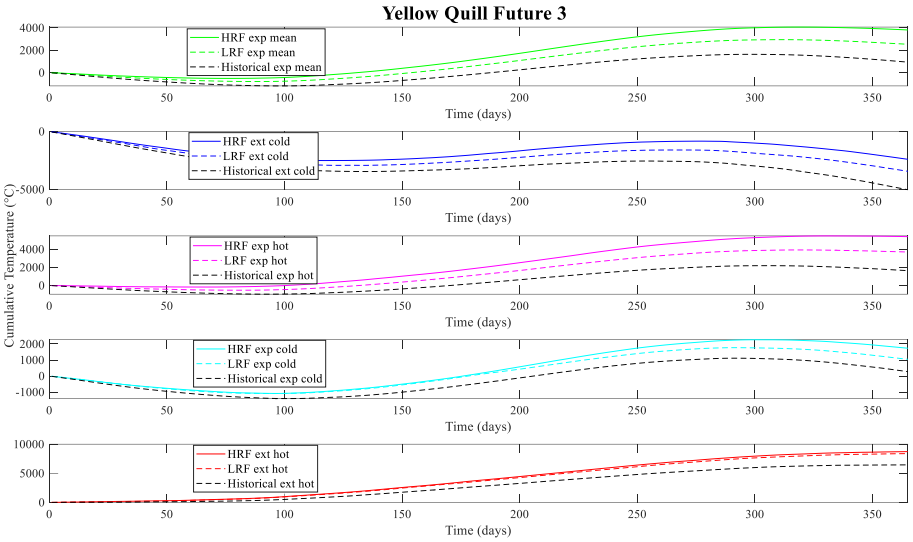

(b)

Figure 5.3 Monitored temperature at point A of Yellow Quill embankment.

5.1.2 At point B

The location of point B is at the critical spot of embankment, where the plastic strain is maximum (will be displayed latterly). The monitored temperatures at point B for both site embankments are shown in Figure 5.4 and 5.5. Similar to point A, the difference of monitored temperatures from Historical to Future-3 are better noticed in cumulative temperature figures.

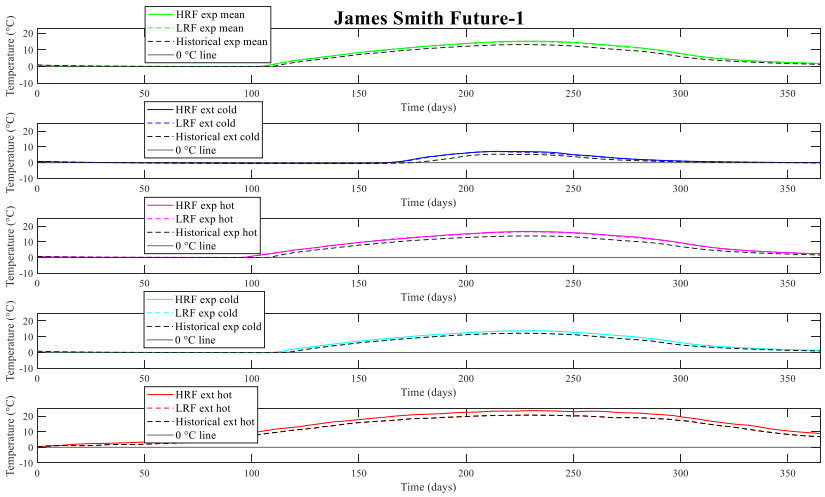

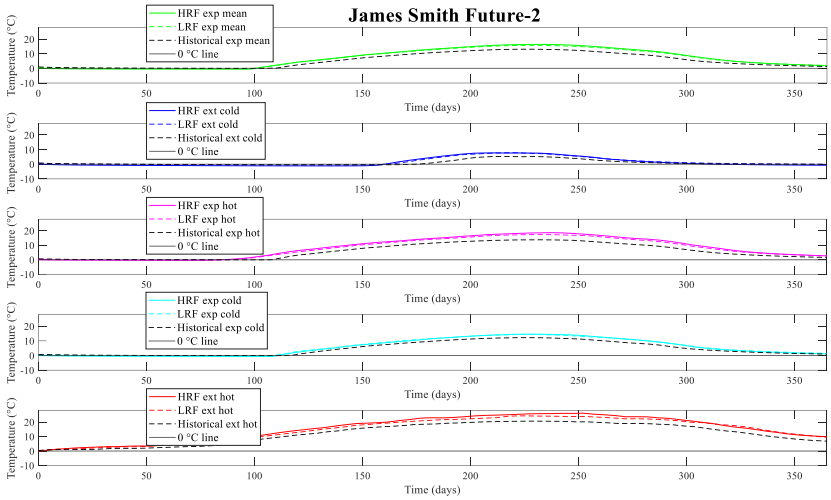
James Smith Future-2
HRF exp mean
LRF exp mean
Historical exp mean
0 °C line
HRF ext cold
LRF ext cold
Historical ext cold
HRF exp hot
LRF exp hot
Historical exp hot
HRF exp cold
LRF exp cold
Historical exp cold
HRF ext hot
LRF ext hot
Historical ext hot
Temperature (°C)
Time (days)

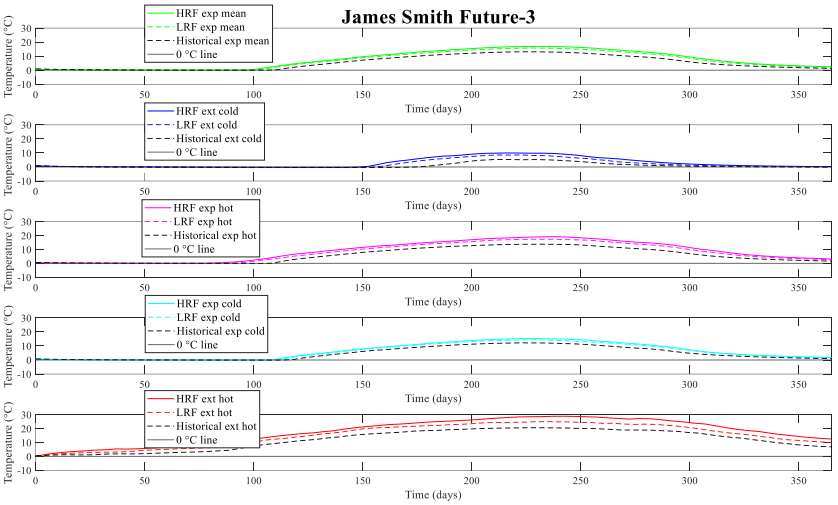
James Smith Future-3
HRF exp mean
LRF exp mean
Historical exp mean
0 °C line
HRF ext cold
LRF ext cold
Historical ext cold
HRF exp hot
LRF exp hot
Historical exp hot
HRF exp cold
LRF exp cold
Historical exp cold
HRF ext hot
LRF ext hot
Historical ext hot
Temperature (°C)
Time (days)

(a)

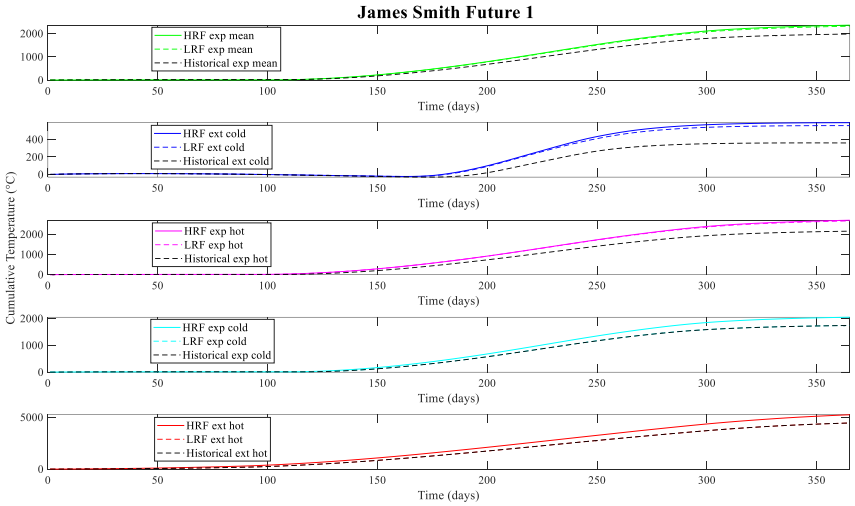
James Smith Future 1
HRF exp mean
LRF exp mean
Historical exp mean
HRF ext cold
LRF ext cold
Historical ext cold
HRF exp hot
LRF exp hot
Historical exp hot
HRF exp cold
LRF exp cold
Historical exp cold
HRF ext hot
LRF ext hot
Historical ext hot
Cumulative Temperature (°C)
Time (days)

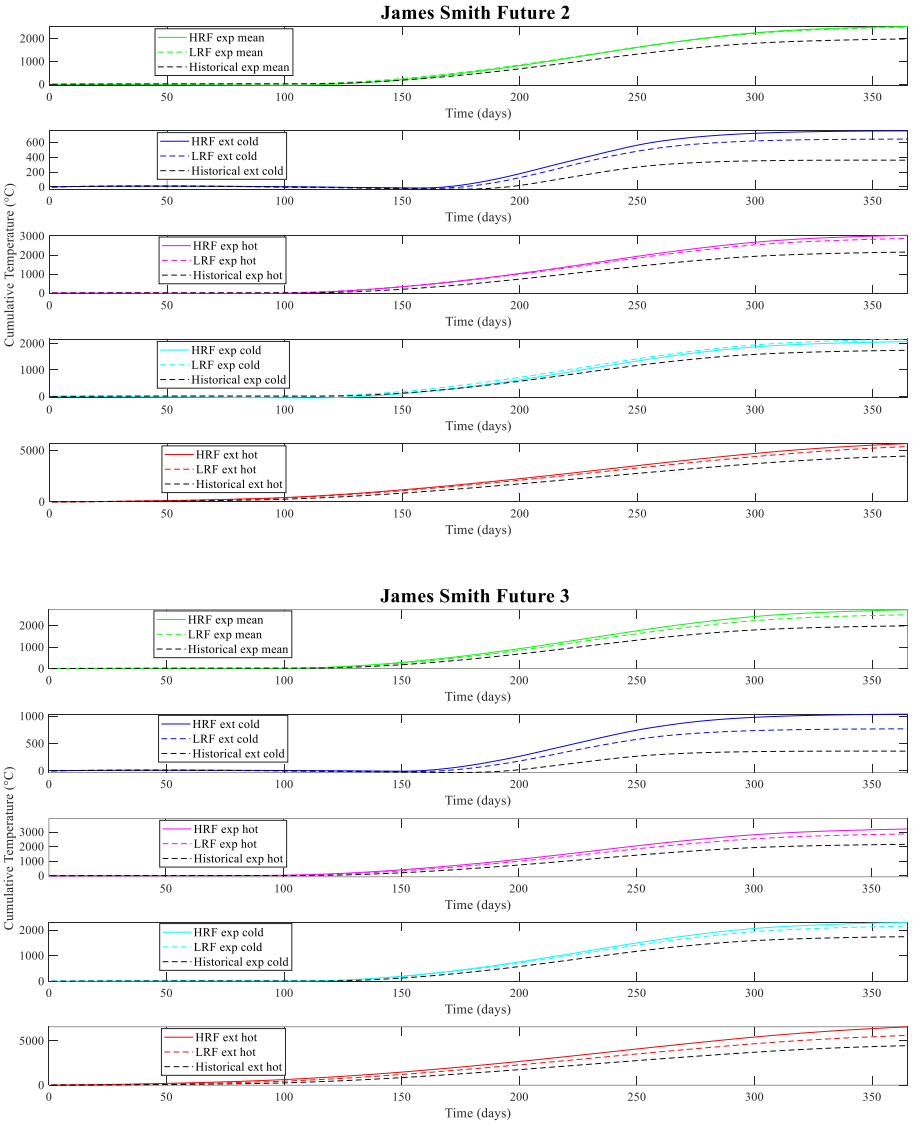

(b)

Figure 5.4 Monitored temperature at point B of James Smith Embankment.

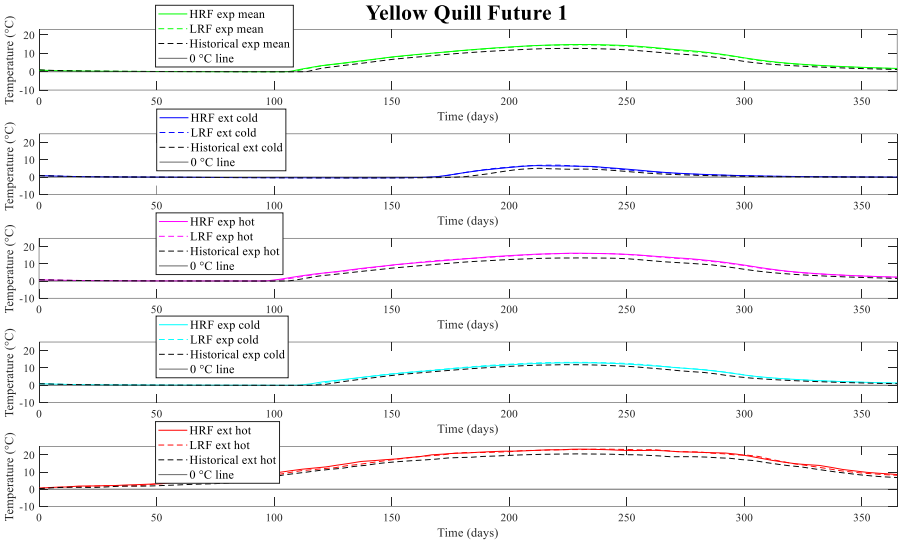
Yellow Quill Future 1
HRF exp mean
LRF exp mean
Historical exp mean
0 °C line
HRF ext cold
LRF ext cold
Historical ext cold
0 °C line
HRF exp hot
LRF exp hot
Historical exp hot
0 °C line
HRF exp cold
LRF exp cold
Historical exp cold
0 °C line
HRF ext hot
LRF ext hot
Historical ext hot
0 °C line
Temperature (°C)
Time (days)

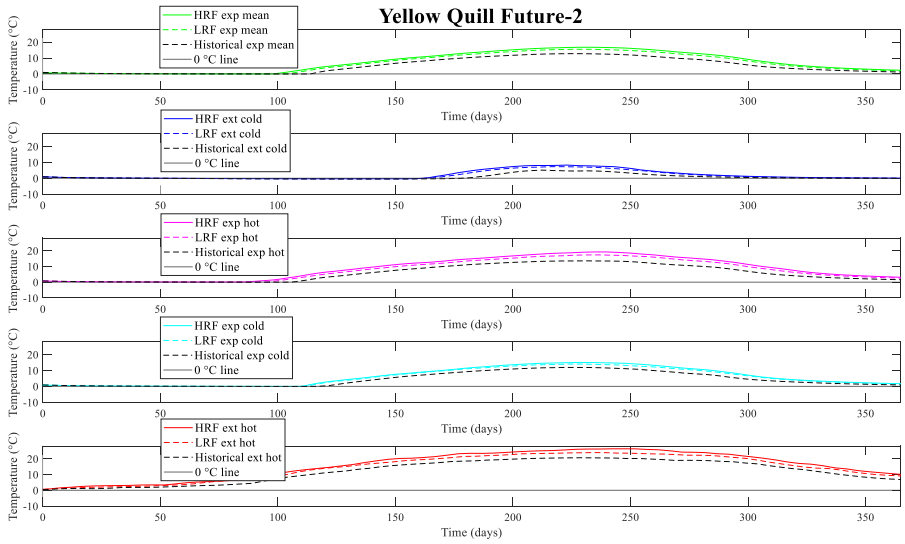
Yellow Quill Future-2
HRF exp mean
LRF exp mean
Historical exp mean
0 °C line
HRF ext cold
LRF ext cold
Historical ext cold
0 °C line
HRF exp hot
LRF exp hot
Historical exp hot
0 °C line
HRF exp cold
LRF exp cold
Historical exp cold
0 °C line
HRF ext hot
LRF ext hot
Historical ext hot
0 °C line
Temperature (°C)
Time (days)

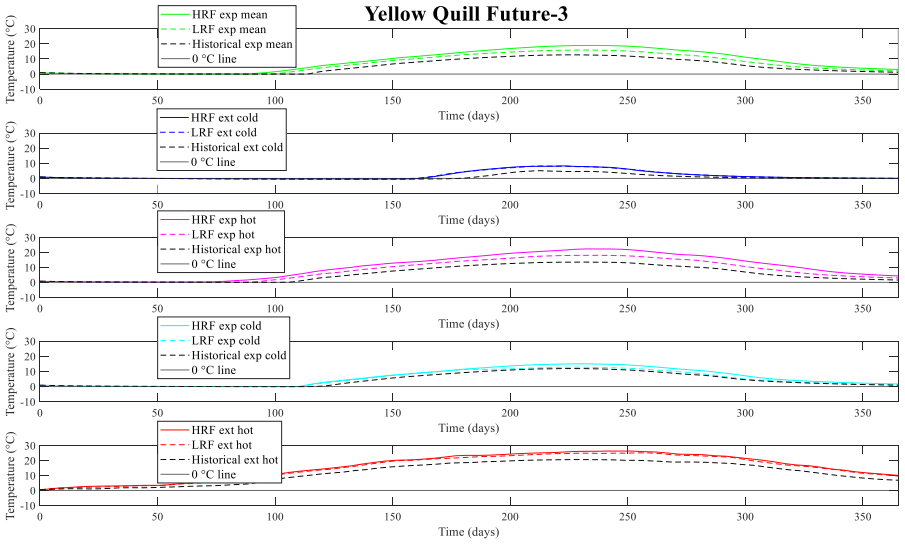
Yellow Quill Future-3
HRF exp mean
LRF exp mean
Historical exp mean
0 °C line
HRF ext cold
LRF ext cold
Historical ext cold
0 °C line
HRF exp hot
LRF exp hot
Historical exp hot
0 °C line
HRF exp cold
LRF exp cold
Historical exp cold
0 °C line
HRF ext hot
LRF ext hot
Historical ext hot
0 °C line
Temperature (°C)
Time (days)

(a)

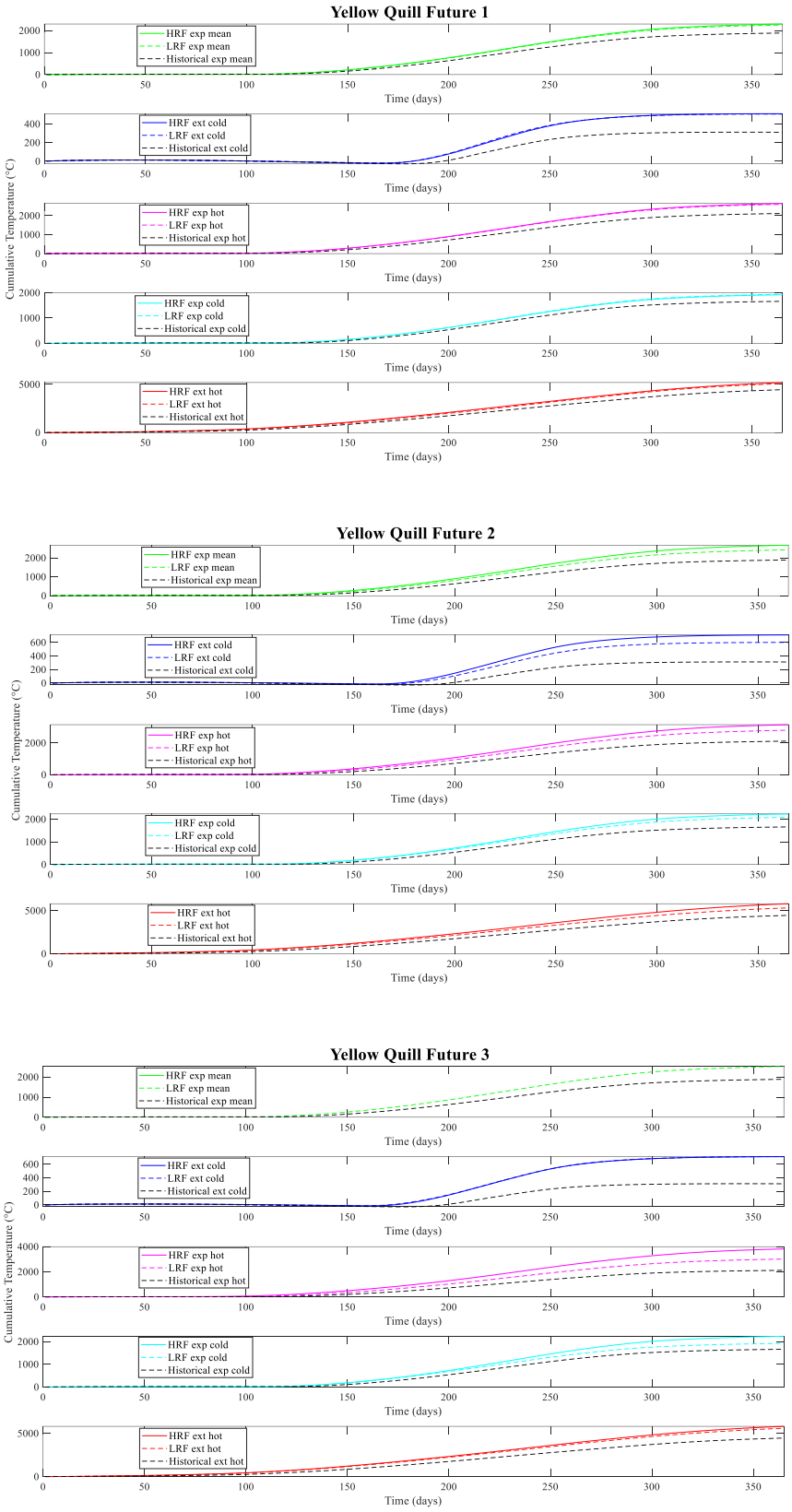

(b)

Figure 5.5 Monitored and cumulative temperature at point B of Yellow Quill embankment.

5.2 Monitored displacement

For all the projected climate scenarios: Historical, Future-1 HRF and LRF, Future-2 HRF and LRF, and Future-3 HRF and LRF of both sites, monitored displacements at point A are presented in Figures 5.6, 5.7 and 5.8. The modeled displacement results from cases of Future-1, Future-2 and Future-3 are compared with the result of historical climate data to understand the effects of climate change and load on the embankments of both locations. There is a noticeable difference between future and historical monitored results, either in traffic load or without traffic load scenarios. It seems that the results from cases of expected mean, expected cold and expect hot are not much affected by climate variation and showing similar trend in expansion and thawing according to seasonal cycle. The case of extreme hot is showing the minimum expansion and settlement, as the soil is in long duration of positive temperature. A noticeable difference in displacement is captured very well in the cumulative displacement (absolute values were accumulated by days) figures of both sites. The results show that the cumulative displacement difference from historical in extreme cold case are increasing, in a sense of showing less displacement in each future case. By contrast, in extreme hot situations, the difference is increasing, but in a sense of showing more displacement in each future case. Among extreme cold cases, it is noticed that from historical to Future 3, there will be much less accumulated displacements when the climate is getting warmer. Nevertheless, the total accumulated displacements

are still quite significant for the extreme cold case (Figure 5.6-5.8). In all cases, HRF's and LRF's of particular period are showing same results in monitored displacements.

As Extreme cold case is most vulnerable to change in climate, that leads to compare the monitored displacements and temperatures at point A of embankments facing only the extreme cold case of all time episodes for each location. The monitored temperatures for both locations show the warmup of surface in every future climate case from Historical to Future-3, as shown in Figure 5.9, which is confirmed also in cumulative displacement figures. Similarly, in the corresponding extreme cold case, the embankment shows less expansion and thawing as pass through each future period, because as the surface is facing more warmup climate, that made it to bend towards unfrozen condition which shows less expansion and settlement as compared to extreme cold of previous climate episodes.

Figure 5.10 shows the simulated displacement results for the extreme hot cases. The results show that that the displacement is increasing in each future case, but even though that is not a big difference in between each future case.

Monitored point B is at the depth of 1.42 meter, and the displacement at point B is zero for all the cases. Due to this non-uniform deformation behavior among different locations of the embankment, the developed shear stress tends to be trapped below the toe of embankment and causes the shear plastic strain. The details will be discussed in the subsequent section.

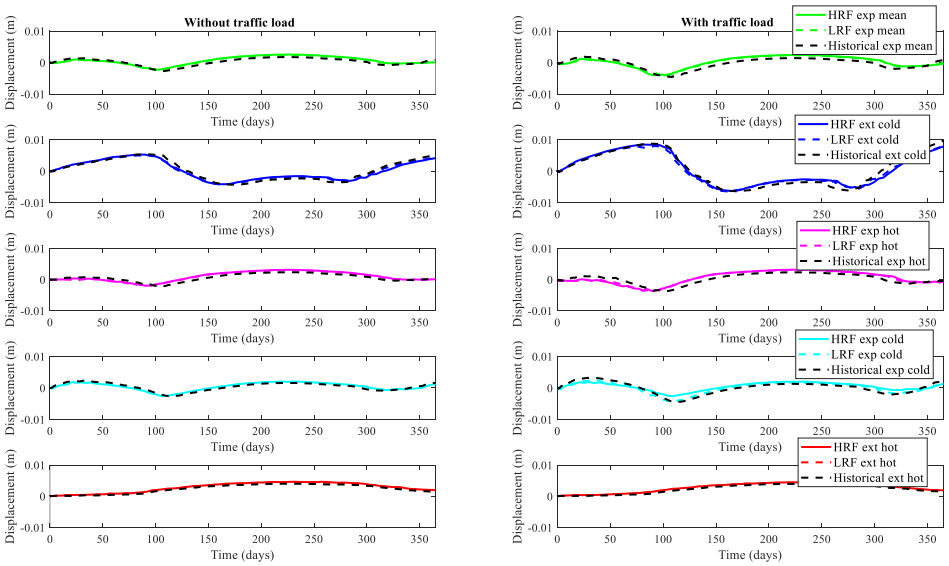
Without traffic load
With traffic load
Displacement (m)
Time (days)
HRF exp mean
LRF exp mean
Historical exp mean
HRF ext cold
LRF ext cold
Historical ext cold
HRF exp hot
LRF exp hot
Historical exp hot
HRF exp cold
LRF exp cold
Historical exp cold
HRF ext hot
LRF ext hot
Historical ext hot

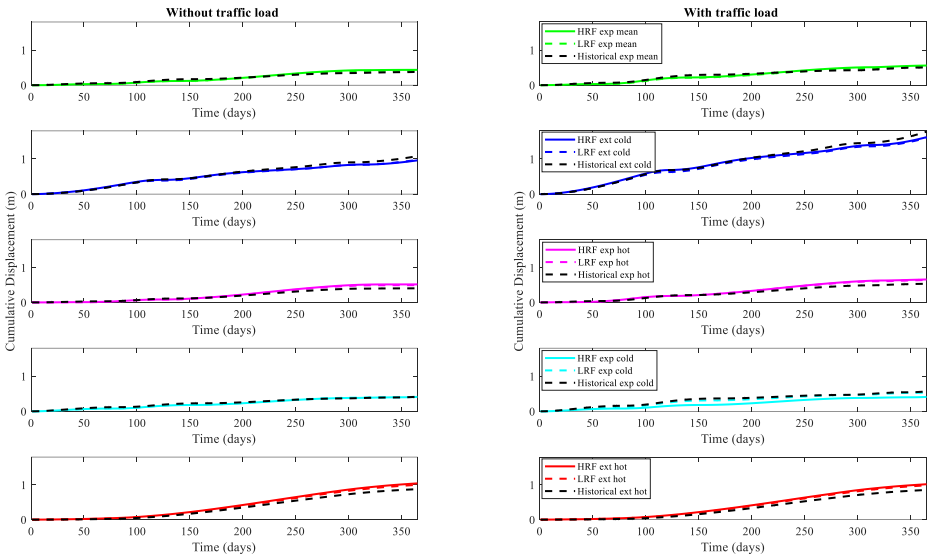
Without traffic load
With traffic load
Cumulative Displacement (m)
Time (days)
HRF exp mean
LRF exp mean
Historical exp mean
HRF ext cold
LRF ext cold
Historical ext cold
HRF exp hot
LRF exp hot
Historical exp hot
HRF exp cold
LRF exp cold
Historical exp cold
HRF ext hot
LRF ext hot
Historical ext hot

(a)

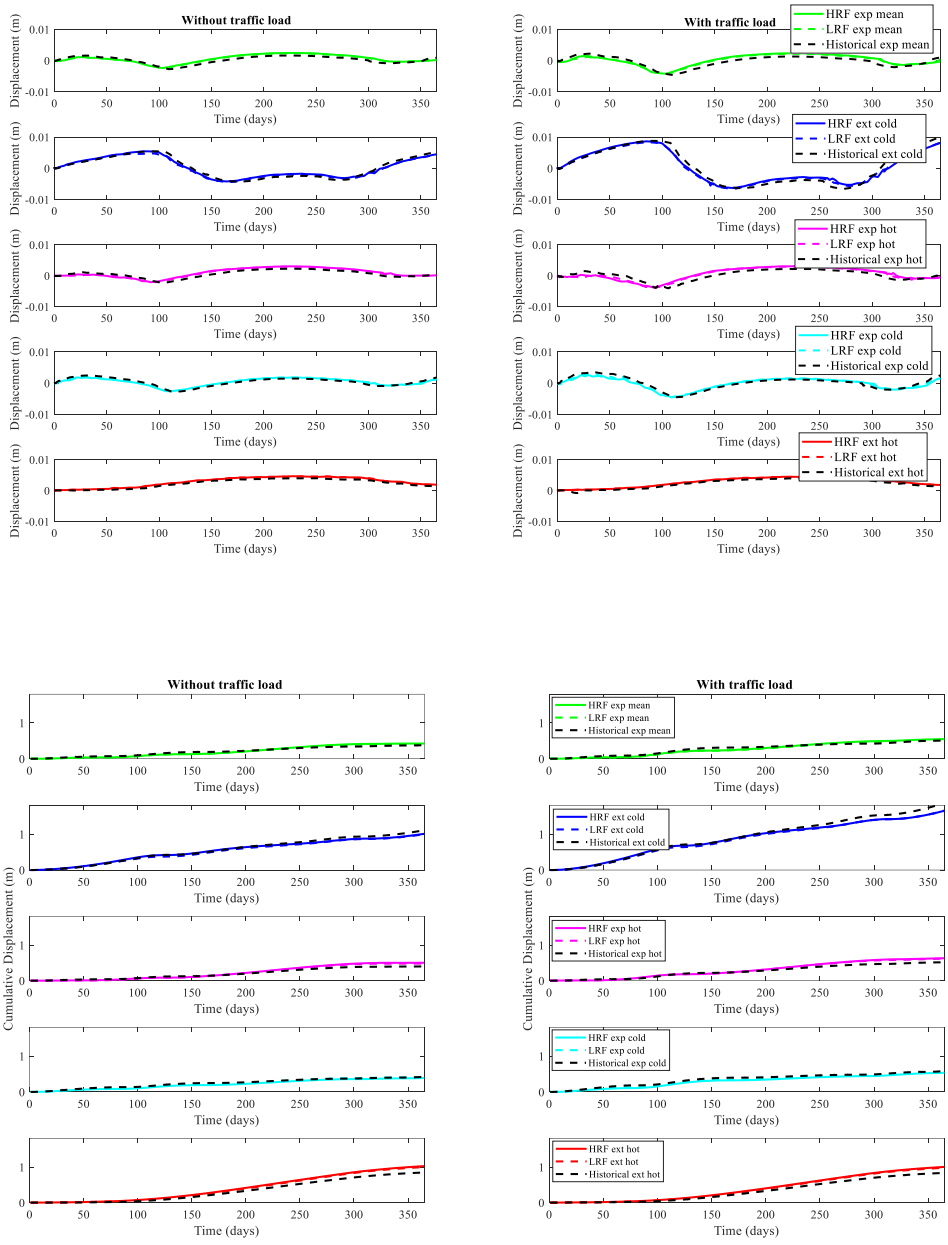

(b)

Figure 5.6 Monitored displacement of Future-1 (2023-2048) at point A (a) James Smith and (b) Yellow Quill

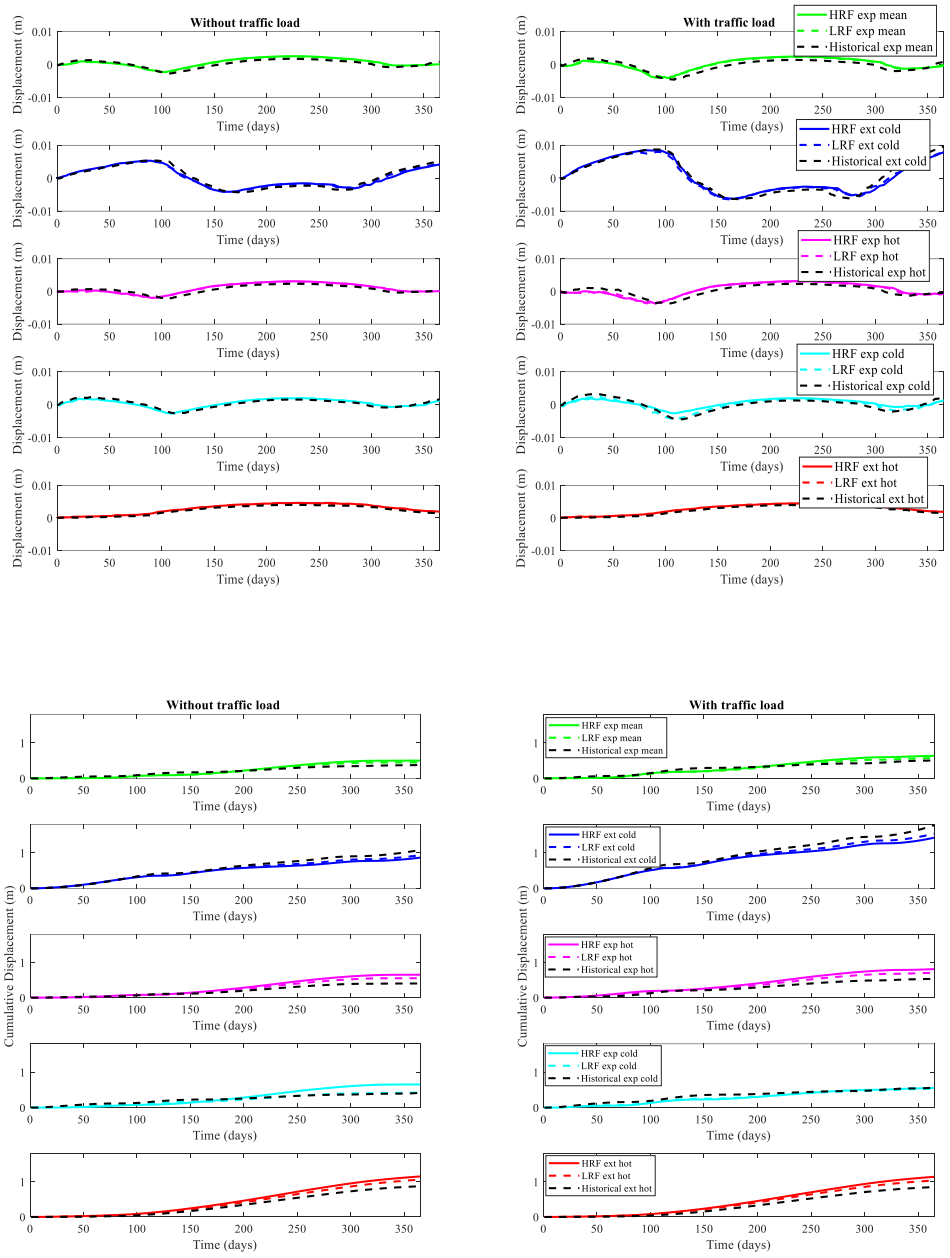
Without traffic load
With traffic load
Displacement (m)
Time (days)
HRF exp mean
LRF exp mean
Historical exp mean
HRF ext cold
LRF ext cold
Historical ext cold
HRF exp hot
LRF exp hot
Historical exp hot
HRF exp cold
LRF exp cold
Historical exp cold
HRF ext hot
LRF ext hot
Historical ext hot
Without traffic load
With traffic load
Cumulative Displacement (m)
Time (days)

(a)

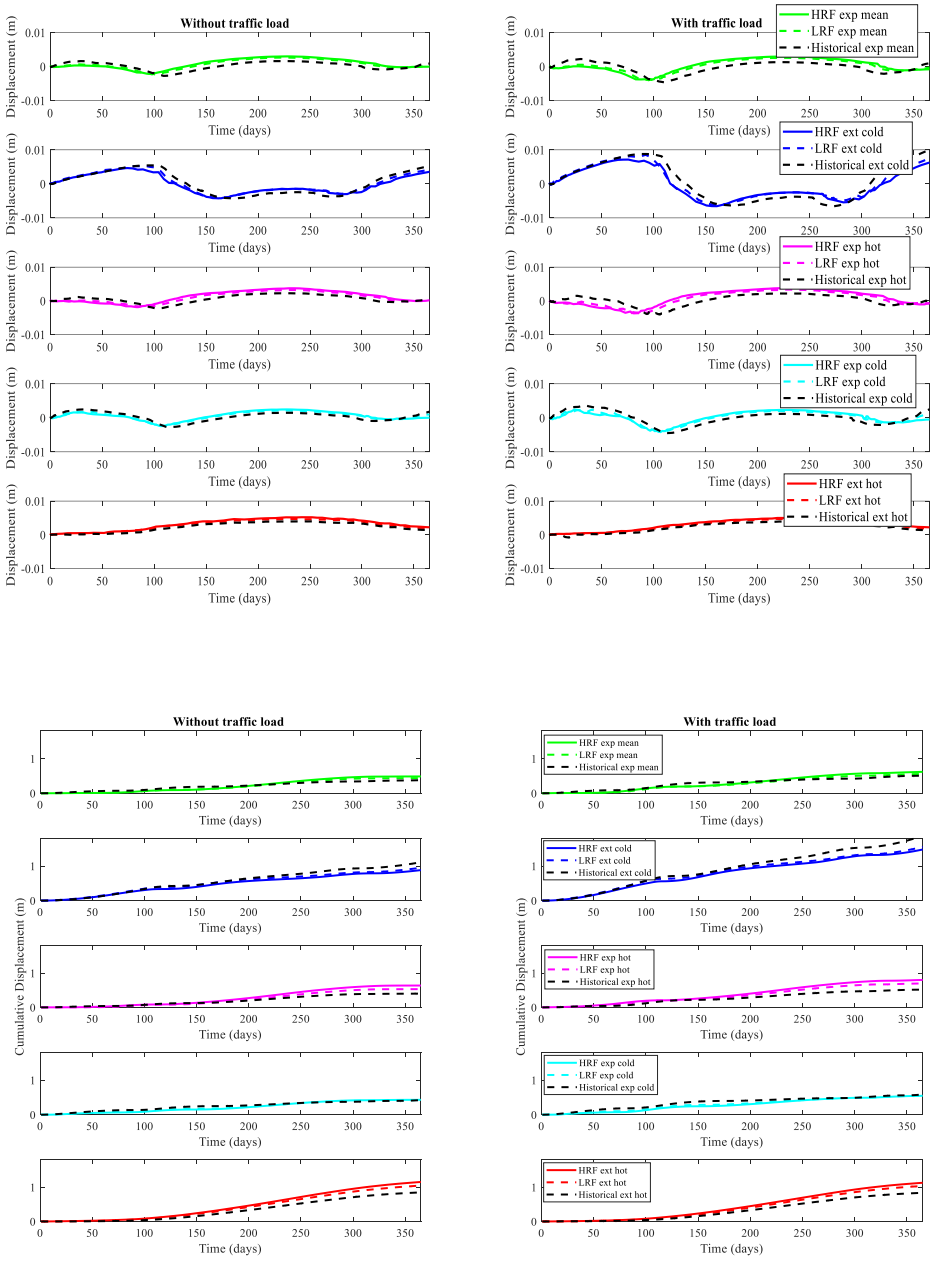

(b)

Figure 5.7 Monitored and cumulative displacement of Future-2 (2049-2074) at point A (a) James Smith and (b) Yellow Quill.

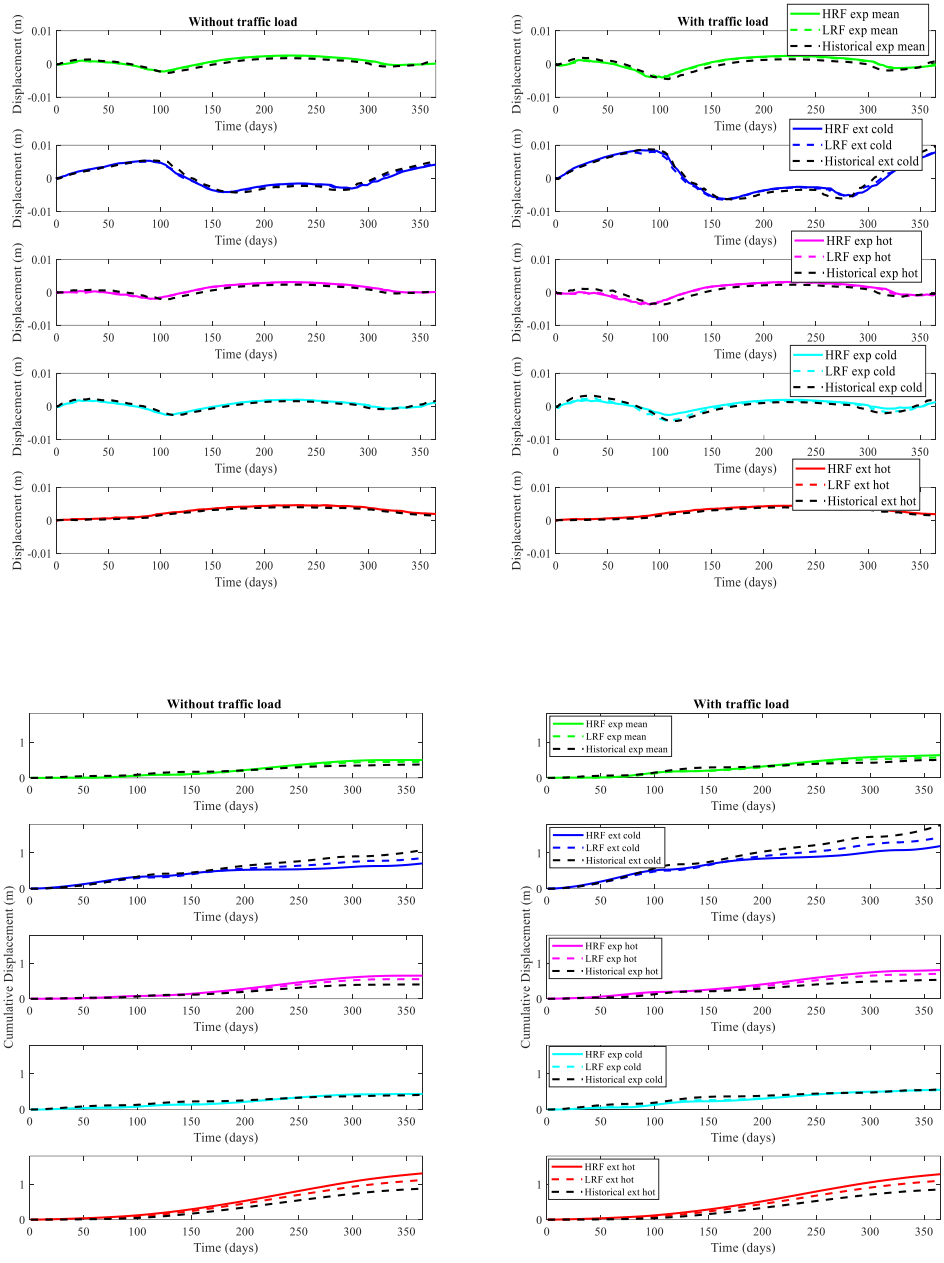
Without traffic load
With traffic load
HRF exp mean
LRF exp mean
Historical exp mean
HRF ext cold
LRF ext cold
Historical ext cold
HRF exp hot
LRF exp hot
Historical exp hot
HRF exp cold
LRF exp cold
Historical exp cold
HRF ext hot
LRF ext hot
Historical ext hot
Displacement (m)
Time (days)
Cumulative Displacement (m)

(a)

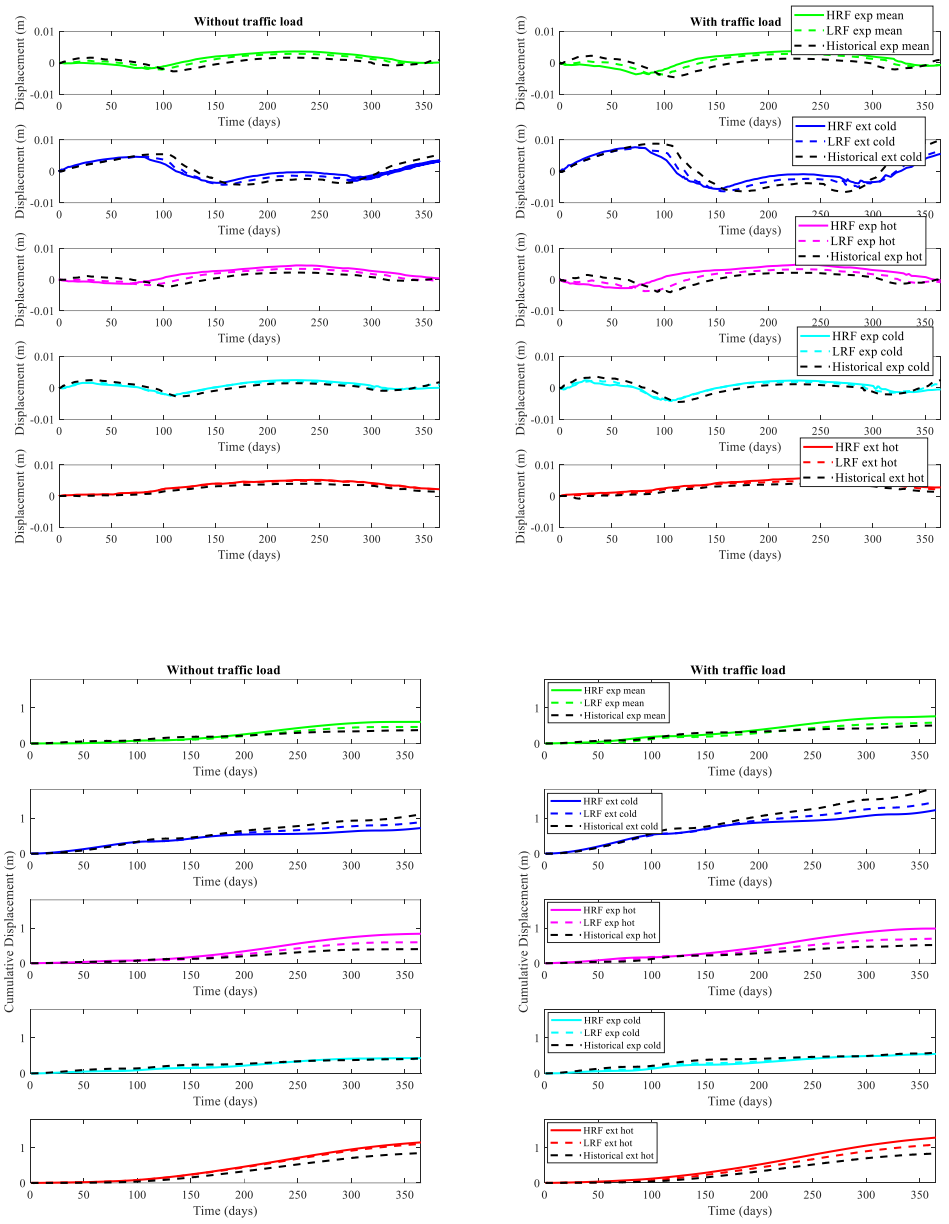

(b)

Figure 5.8 Monitored and cumulative displacement of Future-3 (2075-2100) at point A (a) James Smith and (b) Yellow Quill.

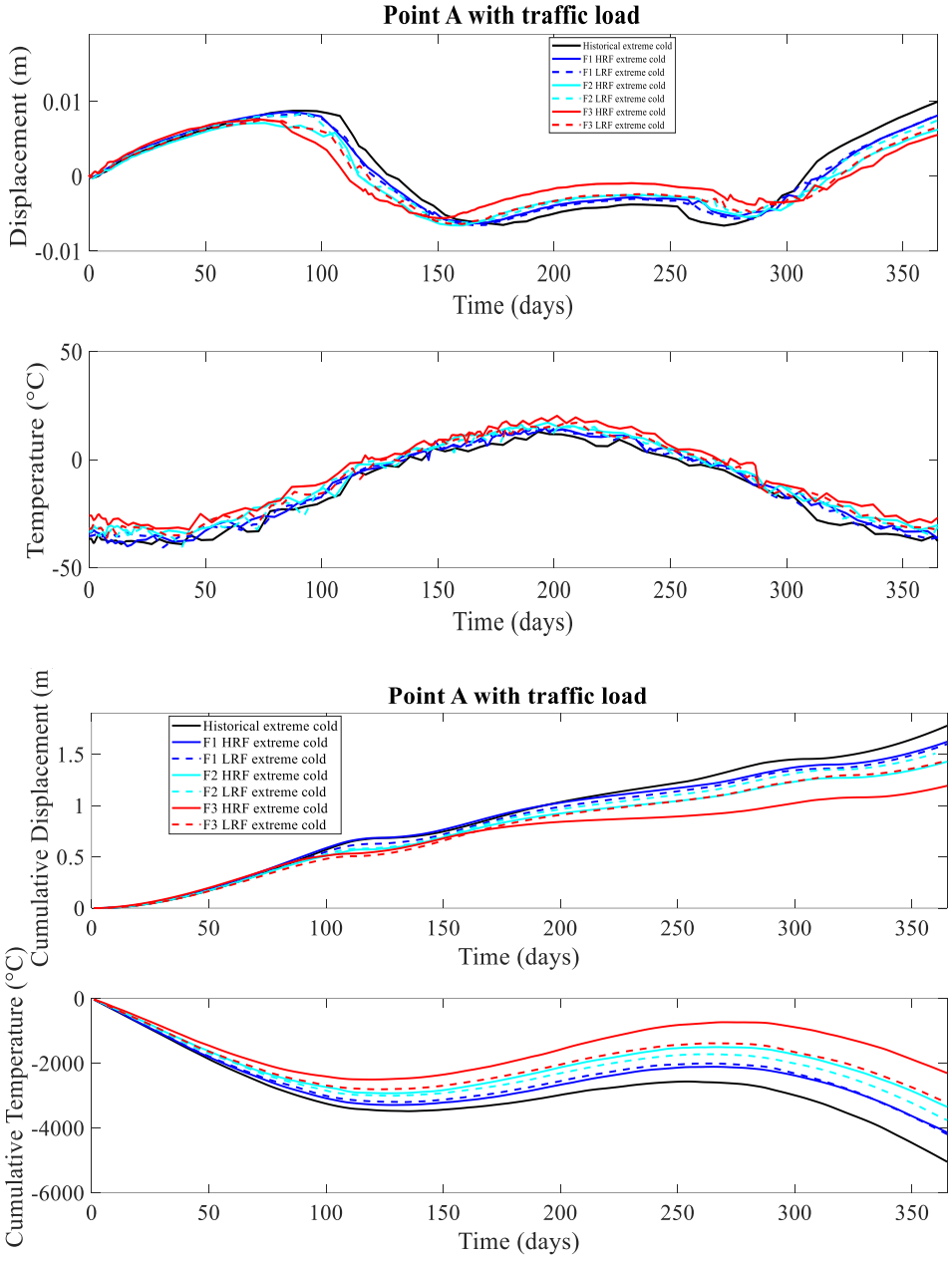
Point A with traffic load
Historical extreme cold
F1 HRF extreme cold
F1 LRF extreme cold
F2 HRF extreme cold
F2 LRF extreme cold
F3 HRF extreme cold
F3 LRF extreme cold
Displacement (m)
Time (days)
Temperature (°C)
Time (days)
Point A with traffic load
Cumulative Displacement (m
Cumulative Temperature (°C)
Time (days)
Time (days)

(a)

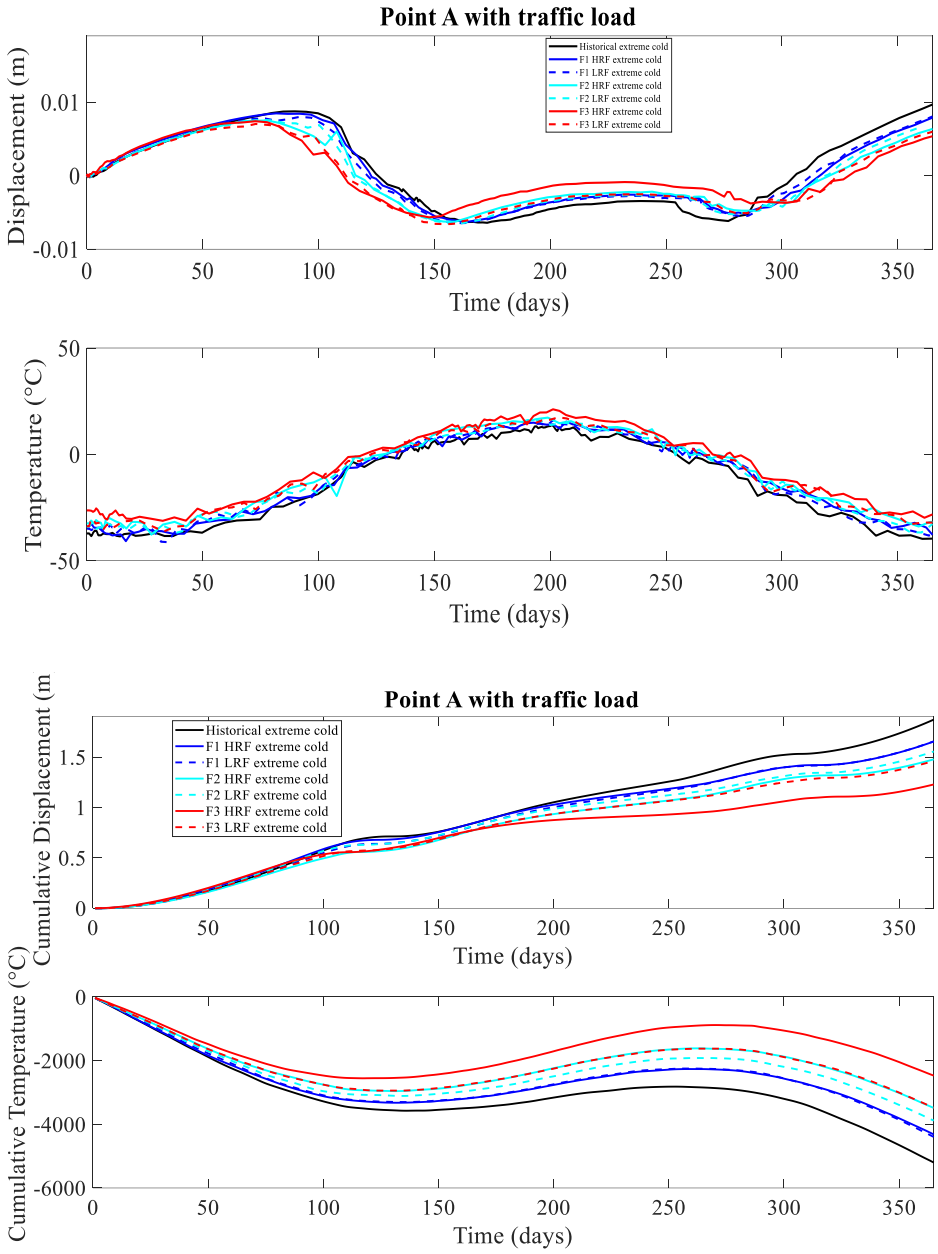

(b)

Figure 5.9 Comparison of displacements cause of extreme cold scenarios in the embankment of (a) James Smith and (b) Yellow Quill.

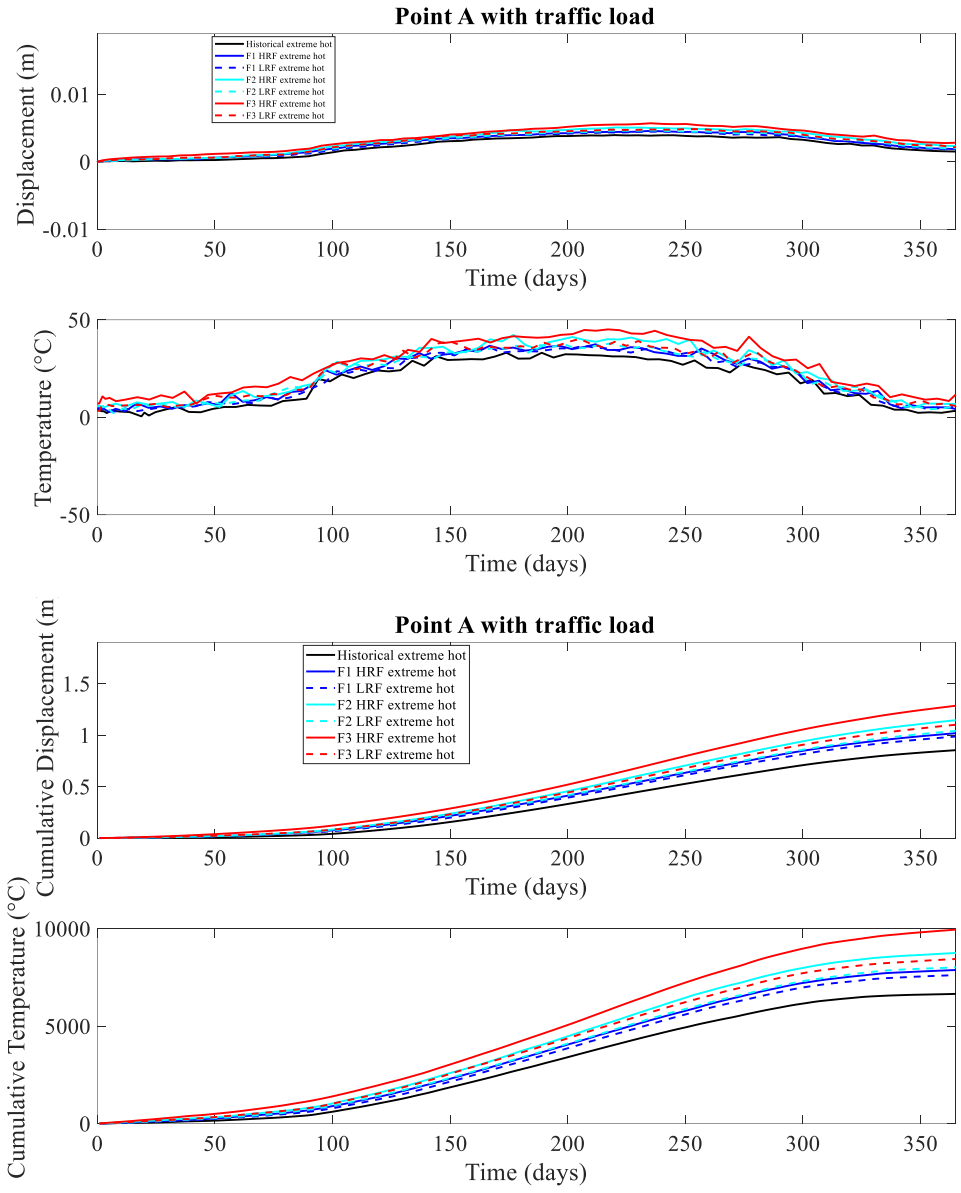
Point A with traffic load
Historical extreme hot
F1 HRF extreme hot
F1 LRF extreme hot
F2 HRF extreme hot
F2 LRF extreme hot
F3 HRF extreme hot
F3 LRF extreme hot
Displacement (m)
Temperature (°C)
Time (days)
Point A with traffic load
Cumulative Displacement (m
Cumulative Temperature (°C)
Time (days)

(a)

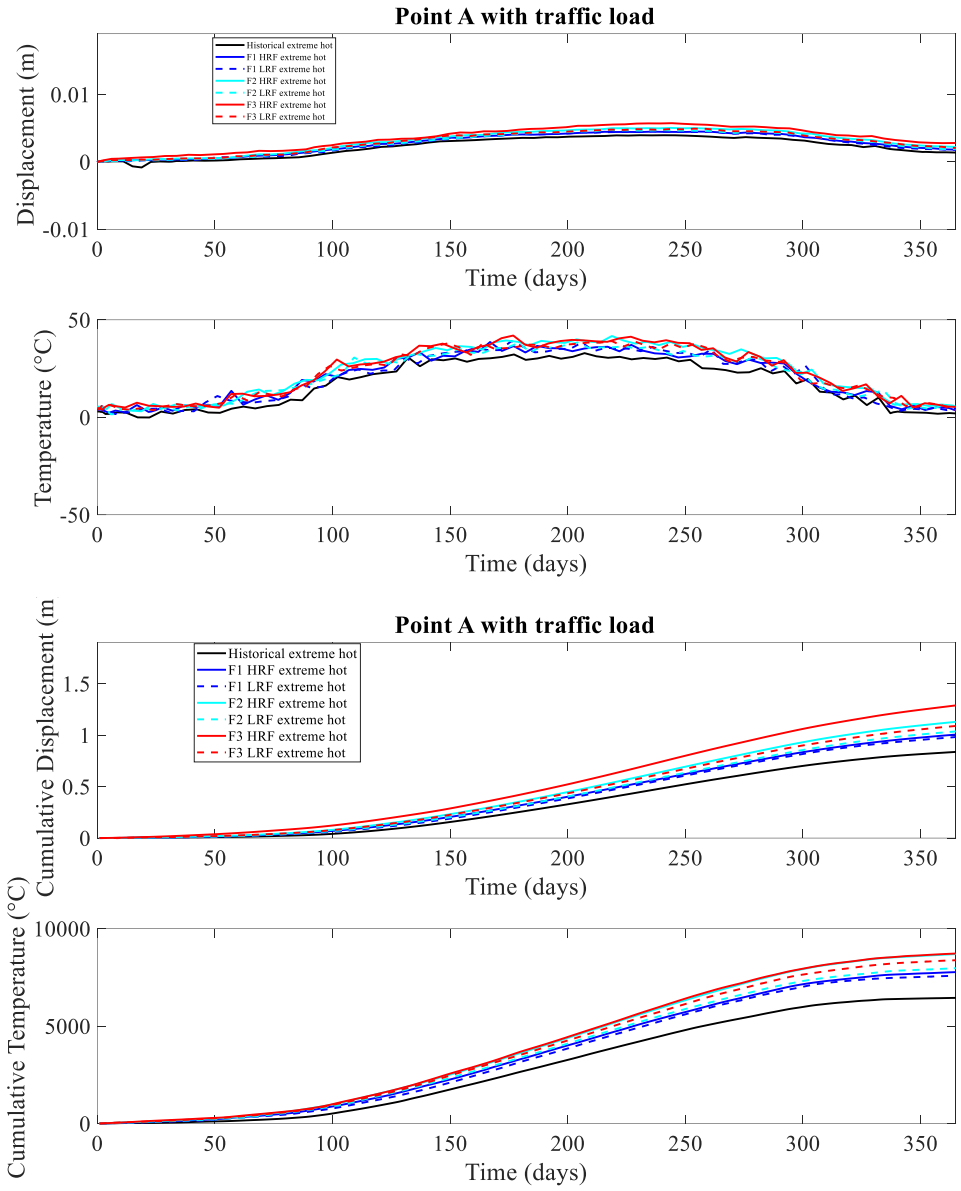

(b)

Figure 5.10 Comparison of displacements cause of extreme hot scenarios in the embankment of (a) James Smith and (b) Yellow Quill.

5.3 Plastic strain profile

The feature of the soil known as plasticity allows it to deform without cracking, fracturing, or rupturing. In this study, the plastic strain profile of all model results for both James Smith and Yellow Quill embankment are considered but here the figure is shown for Future-1 HRF, as shown in Figure 5.11. Because in Plastic strain profile it's

a bit dificult to differenciate between results among various terms; Future-1, Future-2, and Future-3. Since the cases of all projected climate episodes have shown simmilar profile, that indicates that the majority of the strain is created just below the clayey silt layer at the toe , along the gravel in silty clay portion and the point of generation is at the end of gravel where gravel leaves the connection of clayey silt and silty clay. The results show that, with the consideration of traffic load, the embankments generate plastic strain under all climate variables. In cases without the traffic load, the noticeable plastic strain creates only in the extreme cold case, which is in line with the consideration of traffic load and make extreme cold the worse scenario.

The reason for this behaviour of extreme cold is that shown in Figures 5.4 and 5.5, which presents the monitored temperarture at point B. The temperature at that plastic strain spot of extreme cold case shows the ground temperature in winter is around zero °C for short duration and then shows warmup in summer. Which causes the ground to slowly bend towards unfrozen conditions to create more plastic strain as shown in Figure 5.11. The plastic strain profile does not show any noticeable strain difference between HRF and LRF results of both locations.

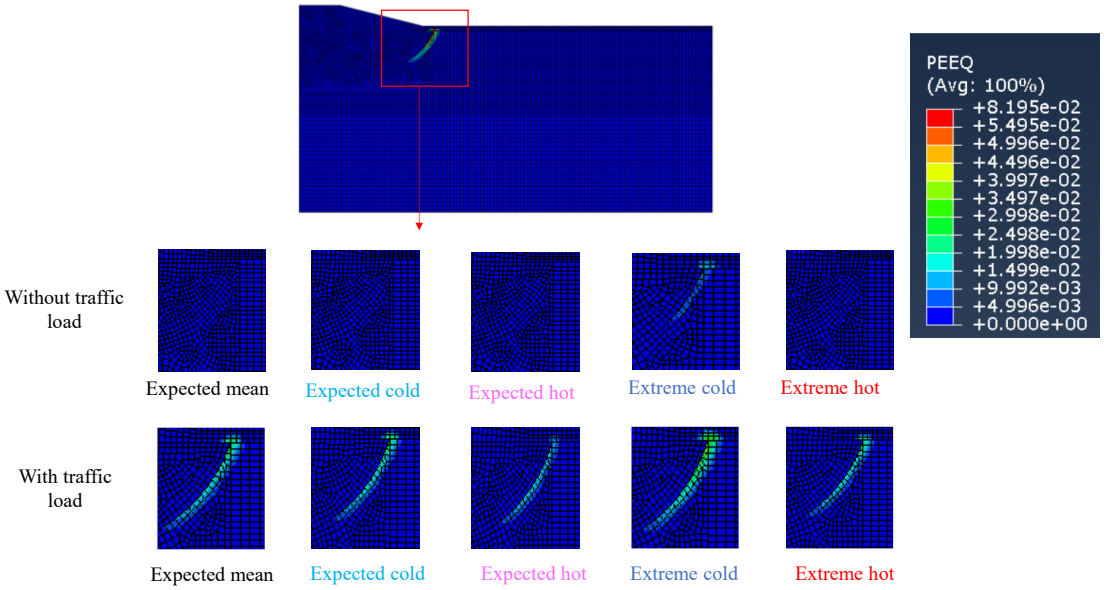

Figure 5.11 Plastic strain profile of James Smith Future-1 HRF (2023-2048).

To make extreme scenario clearer, the comparison of only extreme cold cases of all projected climate terms with the consideration of traffic load are shown in Figure 5.12. Results of extreme hot cases are shown in Figure 5.13. Both of them indicate that there is no significant difference between Historical and Future cases.

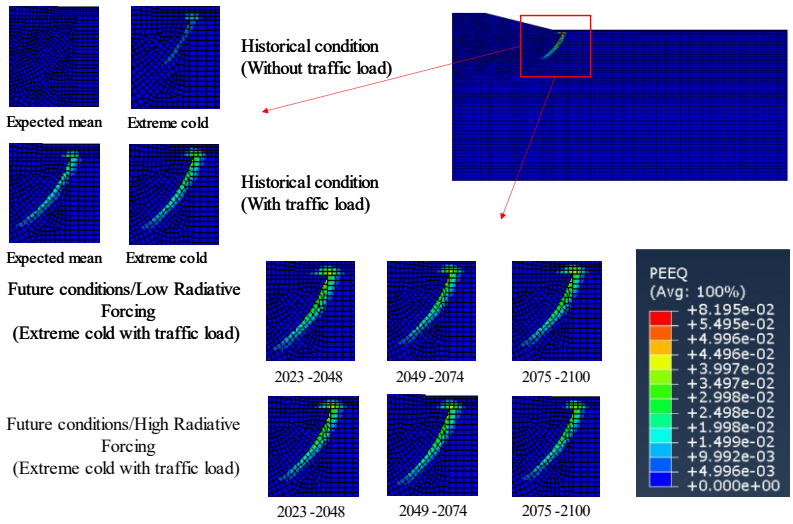

(a)

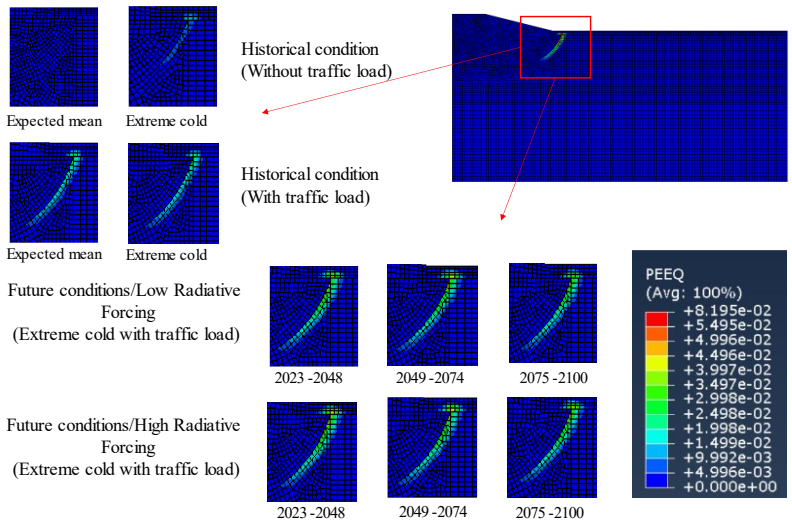

(b)

Figure 5.12 Plastic strain profile of (a) James Smith and (b) Yellow Quill Locations for the extreme cold case.

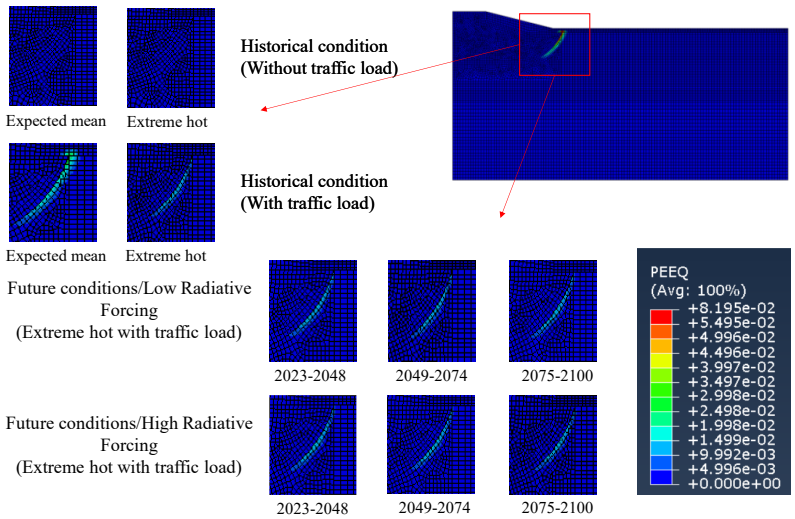

(a)

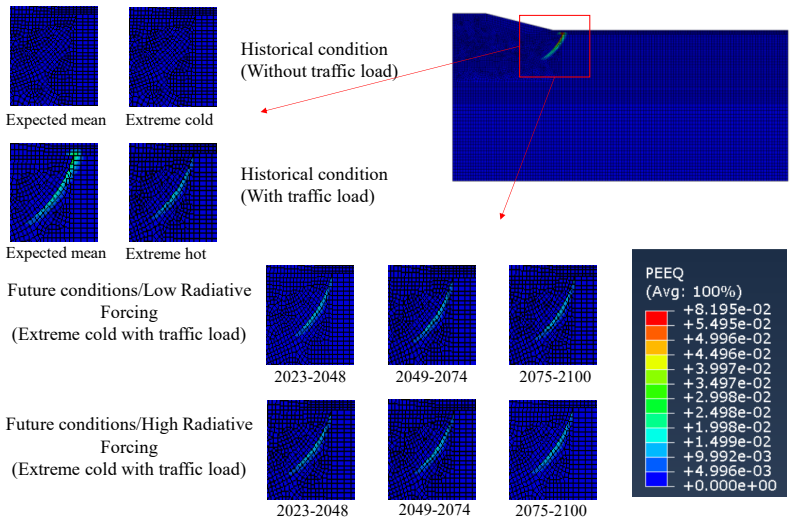

(b)

Figure 5.13 Plastic strain profile of (a) James Smith and (b) Yellow Quill Locations for the extreme hot case.

5.4 Stress path analysis

As mentioned in Chapter 3, this research has used the Linear Drucker-Prager model by considering associative flow rule for yielding in $p' - q$ plane. In the Drucker-Prager yield criteria, the failure line is drawn only for unfrozen soil because of extreme strength of frozen soil and the unfrozen failure surface was derived at 0 °C. So, in warm conditions, the soil fails when the stress path touches this failure line. when the cyclic change in annual temperature occur, the stress line of frozen soil will follow the path to show up stress, which depends on thermal conditions and traffic load on embankment, and when soil temperature becomes equal to or more than 0 °C, the soil will tend to come back to touch the failure surface.

All shown in Figures 5.6, 5.7 and 5.9, soils experience the worst condition when the surface temperature is extreme cold. To check how much the maximum shear stress

can be generated in extreme cold cases, the shear stresses of extreme cold cases from all projected climate scenarios are retrieved and analyzed in this section.

For extreme cold cases, the comparison of stress paths in $p' - q$ plane of all climate scenarios with traffic load consideration for each location are shown in Figures 5.14 and 5.15. Which also includes the monitored temperature at both points A and B of embankments as references. In the embankments of both locations, the monitored temperature at either point A or B shows that the ground is warming up from Historical (1975) to Future (2100). Due to the warmer climate, the ground tends to generate less shear stress, which is more noticeable at the yellow Quill site. Anyway, the stress path lines can clearly indicate that shear stresses gone beyond the shear failure line, thus the extreme cold case is still able to generate large plastic zone in the toe of the embankment in all of the episodes. When there is less shear stress in the toe part of the embankment, it experiences less amount of plastic strain, thus the indirectly it will end up with less disturbance to the road surface. There is a trend that the road surface will have less cumulative displace when the climate is getting warmer for the extreme cold cases as are shown in Fig 5.9.

Similarly, on the consideration of extreme hot case, as shown in Figure 5.16 and 5.17. The results barely show the difference of stress paths from Historical to Future. The stress states are at a state close to the shear failure line, but not do not go much beyond the failure line like the ones shown for the extreme cold cases. Thereby, the displacement on the road surface is due to the thermal expansion/shrinkage of the soil

body and is less influenced by the plastic strain. A warmer temperature will end up with more cumulative displacement Fig 5.10.

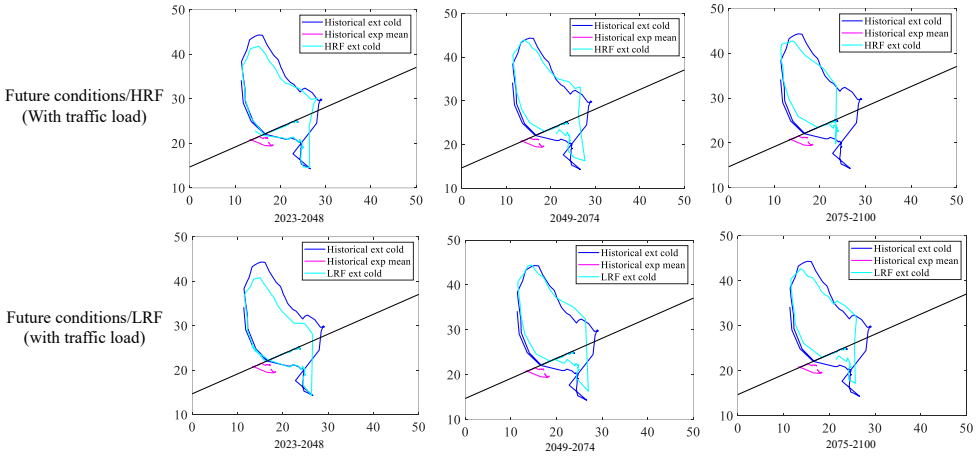

(a)

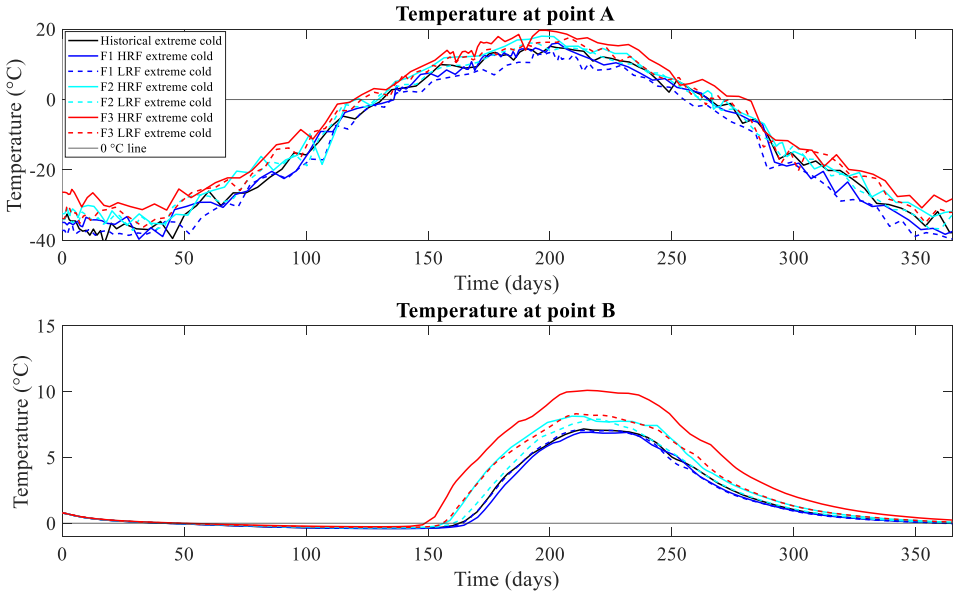

(b)

Figure 5.14 Extreme Cold (a) Monitored Stress path in p'-q plane and (b) temperatures at A and B on the embankment of James Smith location.

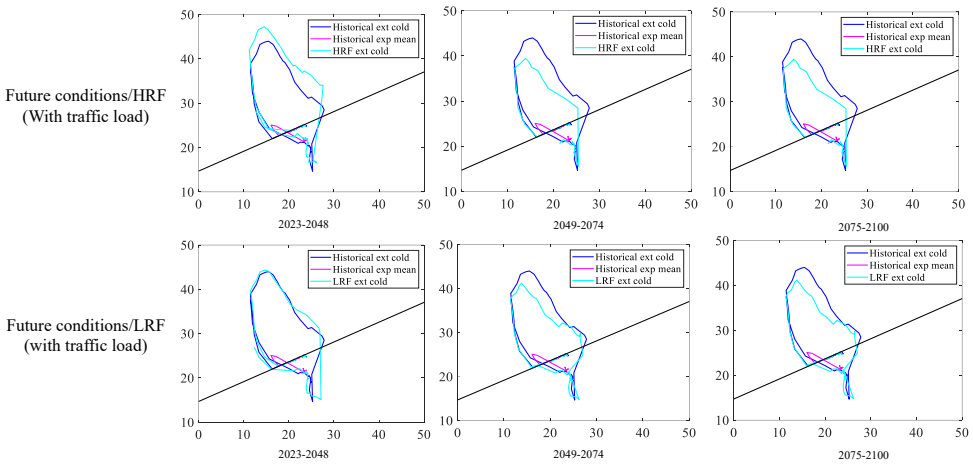

(a)

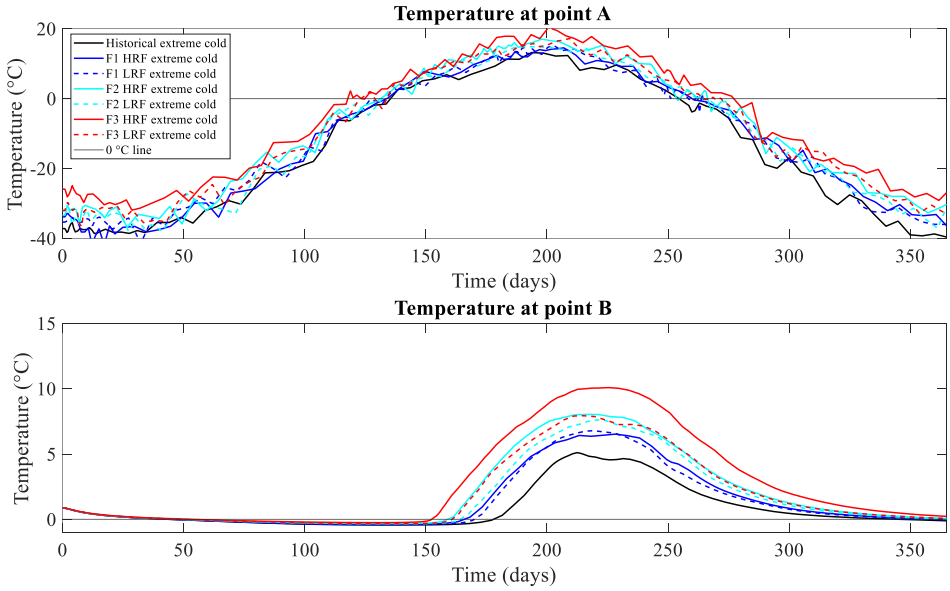

(b)

Figure 5.15 Extreme cold (a) monitored Stress path in p'-q plane and (b) temperatures at A and B on the embankment of Yellow Quill.

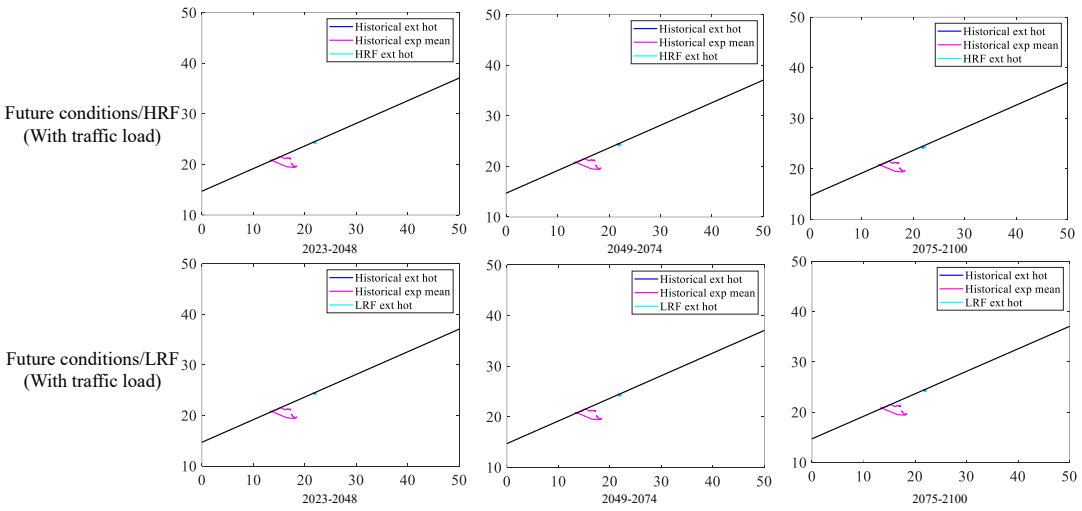

(a)

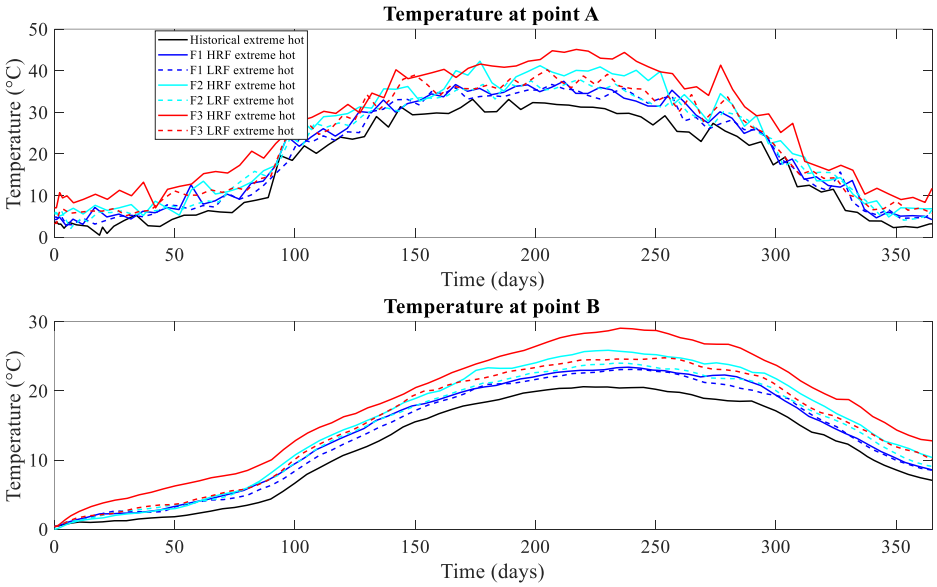

(b)

Figure 5.16 (a) Extreme hot monitored Stress path in p'-q plane and (b) temperatures at A and B on the embankment of James Smith location.

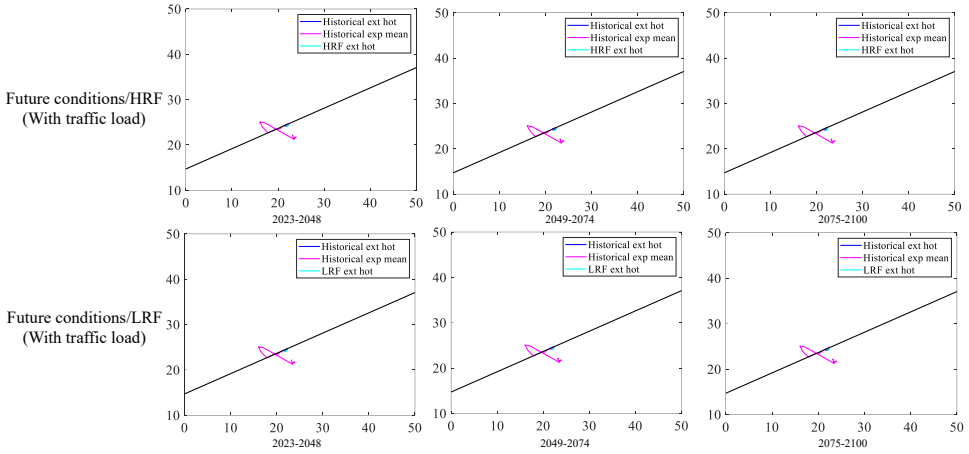

(a)

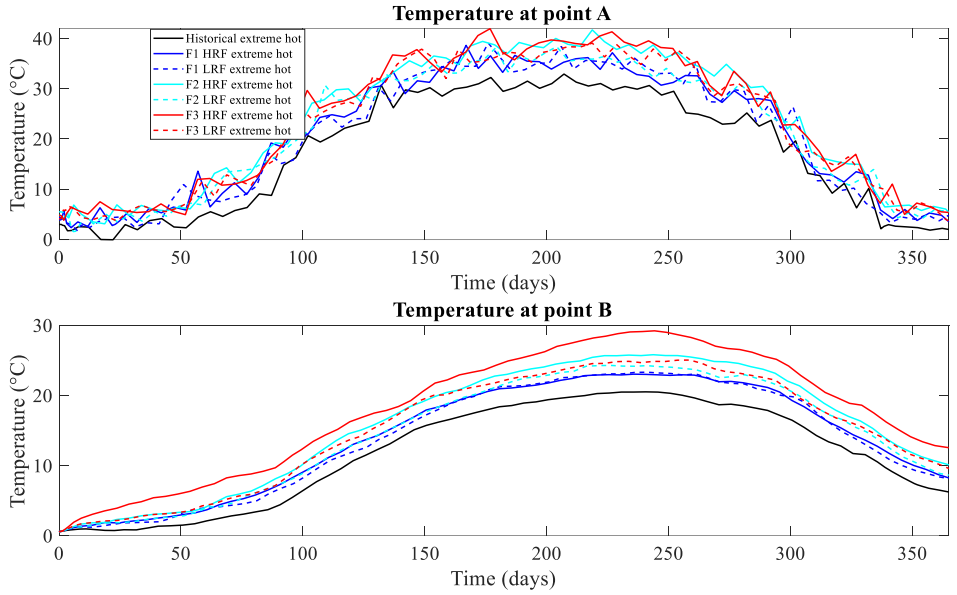

(b)

Figure 5.17 Extreme hot (a) monitored Stress path in p'-q plane and (b) temperatures at A and B on the embankment of Yellow Quill site.

6 Summary, conclusions, and recommendations for future work

6.1 Summary

The goal of the study project was to investigate how global warming affects the thermal-mechanical behavior of the ground in the Canadian non-permafrost zone to examine the effects of climate change on embankment life in these first nation's communities, James Smith, and Yellow Quill, of Saskatchewan. ABAQUS/CAE software is used for the simulation of embankment on both locations.

Since this study was analyzing the embankments of two first nation's communities, the surface air temperature for each location was taken from NASA, and the recent version of the NASA Earth Exchange Global Daily Downscaled Projections (NEX-GDDP) CMIP6 is utilized. The projected climate data contains 7 climate scenarios for each community: Historical, HRFs and LRFs of Future-1,2 and 3, and each of it contains five representative years with varied projected climate data. The results of the coupled thermal-mechanical simulations are reported in Chapter 5. This study not only analyzes the thermal regime of ground or embankments but also considers non-linear thermal-mechanical responses of ground to evaluate the stress re-distributions due to temperature disturbance.

The analysis mainly focusses on the results of extreme cold and extreme hot cases of predicted climate consideration on the embankment. The changing climate conditions on the embankment surface shows the nonlinear behavior of embankment at different parts. The two monitored embankment parts were selected based on the analysis of previous researchers work on the climate related infrastructure failures, which causes the disturbance in the subsurface thermal regime. This study is intended to give a more reliable thermal-mechanical analysis by considering the temperature dependent equivalent thermal expansion coefficients of soils and using FEM based software ABAQUS.

6.2 Conclusions

Based on the study, the following findings were drawn:

- The present investigation is a preliminary attempt of combining climate prediction data with geomechanical analysis for local communities. The combined analysis was successful applied to James Smith and Yellow Quill communities of Saskatchewan. Even though, the study only covers the thermal-mechanical aspect, the procedure can be appliable to a thermal-hydro-mechanical coupled analysis when related data and parameters are available.
- Based on the mixture theory and the unfrozen water content in soils, a model for estimating nonlinear thermal-expansion coefficients of

soils can be established. The model was applied to the studying sites for thermal-mechanical modeling. The including of nonlinear thermal-expansion coefficients is aimed at providing a better characterization of stress redistributions due to temperature disturbance.

- The results of the coupled thermal-mechanical simulations show that projected climate changes will have little effect on the settlement and expansion behavior of soils in the examined Canadian non-permafrost zones. Nevertheless, the extreme cold cases are still able to generate large plastic zone in the toe of the embankment in all of the episodes. The extreme hot cases tend to generate more displacement on the road surface as the climate is getting warmer, thus some attention should be paid to accommodate the climate change.
- In the stress path analysis of extreme cold cases, the results show the generated shear stresses are over the shear failure line of ground soil for cases of all of the episodes even if the climate is getting warmer.
- The plastic strain profile shows that in all results, the plastic strain starts from below the toe of embankment, where the gravel edge is leaving the connection of silty clay with clayey silt and the strain continue down way along the gravel in silty clay soil. In the cases without traffic load, where the climate harshness is the only source of

plastic strain, the strain profile shows that only extreme cold cases have the noticeable plastic strain and HRF and LRF are showing same plastic strain profiles. Upon the consideration of traffic load, all cases show the creation of plastic strain, but the extreme cold climate variable analysis comes up with the maximum plastic strain areas among them.

- This study can provide some preliminary instructions to the engineering society by highlighting the generated plastic zone in the toe part of road embankments under the extreme cold case. In addition, it also implies the trend that the road surface will experience more undulation in the future under the extreme hot condition.

6.3 Recommendations

Many severe problems regarding the short and long-term sustainability of constructions for the benefit of mankind have been raised, to improve ground analysis or to attain the necessary level of soil strength for transportation purposes. The following suggestions are provided for upcoming work:

- The present study only focuses on the thermal-mechanical aspect as a preliminary investigation, the pore water pressure and pore ice pressure should be considered in the subsequent thermal-hydro-mechanical coupled analysis.

- On specific studying sites, field experiments and laboratory testings can be carried out to investigate the geotechnical properties of the ground, the in-situ hydraulic parameters, and the in-situ stress conditions.

- Laboratory freeze-thaw tests can be conducted on soils retrieved from the sites to figure out the cyclic freeze-thaw induced strength degradation of soils.

- Phase transition should be considered while examining the behavior of warm frozen soil. When the applied temperature and stress condition result in melts, micromechanics and thermodynamics theories should be used to determine the large strain behavior of frozen soil.

- A parametric study can be conducted to investigate the impacts of road geometry and soil condition on the results. The parametric study will provide more instructions to engineering projects in cold regions.

References

Abaqus. 2014. Abaqus theory manual, Version 6.14. Simulia.

Alfaro, M.C., Batenipour, H., Graham, J., Kurz, D.R., and Ng, T.N.S. 2009a. Highway embankments on degrading and degraded permafrost. *In*

Proceedings of the 17th International Conference on Soil Mechanics and Geotechnical Engineering: The Academia and Practice of Geotechnical Engineering. IOS Press. pp. 3509–3513.

Alfaro, M.C., Ciro, G.A., Thiessen, K.J., and Ng, T. 2009b. Case study of degrading permafrost beneath a road embankment. Journal of cold regions engineering, **23**(3): 93–111. American Society of Civil Engineers.

Akhtar, S., and Li, B. 2019. Numerical analysis of pipeline uplift resistance in a frozen clay at varying temperatures. *In* Cold Regions Engineering 2019. American society of civil engineers Reston, VA. pp. 345–353.

Akhtar, S., and Li, B. 2020. Numerical analysis of pipeline uplift resistance in frozen clay soil considering hybrid tensile-shear yield behaviors. International Journal of Geosynthetics and Ground Engineering, **6**: 1–12. Springer.

Akhtar, S., and Li, B. 2022. Numerical analysis of pipeline uplift resistance in frozen clay soil considering hybrid tensile-shear yield behaviors. *In* International Journal of Geosynthetics and Ground Engineering. **6**: 1-12.

Aldaeef, A.A., and Rayhani, M.T. 2018. Impact of ground warming on pile-soil interface strength in ice-poor frozen soils. *In* GeoEdmonton 2018 conference, Canadian geotechnical society, Edmonton, Canada.

Andersland, O.B., and Ladanyi, B. 2004. Frozen ground engineering. *In* 4th edition.

Anderson, D.M., Tice, A.R., and McKim, H.L. 1973. The unfrozen water and the apparent specific heat capacity of frozen soils. *In* Second International Conference on Permafrost, Yakutsk, USSR. North American contribution. pp. 289–295.

Armstrong, M.D., and Csathy, T.I. 1963. Frost design practice in canada.

Barron, T.H.K., Collins, J.G., and White, G.K. 1980. Thermal expansion of solids at low temperatures. Advances in Physics, **29**(4): 609–730.

Batenipour, H. 2012. Understanding the performance of highway embankments ondegraded permafrost.

Batenipour, H., Alfaro, M., and Graham, J. 2010. Results from an instrumented highway embankment on degraded permafrost.

Batenipour, H., Alfaro, M., Kurz, D., and Graham, J. 2014a. Deformations and ground temperatures at a road embankment in northern Canada. Canadian

Geotechnical Journal, **51**(4): 260–271. National Research Council of Canada.

Batenipour, H., Alfaro, M., Kurz, D., and Graham, J. 2014b. Deformations and ground temperatures at a road embankment in northern Canada. Canadian Geotechnical Journal, **51**(3): 260–271. National Research Council of Canada.

Batenipour, H., Kurz, D., Alfaro, M., Graham, J., and Ng, T.N.S. 2009a. Highway embankment on degrading permafrost. Proceedings of the International Conference on Cold Regions Engineering,: 512–521.

Batenipour, H., Kurz, D., Alfaro, M.C., and Graham, J. 2009b. Effect of temperature on the 1-D behaviour of plastic clay. *In* Proceedings of the 62nd Canadian geotechnical conference and 10th joint CGS/IAH-CNC groundwater conference, Halifax, NS.

Bo, M.W., Fabius, M., and Fabius, & K. 2008. Impact of global warming on stability of natural slopes.

Burgess, M.M., Riseborough, D.W., and Smith, S.L. 2001. Permafrost and glaciers/icecaps monitoring networks workshop, January 27-28, 2000: report on the permafrost sessions.

Bush, E., and Lemmen, D.S. 2019. Rapport sur le climat changeant du Canada.

Chen, H., Guo, H., Yuan, X., Chen, Y., and Sun, C. 2020. Effect of temperature on the strength characteristics of unsaturated silty clay in seasonal frozen region. KSCE Journal of Civil Engineering, **24**: 2610–2620. Springer.

Chen, R., von Deimling, T.S., Boike, J., Wu, Q., and Langer, M. 2023. Simulating the thermal regime of a railway embankment structure on the Tibetan Plateau under climate change. Cold Regions Science and Technology, **212**: 103881. Elsevier.

Crawford, C.B., and Legget, R.F. 2002. NRC publications archive. Archives des publications du CNRC Cool under fire.

Dasog, G.S., Acton, D.F., and Mermut, A.R. 1987. Genesis and classification of clay soils with vertic properties in Saskatchewan. Soil Science Society of America Journal, **51**(5): 1243–1250. Wiley.

De Bruyn, D., Thimus, J-F. 1996. The influence of temperature on mechanical characteristics of Boom clay: the results of an initial laboratory programme. *In* Engineering Geology. **41**(1-4): 117-126.

Doré, G., and Zubeck, H. 2009. Cold regions pavement engineering.: 416.

Drucker, D.C., and Prager, W. 1952. Soil mechanics and plastic analysis or limit design. Quarterly of Applied Mathematics, **10**(2): 157–165. American Mathematical Society (AMS).

Dysli, M. 1997. Related effects on frost action: Freezing and solar radiation indices. Ground freezing 97,: 3–23.

E. G. Johnson, Arvind Phukan, and Wilbur H. Haas. 1998. Geotechnical thermal analysis. *In* Embankment design and construction in cold regions. *Edited by* J.P. Zarling and W.A. Braley.

Extended Drucker-Prager models. 1995.

Faroukia, O.T. 1985. Section 7.0 Ground thermal properties. Thermal design considerations in frozen ground engineering, 186. ASCE Publications.

Flynn, D., Kurz, D., Alfaro, M., Graham, J., and Arenson, L.U. 2016a. Forecasting ground temperatures under a highway embankment on degrading permafrost. Journal of cold regions engineering, **30**(4). American society of civil engineers (ASCE).

Flynn, D., Kurz, D., Alfaro, M., Graham, J., Arenson, L.U., and Emeritus, P. 2016b. Forecasting ground temperatures under a highway embankment on degrading permafrost. J. Cold Reg. Eng. J. Cold Reg. Eng, (4): 30.

Flynn, D.J. 2015. Field and numerical studies of an instrumented highway embankment in degrading permafrost. University of Manitoba, Winnipeg.

Fortier, R., LeBlanc, A.M., and Yu, W. 2011a. Impacts of permafrost degradation on a road embankment at Umiujaq in Nunavik (Quebec), Canada. Canadian Geotechnical Journal, **48**(5): 720–740.

Forster, P., Storelvmo, T., and Alterskjæ, K. 2021. IPCC sixth assessment report (AR6) working group 1: the physical science basis, chap. 7. University press, UK.

Geology and geosciences. 2019. Available from https://natural-resources.canada.ca/maps-tools-and-publications/maps/geology-and-geosciences/16876. [accessed 11 April 2023].

Gholamzadehabolfazl, A. 2015. A numerical study of a highway embankment on degrading permafrost. University of Manitoba, Winnipeg.

Girgis, N., Li, B., Akhtar, S., and Courcelles, B. 2020. Experimental study of rate-dependent uniaxial compressive behaviors of two artificial frozen sandy clay soils. *In* Cold Regions Science and Technology. **180**: 103166

Global Temperature | Vital Signs – Climate Change: Vital Signs of the Planet. (n.d.). Available from https://climate.nasa.gov/vital-signs/global-temperature/. [accessed 10 April 2023].

Government of Canada. 2019. Climate data viewer (canada.ca)

Heginbottom, J.A., Dubreuil, M.A., and Harker, P.A. 1995. Canada, permafrost. National atlas of Canada. Natural resources Canada, 5th Edition, MCR, **4177**.

Hu, J., Che, T., Sun, H., and Yang, X. 2022. Numerical modeling and simulation of thermo-hydrologic processes in frozen soils on the Qinghai-Tibet plateau. Journal of hydrology: Regional studies, **40**. Elsevier B.V.

Jansson, P.-E. 2012. Coup-Model: model use, calibration, and validation. Transactions of the ASABE, **55**(4): 1337–1344. American society of agricultural and biological engineers.

J.Smith, C., J. Kramer, R., Myhre, G., Alterskjr, K., Collins, W., Sima, A., Boucher, O., Dufresne, J.L., Nabat, P., Michou, M., Yukimoto, S., Cole, J., Paynter, D., Shiogama, H., M. O'Connor, F., Robertson, E., Wiltshire, A., Andrews, T., Hannay, C., Miller, R., Nazarenko, L., Kirkevg, A., Olivi, D., Fiedler, S., Lewinschal, A., MacKallah, C., Dix, M., Pincus, R., and M. Forster, P. 2020. Effective radiative forcing and adjustments in CMIP6 models. Atmospheric Chemistry and Physics, **20**(16): 9591–9618. Copernicus GmbH.

Kersten, M.S., and Cox, A.E. 1951. The effect of temperature on the bearing value of frozen soils. Highway research board bulletin, (40).

Klene, A.E., Nelson, F.E., Shiklomanov, N.I., and Hinkel, K.M. 2001. The n-factor in natural landscapes: variability of air and soil-surface temperatures, Kuparuk river basin, Alaska, USA. Arctic, Antarctic, and Alpine research, **33**(2): 140–148. Taylor & Francis.

Kurz, D., Alfaro, M., and Graham, J. 2015. Thermal conductivities of frozen and unfrozen soil in the active layer. Cold Regions Science and Technology.

Kurz, D.R. 2014. Understanding the effects of temperature on the behaviour of clay. University of Manitoba, Winnipeg.

Lachenbruch, A.H. 1988. Permafrost temperature and the changing climate. *In* 1988, Proceedings of the fifth international conference on permafrost, Trondhelm, Norway. pp. 9–17.

Ladanyi, B., and Andersland, O.B. 2004. Frozen ground engineering. Wiley.

Lepage, J.M., and Mémoire, Y. 2016. Experimentation of mitigation techniques to reduce the effects of permafrost degradation on transportation infrastructures at Beaver Creek experimental road site.

Li, B and Akhtar, S. 2022. Characterizations of tensile yield and failure processes of frozen clay soils: laboratory testing and numerical modeling. *In* Bulletin of Engineering Geology and the Environment. **81**(10): 429

Li, B., and Wong, R.C.K. 2017. A mechanistic model for anisotropic thermal strain behavior of soft mudrocks. Engineering Geology, **228**: 146–157.

Li, L. 2022. Numerical modeling in civil and mining geotechnical engineering. Numerical modeling in civil and mining geotechnical engineering, MDPI, Basel.

Li, S., Zhang, M., Pei, W., and Lai, Y. 2018. Experimental and numerical simulations on heat-water-mechanics interaction mechanism in a freezing soil. Applied thermal engineering, **132**: 209–220. Elsevier Ltd.

Li, S., Zhang, M., Tian, Y., Pei, W., and Zhong, H. 2015. Experimental and numerical investigations on frost damage mechanism of a canal in cold regions. Cold regions science and technology, **116**: 1–11. Elsevier.

Lim Kam Sian, K.T.C., Wang, J., Ayugi, B.O., Nooni, I.K., and Ongoma, V. 2021. Multi-decadal variability and future changes in precipitation over Southern Africa. Atmosphere, **12**(6): 742. MDPI.

Lunardini, V. 1978. Theory of n-factors and correlation of data. *In* Proceedings of the Third International Conference on Permafrost. National Research Council of Canada Ottawa. pp. 40–46.

Luo, X., Ma, Q., Niu, F., Su, W., and Hu, H. 2019. Experimental and numerical analyses of freezing behavior of an embankment in cold regions. Mathematical Problems in Engineering, **2019**. Hindawi Limited.

Marrah, M. 2021. Numerical modeling of thermal and geotechnical response of soils in Canadian no-permafrost regions to climate warming. University of Ottawa, Ottawa.

McAdams 1892-, W.H. (William H. 1954. Heat transmission [by] William H. McAdams. McGraw-Hill, New York.

Ming, F., Yu, Q. hao, and Li, D. qing. 2018. Investigation of embankment deformation mechanisms in permafrost regions. Transportation Geotechnics, **16**: 21–28. Elsevier Ltd.

Nixon, J.F. 1991. Discrete ice lens theory for frost heave in soils. Canadian geotechnical journal, **28**(6): 843–859.

Pavlov, A.V. 1976. Heat transfer of the soil and atmosphere at northern and temperate latitudes. Heat transfer of the soil and atmosphere at northern and temperate latitudes Transl. into ENGLISH of the book"" Temploo'men pochvy s atmosferoi v severn'ikh i umerenn'ikh shirotakh territorii''SSSR,.

Phillips, Marcia., Springman, S.M., and Arenson, L.U. 2003. Permafrost : proceedings of the 8th international conference on permafrost, 21-25 July 2003, Zurich, Switzerland. A.A. Balkema.

Pk, S., and Bashir, R. 2018. Effect of climate change on the stability of earthen embankments. GeoEdmonton 2018, The 71 st Canadian Geotechnical Conference, September 23-26, 2018 in Edmonton, Alberta, Canada.

Pörtner, H.-O., Roberts, D.C., Adams, H., Adler, C., Aldunce, P., Ali, E., Begum, R.A., Betts, R., Kerr, R.B., and Biesbroek, R. 2022. Climate change 2022: Impacts, adaptation and vulnerability. IPCC Geneva, Switzerland.

Puzrin, A.M. 2012. Constitutive modelling in geomechanics: Introduction. Constitutive modelling in geomechanics: Introduction,: 1–312. Springer Berlin Heidelberg.

Qi, J., Yao, X., Yu, F., and Liu, Y. 2012. Study on thaw consolidation of permafrost under roadway embankment. Cold Regions Science and Technology, **81**: 48–54.

Rasmussen, L.H., Zhang, W., Hollesen, J., Cable, S., Christiansen, H.H., Jansson, P.E., and Elberling, B. 2018. Modelling present and future permafrost thermal regimes in Northeast Greenland. Cold Regions Science and Technology, **146**: 199–213. Elsevier B.V.

Reidmiller, D., Avery, C.W., Easterling, D.R., Kunkel, K., Lewis, K., Maycock, T., and Stewart, B. 2018. Fourth national climate assessment. Volume II: Impacts, risks, and adaptation in the United States.

Resources. 1996. Available from http://www.otc.ca/resource/purchase/first_nations_of_saskatchewan_languagedialect_groups.html?page=1. [accessed 11 April 2023].

Riseborough, D W. 2003.Thawing and freezing indices in the active layer. *In* Proceedings of the 8th International Conference on Permafrost. pp. 953–958.

Scenarios and climate models - Canada.ca. 2018. Available from https://www.canada.ca/en/environment-climate-change/services/climate-change/canadian-centre-climate-services/basics/scenario-models.html#toc1. [accessed 12 April 2023].

Shen, Y. jun, Wang, Y. zhi, Zhao, X. dong, Yang, G. she, Jia, H. liang, and Rong, T. long. 2018. The influence of temperature and moisture content on sandstone thermal conductivity from a case using the artificial ground freezing (AGF) method. Cold Regions Science and Technology, **155**: 149–160. Elsevier B.V.

Shi, X., Niu, F., Qu, T., Zhang, H., Jiang, M., Jiang, H., Zhang, Z., and Wang, X. 2022. Stability analysis of Shiwei-Labudalin highway in inner mongolia, Northeastern China using sentinel-1 InSAR. Cold regions science and technology, **202**: 103647. Elsevier.

Smith, S.L., Burgess, M.M., and Nixon, F.M. 2001. Response of active-layer and permafrost temperatures to warming during 1998 in the Mackenzie Delta, Northwest territories and at Canadian forces station alert and Baker lake, Nunavut. Natural resources Canada, geological survey of Canada Nunavut.

Smith, S.L., Burgess, M.M., Riseborough, D., and Nixon, F.M. 2005. Recent trends from Canadian permafrost thermal monitoring network sites. Permafrost and Periglacial Processes, **16**(1): 19–30.

Taylor, A.E. 1995. Field measurements of n-factors for natural forest areas, Mackenzie Valley, Northwest territories. Interior plains and arctic Canada, 5.

Taylor, G.S., and Luthin, J.N. 1978. Model for coupled heat and moisture transfer during soil freezing. Canadian geotechnical journal, **15**(4): 548–555..

Thrasher, B., Wang, W., Michaelis, A., Melton, F., Lee, T., and Nemani, R. 2022. NASA global daily downscaled projections, CMIP6. Scientific Data 2022 9:1, **9**(1): 1–6. Nature Publishing Group.

Topolnicki, M. 2020. Road traffic loads for geotechnical analyses of embankments. Ground engineering.

Van Everdingen, R.O. 1998. Multi-language glossary of permafrost and related ground-ice terms. International Permafrost Association.

Veinović, Ž., Uroić, G., Domitrović, D., and Kegel, L. 2020. Thermo-hydro-mechanical effects on host rock for a generic spent nuclear fuel repository. Rudarsko Geolosko Naftni Zbornik, **35**(1): 65–80. University of Zagreb, Faculty of Political Sciences.

Williams, P.J. 1964. Unfrozen water content of frozen soils and soil moisture suction. Géotechnique, **14**(2): 133–142.

Wood, A.W., Leung, L.R., Sridhar, V., and Lettenmaier, D.P. 2004. Hydrologic implications of dynamical and statistical approaches to downscaling climate model outputs. Climatic change, **62**(1–3): 189–216. Springer.

Wu, Z.W., and Liu, Y.Z. 2005. Frozen subsoil and engineering. Ocean Press, Beijing.

Xu, X., Li, Q., Lai, Y., Pang, W., and Zhang, R. 2019. Effect of moisture content on mechanical and damage behavior of frozen loess under triaxial condition along with different confining pressures. Cold regions science and technology, **157**: 110–118. Elsevier B.V.

Yip, W. 2021. Global daily downscaled projections (NEX-GDDP-CMIP6).

Yukselen-Aksoy, Y., and Kaya, A. 2010. Method dependency of relationships between specific surface area and soil physicochemical properties. applied clay science, **50**(2): 182–190.

Zarling, J.P., and Braley, W.A. 1988. Geotechnical thermal analysis. School of engineering, university of Alaska Fairbanks.

Zhang, H., Wang, X., Zhao, X., and Liu, P. 2020. In-situ experiment investigations of hydrothermal process of highway in deep seasonal frozen soil regions of Inner Mongolia, China. Journal of central south university, **27**(7): 2082–2093. Springer.

Zhang, M., Lu, J., Lai, Y., and Zhang, X. 2018. Variation of the thermal conductivity of a silty clay during a freezing-thawing process. International journal of heat and mass transfer, **124**: 1059–1067. Elsevier Ltd.

Zheng, H., Kanie, S., and Niu, F. 2018. The thermal regime evaluation of high-speed railway foundation by mixed hybrid FEM. Cold Regions Science and Technology, **155**: 333–342. Elsevier